Real-time dynamics of spins coupled to a conduction-electron system

Dissertation

with the aim of achieving a doctoral degree at the Faculty of Mathematics, Informatics and Natural Sciences
Department of Physics | University of Hamburg.

submitted by
Mohammad Sayad

Hamburg | January 2017

Day of oral defense: Hamburg | April 19, 2017
The following evaluaters recommend the admission of the dissertation:

Committee for Dissertation:	**Prof. Dr. Michael Potthoff** **Prof. Dr. Alexander Lichtenstein**
Committee for Disputation:	**Prof. Dr. Michael Potthoff** **Prof. Dr. Roland Wiesendanger**
Chairman of the Board of Examiners:	**Prof. Dr. Wolfgang Hansen**
Chairman of the Doctoral Committee:	**Prof. Dr. Wolfgang Hansen**
Head of Physics Department:	**Prof. Dr. Michael Potthoff**

Abstract

The static hybridization mean-field (HybMF) approach is generalized to the nonequilibrium case for Kondo systems by employing the nonequilibrium perturbation theory for Keldysh-Matsubara Green's functions. This time-dependent hybridization mean-field (tHybMF) is a conserving approximation, readily accessible by Runge-Kutta methods and can be generally used to address various problems concerning Kondo systems far from thermal equilibrium, such as time-dependent Kondo screening as well as the time- dependent competition of the Kondo effect with the Ruderman-Kittel-Kasuya-Yosida indirect magnetic exchange interaction. Another line of research comprises the Kondo model as a paradigmatic system to study the longitudinal and transversal dynamics of spins coupled to a conduction-electron system, which will be in the focus of the present work. Here, the equations of motion for charge, hybridization and spins are derived. Subsequently, the focus is set on the transversal spin dynamics, which appears to be a more classical phenomenon, and relations to previous approaches to classical spin dynamics such as the quantum-classical hybrid method and the linear-response spin dynamics are established. In addition the Landau-Lifshitz-Gilbert equation and in particular the Gilbert-damping term is re-derived revealing that this concept is ill-defined for the case of a non-interacting one-dimensional system. Moreover, a numerical study of the real-time dynamics of a classical spin subject to an external magnetic field and locally exchange coupled to a one-dimensional system of conduction electrons is performed. It is shown, that (i) the relaxation of the spin results from retardation effects in the coupled electron-spin dynamics; (ii) as total energy and spin are conserved in the relaxation process, energy and spin carried by dispersive wave packets of excitations are dissipated into the bulk of the system; (iii) in contrast to the classical theory, the nutational motion of a quantum spin is efficiently damped on a femtosecond time scale, which is explained in the strong-coupling ($JS \to \infty$) limit as quantum dephasing of the eigenmodes in an emergent two-spin model that is weakly coupled to the bulk of the system. Finally, the effect of electron correlations on the spin dynamics is explored. At quarter-filling, correlation-induced time-scale separation is observed in terms of two main electronic dissipation channels, namely the transport of excitations via correlated hopping and via excitations of correlation-induced magnetic moments become active on largely different time-scales. At half-filling, it is demonstrated that strong electron correlations can lead to an incomplete relaxation on intermediate time scales which is reminiscent of prethermalization and so far has been observed in purely electronic systems only.

Zusammenfassung

Die Hybridisierungs-Mean-Field Theorie wird unter Verwendung der diagrammatischen Störungstheorie für die Keldysh-Matsubara Greensche Funktion verallgemeinert, um Kondo-Systeme im Nichtgleichgewicht zu beschreiben. Die zeitabhängige Mean-Field Näherung respektiert mikroskopische Erhaltungsgrößen, ist numerisch effizient lösbar mit Runge-Kutta Methoden und erlaubt im Allgemeinen die Behandlung verschiedener Probleme im Bereich der Kondo-Physik, darunter die zeitliche Entwicklung des Kondo-Effektes sowie die Beschreibung der konkurrierenden Wechselwirkung zwischen Kondo-Effekt und der Ruderman-Kittel-Kasuya-Yosida indirekten magnetischen Wechselwirkung im Nichtgleichgewicht. Insbesondere kann die longitudinale und transversale Dynamik von an Leitungselektronen gekoppelten Spins, beschrieben durch das Kondo-Modell, untersucht werden, was den Forschungsschwerpunkt dieser Arbeit darstellt. Zunächst werden Bewegungsgleichungen für die Ladung, die Hybridisierung sowie die Spins hergeleitet. Anschließend wird der Fokus auf die transversale Spindynamik gelegt, welche eher ein klassisches Phänomen darstellt. Diese wird mit bereits existierenden Methoden in der Li-teratur verglichen, darunter die quanten-klassische Hybridmethode sowie Linear-Response Spindynamik. Weiterhin werden die Landau-Lifshitz-Gilbert Bewegungsgleichung sowie die Gilbert-Dämpfungskonstante aus der transversalen Spindynamik hergeleitet und es wird gezeigt, dass diese für nicht-korrelierte Systeme in einer Dimension nicht wohldefiniert sind. Darüberhinaus wird die Dynamik von einem klassischen Spin im äußeren Magnetfeld, welcher lokal durch die Austauschwechselwirkung an ein itinerantes Elektronensystem gekoppelt ist, numerisch untersucht. Hierbei wird Folgendes gezeigt: (i) Retardierungseffekte in der gekoppelten Spin- und Elektronendynamik führen zur Relaxation des Spins. (ii) Da der Gesamtspin sowie die Gesamtenergie erhalten sind, werden während des Relaxationsprozesses Energie und Spin, getragen durch dispersive Wellenpakete, an das Elektronensystem abgeleitet. (iii) Im Gegensatz zum klassischen Spin, ist die Nutation eines Quantenspins sehr wirksam innerhalb von wenigen Femtosekunden gedämpft. Dies wird im Limes starker Kopplung ($JS \to \infty$) als Dephasierung der Eigenmoden eines Zwei-Spin Systems erklärt, welches schwach an ein Elektronensystem gekoppelt ist. Abschließend wird der Einfluss der elektronischen Korrelation auf die Spindynamik numerisch untersucht. Bei Viertelfüllung führen Korrelationen im elektronischen System zu einer Separation der Zeitskalen, was zur Aktivierung zweier Dissipations- Kanälen auf sehr unterschiedlichen Zeitskalen führt, nämlich Transport von Anregungen über korrelierte Hoppingprozesse sowie über magnetische Anregungen. Bei Halbfüllung wird gezeigt, dass starke Elektronenkorrelation die Relaxation des Spins zwischenzeitlich unterdrückt, ähnlich wie bei dem Phänomen der Präthermalisierung, was bisher nur in rein elektronischen Systemen beobachtet wurde.

Contents

1 Motivation and Introduction

The advent of ground breaking development of electronic devices based on semiconductor transistors has lead to the ubiquitous information society in which we are living today. This progress has been achieved by the miniaturization of electronic devices, i.e. a shrinking in size of the semiconductor transistors in previous decades, as postulated by Moore [1965]. However, transistors cannot be scaled down infinitely due to fundamental physical limitations [Lundstrom, 2003] and Moore's law may reach its end in the very near future [Iwai, 2016; Waldrop, 2016]. The emerging scaling limits of the charge-based semiconductor devices towards atomic-scale structures have led to a rethinking and the development of alternative information processing technologies. One promising approach is called *spintronics* [Wolf et al., 2001], which either adds the spin degree of freedom to conventional charge-based electronic devices in macro-scale systems or exploits the spin alone to develop atomic-scale spin-based devices.

In particular, the all-spin-based device concept realized by Khajetoorians et al. [2011] to process information is a promising approach with key advantages compared to the charge-based concepts, such as non-volatility, and as a result shows high energy efficiency and compatibility with non-volatile storage technology. Further advantages comprise increased data processing speed as well as increased integration densities. Also, non-volatile storage technology based on spin degrees of freedom has made striking progress in recent years. Here, the ultimate objective to code data in single-atom bits is clearly reached [Donati et al., 2016; Natterer et al., 2016]. The fabrication of such systems, i.e. atomic-scale spin chains or single atoms adsorbed on a metallic substrate is readily technically viable either by self-assembly [Bode et al., 2007; Nadj-Perge et al., 2014] or by combined bottom-up atomic fabrication with spin-resolved scanning-tunneling microscopy (STM) [Wiesendanger, 2009]. Moreover, STM-based methods are established as reliable tools to resolve magnetic structures with subnanometer spatial resolution. In particular, the time-resolution of STM-based tools has been recently improved to characterize localized spin dynamics and detect spin relaxation times [Loth et al., 2012, 2010; Nunes and Freeman, 1993; Spinelli et al., 2014; Yoshida et al., 2014].

The theoretical analysis of the spin dynamics and relaxation observed in the above STM-based experiments is a demanding and interesting task. A localized spin switched by an external magnetic field shows precessional motion. However, if the spin is coupled to an extended bath, e.g. a conduction electron system, the spin relaxes and eventually reaches a new equilibrium state, as the energy and angular momentum can be transferred into the electronic system.

This process has been extensively studied on a phenomenological level by means of the Landau-Lifshitz-Gilbert equation (LLG) [Gilbert, 2004; Landau and Lifshitz, 1935], consisting of precessional and a pure phenomenological damping terms. The LLG equation was originally developed to study magnetization dynamics of macroscopic samples, but nowadays it has become an essential approach to atomistic simulations of magnetic materials [Evans et al., 2014; Skubic et al., 2008; Tatara et al., 2008]. The obvious advantage of the LLG approach is its broad applicability to systems of practical interest up to a 100-nanometer length scale and time regimes up to picoseconds Evans et al. [2014], which comes from the fact that in the LLG equation, only the time-scale of the spins must be taken into account. However, the LLG concept has some significant weakpoints: Firstly, although the Gilbert damping constant has been computed numerically from a more fundamental model including electron degrees of freedom explicitly [Bhattacharjee et al., 2012; Onoda and Nagaosa, 2006; Umetsu et al., 2012] or in some cases even from first principles [Antropov et al., 1995; Capelle and Gyorffy, 2003; Ebert et al., 2011; Kuneš and Kamberský, 2002a; Sakuma, 2012], in general it is not clear how to define Gilbert damping for atomistic models. Thus in general, the LLG approach possesses no predictive power due to the inherent phenomenological damping term. The same applies to inertia effects which become important for ultrafast processes on a femtosecond time-scale [Kimel et al., 2009], which have been introduced and studied phenomenologically by an additional term to the LLG equation with a second-order time derivative of the spin [Ciornei et al., 2011; Olive et al., 2012]. As in the case of the damping term, the nutational term can also be derived on a microscopic level [Bhattacharjee et al., 2012; Kikuchi and Tatara, 2015]. However, there have been only few studies with realistic parameters taken from first-principles calculations [Böttcher and Henk, 2012; Thonig et al., 2016]. Secondly and more importantly, the LLG theory relies on two partially related assumptions: (i) the electron-spin coupling is assumed to be weak and can be treated perturbatively to lowest order. (ii) a separation of time-scales is assumed, i.e. the impurity spin dynamics is slow compared to the electron dynamics. Consequently this concept must break down, for (i) strong spin-electron couplings and (ii) when time scale of the impurity spin becomes comparable to the electronic dynamics. This situation occurs in fast magnetization processes in a sub-femtosecond regime, experimentally realized, e.g., by ultrafast optical manipulation of magnetic order [Kirilyuk et al., 2010].

On the atomistic level, the Gilbert damping must originate from the coupling of the spin to its environment. Thus, a successful approach beyond the LLG concept must in general take into account the interdependent interactions of the impurity spin to the host material [Koopmans et al., 2010], which are active on different length and time scales, such as the coupling of the spin to the conduction-electron system [Cinchetti et al., 2006] and lattice degrees of freedom (phonons) [Koopmans et al., 2010] and electron-magnon scattering [Carpene et al., 2008]. In addition, such an approach must overcome assumptions (i) and

(ii) in order to be valid for all coupling strengths and time-scales to explore the physics beyond the LLG theory.

This is the starting point of our work, which is devoted to the development of a computationally efficient formulation in terms of the electronic one-particle reduced density matrix explicitly including electronic degrees of freedom, which is applicable to arbitrary coupling strengths and does not assume a separation of electron and spin time-scales. Here, we neglect lattice degrees of freedom as well as electron-magnon interactions and rather focus on the interaction of the impurity spins with the conduction-electron system as presented by the well known Kondo model [Kondo, 1964] as a paradigmatic system to study the real-time dynamics of the spins. To this end, we generalize the static hybridization mean-field theory [Lacroix and Cyrot, 1979] to the nonequilibrium case and multi-impurity Kondo systems. This time-dependent hybridization mean-field (tHybMF) approach can be numerically evaluated by standard Runge-Kutta methods [Verner, 2010] and opens up different interesting lines of research: Firstly, the spatial and temporal formation or breaking of a Kondo singlet [Lechtenberg and Anders, 2014; Medvedyeva et al., 2013; Nuss et al., 2015a] can be studied on a mean-field level. (ii) Secondly, the competition of the Kondo effect with the Ruderman-Kittel-Kasuya-Yosida (RKKY) indirect magnetic exchange interaction for systems with many magnetic impurities, which has yet not been studied on the time domain, is accessible to the tHybMF theory. (iii) Finally, another line of research comprises longitudinal and transversal spin dynamics on an atomistic level representing the main focus of this thesis, which is organized as follows:

After this introduction, the correlated quantum lattice models of interest, such as the Hubbard, Anderson and Kondo model and physics behind these models are introduced first in *Chapter 2*. Subsequently, the nonequilibrium theory for quantum many-body systems as well as the nonequilibrium perturbation theory in the context of the Kadanoff and Baym [1962] equation are presented. Finally, a time-dependent mean-field equation for the reduced one-particle density matrix is derived.

Based on the preliminary work of *Chapter 2*, we formulate the time-dependent hybridization mean-field theory in *Chapter 3*. In addition we derive equations of motion for hybridization, charge and spin dynamics for the multi-impurity Kondo model and discuss potential applications of the tHybMF theory to impurity systems far from equilibrium.

In the following *Chapter 4*, we relate our theory to previous approaches in the literature. To this end, we neglect the hybridization terms reflecting the longitudinal spin dynamics and the time-dependent Kondo effect and focus mainly on transversal spin dynamics, which appears to be a more classical phenomenon. Thereby the exact quantum-classical hybrid spin dynamics (QCH-SD) [Elze, 2012; Hall, 2008] for the classical-spin Kondo model is recovered, which includes electronic degrees of freedom explicitly. In addition, LLG theory and in particular the Gilbert damping term is re-derived from the quantum-classical hybrid approach in two steps: Firstly, in the weak-coupling limit, applying

lowest-order linear-response theory in the spin-electron coupling, the electron degrees of freedom can be integrated out altogether [Bhattacharjee et al., 2012; Onoda and Nagaosa, 2006], resulting in an equation of motion for the classical spins only, denoted as linear-response spin dynamics (LR-SD), which possesses a temporally and spatially non-local structure. Secondly, assuming a separation of time-scales, the LR-SD can be simplified further by applying a Markov approximation resulting in the LLG equation. Finally, we discuss the dependency of the Gilbert damping constant on the low-energy electronic structure.

Chapter 5 is devoted to a comprehensive numerical study of the real-time dynamics of a single classical spin coupled to a conduction electron system subject to a local magnetic field. In Secs. 5.1 and 5.2 a noninteracting conduction electron system is addressed. Later on, in Sec. 5.3, we focus on a strongly correlated conduction electron system to which the spin is coupled. Following a sudden quench of the magnetic field, the real-time dynamics of the classical spin and of the conduction electron spins are examined rigorously. In particular, the microscopic cause of the relaxation is identified and the reversal time as a function of the interaction and the field strength is analyzed. In addition, we study the nutational behavior in the dynamics of a classical spin as well as a quantum spin in Secs. 5.2. Moreover, we explore quantum effects by a systematic time-dependent density-matrix renormalization group (tDMRG) [Haegeman et al., 2011, 2016; Schollwöck, 2011] study for different spin quantum numbers S and by comparing with QCH-SD theory for the classical-spin Kondo model. In the following Sec. 5.2, we study directly the effect of electronic correlations on the real-time dynamics of a classical spin coupled to a Hubbard chain by means of a combination of the LR-SD approach [Bhattacharjee et al., 2012; Onoda and Nagaosa, 2006] for the spin dynamics and the tDMRG method for the correlated electronic system. We demonstrate that correlation-induced time-scale separation elicits qualitatively new effects in the spin dynamics similar to prethermalization [Kollar et al., 2011; Marcuzzi et al., 2013; Moeckel and Kehrein, 2008, 2010] or metastability of excitations due to lack of phase space for decay [Hofmann and Potthoff, 2012; Rausch and Potthoff, 2016; Rosch et al., 2008; Strohmaier et al., 2010], i.e., physics which so far has been observed in purely electronic quantum systems only.

Finally, in *Chapter 6*, we conclude this thesis by giving a summarized overview followed by a brief outline of future prospects and potential applications of the time-dependent hybridization mean-field theory as well as the quantum-classical hybrid spin dynamics.

2 Models and methods

In this chapter we briefly introduce fermionic Hamiltonians for quantum many-body problems in solid state systems. To this end, it is convenient to use the formalism of the second quatization for interacting many electron systems, as the proper symmetry of the many-electron wave function is imposed from the very beginning in terms of commutation rules for electron creation and annihilation operators. The Hamiltonian itself is written in terms of field operators and reads:

$$H = \sum_{\alpha\beta} T_{\alpha\beta}\, c^\dagger_\alpha c_\beta + \frac{1}{2} \sum_{\alpha\beta\delta\gamma} V_{\alpha\beta\gamma\delta}\, c^\dagger_\alpha c^\dagger_\beta c_\delta c_\gamma \,, \tag{2.1}$$

where the Greek letters label the spin projection, orbitals and lattice sites. The first term in the Hamiltonian is an one-particle operator and describes the hopping of Fermions between arbitrary sites with amplitude $T_{\alpha,\beta}$, which is in general determined by an overlap integral between the local wave functions and the crystalline structure. $c^\dagger_\alpha$ and c_α are the corresponding creation and annihilation operators. The second term is a two-particle operator and represents the interaction between fermions on different sites, where $V_{\alpha\beta\gamma\delta}$ denotes the interaction matrix element between two-particle states. In solid state systems the two-particle matrix element describes the screened Coulomb interaction.

In Sec. 2.1 and Sec. 2.2 we briefly introduce the Hubbard, Anderson and Kondo Hamiltonian as paradigmatic models for interacting fermionic quantum lattice systems. These models capture the relevant elementary electro-magnetic interactions between electrons in a solid state system, which leads to interesting phenomena such as collective magnetism, Mott insulating behavior, super conductivity, Kondo screening or non-Fermi liquid behavior [Coleman, 2016].

The nonequilibrium theory for quantum many-body systems is presented in Sec. 2.3. Here, we introduce the contour Green's function method and discuss the nonequilibrium perturbation theory in the context of the Kadanoff and Baym [1962] equation. Finally, a time-dependent equation for the reduced one-particle density matrix is derived.

2.1 Hubbard model

In this section, we begin with the simplest paradigm model of correlated electrons, the single-band Hubbard model and discuss the metal-insulator transition based on the book

by Gebhard [1997]. The nowadays so-called Hubbard model was introduced to approximately model of electron interaction in narrow energy band models independently by Gutzwiller [1963], Hubbard [1963] and Kanamori [1963]. The Hamiltonian of the single-band Hubbard model reads as

$$H = \sum_{ij\sigma} T_{ij} c^{\dagger}_{i\sigma} c_{j\sigma} + \frac{U}{2} \sum_{i\sigma} n_{i\sigma} n_{i-\sigma} \,. \tag{2.2}$$

The parameters of the Hubbard model are the interaction U (local screened Coulomb interaction), the lattice dimension d and the structure of the lattice, which is determined by the hopping matrix elements T_{ij}. Further parameters are given by the temperature $k_B T/W$ and the density of electrons with spin σ denoted as $n_\sigma = N_\sigma/L$, where L stands for the number of sites, $N_\sigma = \sum_{i=1}^{L} n_{i\sigma}$ for the number of electrons with spin σ and W denotes the bandwidth.

The Hubbard Hamiltonian (2.2) is a minimal model for studying low-energy and low-temperature phenomena as the theory of itinerant magnetism [Tasaki, 1998], the metal-insulator transition [Imada et al., 1998] and recently also superconductors in doped Mott insulators. In the following, we describe basic properties of the Hubbard model, in particular we will focus on the metal to insulator transition, as we will address this effect in Sec. 5.3 in the context of the relaxation of a classical spin coupled to a one-dimensional Hubbard model. The Hubbard model is integrable [Shastry, 1986] in $1d$ and was solved analytically by Lieb and Wu [1968] via the Bethe approach. However, in higher dimension $d > 1$ the model is not integrable and an exact solution is accessible only in a few limiting cases like the Fermi-gas limit and the atomic limit [Hubbard, 1963]. Now we focus on the large-U limit and discuss the metal to Mott insulator transition. In the case of $N < L$ with $N = N_\uparrow + N_\downarrow$ (less than half band-filling) the Hamiltonian (2.2) describes in any dimension an ideal metal, as holes are mobile charge carriers. In the case of an exactly half filled band $N_\uparrow = N_\downarrow = L/2$ the Hubbard model describes a metal for $U < U_c$, where U_c is the critical interaction which depends on the microscopic detail of the model. However, for large interactions $U \gg W$, electrons becomes localized and the model Hamiltonian (2.2) describes an antiferromagnetic insulator and can be mapped via the Schrieffer-Wolff transformation to the antiferromagnetic Heisenberg model, namely

$$H = J_H \sum_i \boldsymbol{s}_i \boldsymbol{s}_{i+1} \,, \tag{2.3}$$

where $J_H \sim {}^{4T^2}/_{U} > 0$ is the antiferromagnetic exchange interaction between rigid $s = {}^1/_2$ spins. Proceeding from the aforementioned behavior at small $U < U_c$ and large $U \gg W$, the Hubbard model should be able to capture the Mott transition at a critical interaction U_c. One exception is the $1d$ Hubbard model. Taken literally, in $1d$ the metallic phase only occurs at $U = 0$ and the system is an insulator for any finite value of U. However a residual hopping processes remains, as the charge gap $\Delta \sim e^{-1/U}$ is small compared

to the hopping amplitude T in the weak-coupling limit $U \to 0$ as obtained from Bethe approach by Ovchinnokov [1969].

2.2 Quantum impurity models in a nutshell

This section is based on the textbooks of Coleman and Hewson and describes the physics of local moment formation and subsequently the interaction of this local moment with the itinerant electrons of a non-magnetic host material, which leads to the Kondo effect, a paradigm example of collective phenomena in the field of strongly correlated electrons. The Kondo problem, and later the heavy Fermion physics, started essentially with the observation of the so-called 'resistance minimum' in the resistivity of gold, copper and lead reported by de Haas et al. [1934]. However, the study of individual impurities became technically manageable only 30 years later. In 1962 Clogston et al. published experimental studies on local magnetic moment formation, with an iron atom dissolved in various transition metal alloys and demonstrated that the magnetic moments does not always survive. Later on, in 1964 Sarachik et al. confirmed the former experimental study by de Haas et al. with a measurement of the resistivity of *Mo-Nb* and *Mo-Re* alloys containing only 1% Fe concentration. These seminal experimental discoveries raised two important questions for theoreticians:

- How is the formation of local magnetic moments possible in a host metal?
- How does the localized magnetic moment interact with the see of the itinerant conduction electrons of the host metal?

In the following we will briefly discuss theoretical attempts to explain both questions in almost historical order. Initial studies, focused on identifying the cause of local moment formation in metals, were made by Mott and Peierls [1937] and also Van Vleck [1953]. Their studies suggested that a sufficiently strong Coulomb interaction between electrons on an atomic state would lead to localization of electrons and transform a metal into a Mott insulator. However, the question of interaction between a magnetic impurity and the host metal remained unstudied. Friedel and Blandin [1956] addressed the problem of a magnetic impurity without local Coulomb interaction, coupling to the conduction electron system and argued that the electrons scattering off metal transition atoms will hybridize with the Bloch states of the host metal leading to resonant bound states. However, in the absence of Coulomb interaction this concept does not explain the formation of localized magnetic moments and also the resistance minimum as a consequence of screening of the local moments remains unclear. Hence we need a unification of both above ideas, which was realized by Anderson [1978] by the proposition of an appropriate Hamiltonian, which nowadays is well-known as the Anderson model.

2.2.1 Anderson model

The Anderson model in its simplest form as introduced by Alexander and Anderson [1964] reads as

$$\begin{aligned} H &= H_c + H_f + H_{cf} \\ &= \sum_{\boldsymbol{k}\sigma} \epsilon_{\boldsymbol{k}} c^\dagger_{\boldsymbol{k}\sigma} c_{\boldsymbol{k}\sigma} + \epsilon_f \sum_\sigma n_{f\sigma} + U n_{f\uparrow} n_{f\downarrow} + \sum_{\boldsymbol{k},\sigma} (V(\boldsymbol{k}) c^\dagger_{\boldsymbol{k}\sigma} f_\sigma + \text{H.c}) \,, \end{aligned} \tag{2.4}$$

where H_c describes the non-interacting conduction-electron sea, H_f captures the atomic physics of the impurity state and H_{cf} denotes the interaction between the impurity state and the conduction band. $c^\dagger$ (c) and $f^\dagger$ (f) are, respectively, the creation (annihilation) operators for the conduction and the impurity electrons. $\epsilon_{\boldsymbol{k}}$ stands for the energy of an electron with momentum $\boldsymbol{k}$ and ϵ_f is the energy of the impurity state in absence of U, which is the Coulomb repulsion between two electrons in the impurity state. The impurity local moment results from partially filled d- or f- orbitals, as they are highly localized and narrow in shape and one cannot neglect the Coulomb repulsion in contrast to the s-orbitals. The tunneling process between localized d- or f-orbitals and the Bloch states of the conduction band, the hybridization process, with the amplitude $V(\boldsymbol{k})$ is given by the third expression H_{cf}.

The atomic limit: If the hybridization vanishes ($V = 0$), the Hamiltonian H_f remains and describes the atomic physics of an isolated ion and one can study local moment formation. Neglecting orbital degeneracy the atomic Hubbard model spectrum is given by $E(|n_f = 0\rangle) = 0$ (empty), $E(|n_{f\sigma} = 1\rangle) = \epsilon_f$ (singly occupied with spin degeneracy) and $E(|n_{f\sigma} = 2\rangle) = 2\epsilon_f + U$ (doubly occupied). For $^U/_2 > |\epsilon_f + ^U/_2|$ and repulsive $U > 0$ a singly occupied state with only two-fold spin degenerate degrees of freedom remains and the d- or f-orbitals act effectively as a local moment. The immersion ($V \neq 0$) of this system to a conduction-electron sea leads to different phenomena dependent on the parameters of the model and the temperature.

Virtual bound state: If $U = 0$, the formation of electronic resonance, i.e. the concept of Friedel and Blandin [1956] is recovered, which states that hybridization in the absence of interaction broadens the localized impurity density of states. The width of the latter can be calculated via Fermi's golden rule and results in an average of the density of state and the hybridization $|V(\boldsymbol{k})|^2$ given by $\Delta = \pi \sum_{\boldsymbol{k}} |V(\boldsymbol{k})|^2 \delta(\epsilon_{\boldsymbol{k}} - \epsilon_f)$. The mean-field treatment of the full Hamiltonian (2.4) [Anderson, 1961], where both Coulomb interaction and hybridization are active and competing with each other, confirms the result of Friedel and Blandin [1956] at weak $U < \pi\Delta$. In contrast, in the case of strong coupling $U > \pi\Delta$ two Lorentzian peaks corresponding to the up and down components of the resonance are found at $E \sim \pm^U/_2$ for the particle-hole symmetric case. Hence, the mean-field results presented by Anderson [1961] explain qualitatively the experimentally observed formation of local moments. However the immersion of a local moment to a conduction-electron sea at low temperatures is more involved as it leads to a strongly

correlated collective phenomenon called Kondo effect. The very fundamental manifestation of the Kondo effect is the appearance of a resonance peak in the impurity density of states, the Kondo resonance at the Fermi energy, which occurs below the so-called Kondo temperature $T_K \propto \exp(-U/\Delta)$ (for the symmetric Anderson model). However the Kondo effect cannot be captured by the mean-field solution of Anderson [1961] and is only accessible by non-perturbative methods. The Kondo effect arises primarily due to the interaction between a localized magnetic moment or spin with the spin of the itinerant electrons of the host metal, consequently an effective spin Hamiltonian describing the interaction between the spin of localized and itinerant electrons would be essentially adequate to describe the Kondo effect. Such an effective Hamiltonian can be derived from the Anderson model in the limit $V^2/U \ll 1$ by the Schrieffer-Wolff transformation [Schrieffer and Wolff, 1966] leading to the Kondo model which we will discuss in the following section.

2.2.2 Kondo model

Historically, the Kondo effect is associated with electron transport at low temperature and in particular with the resistance minimum in metals doped with magnetic impurities. The experimental evidence of the correlation of a local magnetic moment (Curie-Weiss term in the impurity susceptibility) and the resistance minimum in the host metal by Sarachik et al. suggests to focus primarily on the interaction between the spins of localized and conduction electrons and neglect all remaining hypothetical effects coming for instance from the impurity charge or the crystal field. Therefore Kondo [1964] used the *s-d* interaction model or, equivalently, the Kondo model to calculate the scattering probability of the conduction electrons up to the second Born approximation.

The Kondo model captures the interaction between the spins of a localized (impurity spin) and itinerant conduction electrons of the host material. Its Hamiltonian reads

$$H = \sum_{\boldsymbol{k}\sigma} \epsilon_{\boldsymbol{k}} c^\dagger_{\boldsymbol{k}\sigma} c_{\boldsymbol{k}\sigma} + J \boldsymbol{S} \boldsymbol{s}_{i_0} \,, \tag{2.5}$$

where $\boldsymbol{S}$ denotes the impurity spin operator and $\boldsymbol{s}_{i_0}$ the conduction-electron spin at site i_0 with $\boldsymbol{s}_{i_0} = 1/2 \sum_{\sigma\sigma'} c^\dagger_{i_0\sigma} \boldsymbol{\sigma}_{\sigma\sigma'} c_{i_0\sigma'}$. The exchange coupling parameter is given by J and the Kondo effect is obtained for anti-ferromagnetic coupling i.e. $J > 0$. Using the above Hamiltonian (2.5), Kondo [1964] discovered that the resistivity contribution from the spin scattering to the local moment is temperature dependent and scales as $R \sim -\ln(T)$ which combined with the other contributions to the resistivity arising from phonon-interaction ($R \sim T^5$) and a temperature-independent term coming from the impurity potential explains the experimental studies by Sarachik et al. rigorously. As a result at low temperatures, the resistance of a metal increases logarithmically when the temperature is decreased. Kondo's observation solved the longstanding and fundamental question about

the resistance minimum in metals. Nevertheless, it makes also wrong predictions as the observed upturn in the resistance, occurring approximately at the Kondo temperature T_K, does not saturate and diverges in the limit $T \to 0$, indicating that Kondo's perturbation theory breaks down below the Kondo temperature T_K.

A loophole theoretical framework for understanding the nature of the strongly correlated many-particle quantum state below the Kondo temperature was introduced by Kenneth Wilson [1975] with a non-perturbative approach called Numerical Renormalization Group, which provides exact numerical results. A new picture emerges from Wilson's calculation, which describes the following crossover: At energies larger than $T_K \propto \exp(-1/J)$ the impurity is asymptotically free. In contrast at energies below the characteristic Kondo scale T_K the impurity is progressively screened into a singlet state by the itinerant electrons of the host metal with energies close to the Fermi energy ϵ_F. This screening process happens via virtual excitation which effectively flip the spin of the impurity and create at the same time a spin excitation in the Fermi sea. Many of such processes coming together lead to a new state, the Kondo resonance at the Fermi level, which relates to a singlet ground state between impurity and conduction electrons. The singlet state consists of the impurity and a screening cloud, which loosely speaking contains all itinerant conduction electrons which are entangled with the impurity spin. The length scale of the Kondo interaction, which describes the spatial extent of the Kondo screening cloud, is given by the Kondo length scale $\xi_K \sim v_F/T_K$, where v_F is the Fermi velocity. The scattering of the itinerant electrons with energies close to ϵ_F, which are relevant for the conductivity, at the Kondo cloud results in enhanced resistivity in metals at low temperatures when doped with magnetic impurities. After Wilson's numerical renormalization approach, also analytic solutions via Bethe ansatz were presented independently by Andrei [1980] and Wiegmann [1980a], which revealed the integrable nature of the Kondo model and thus its full many body spectrum can be exactly diagonalized. Later on Paul Wiegmann [1980b] proved that the original Anderson impurity model is also completely integrable.

Today, in theoretical physics the Kondo and the Anderson impurity models are often used as "impurity solvers" for the dynamical mean-field approach to the physics of strongly correlated materials in equilibrium [Georges et al., 1996] as well as in non-equilibrium [Aoki et al., 2014]. Furthermore, the Kondo model is considered as a paradigmatic system to study the real-time dynamics of a spin coupled to a conduction electron systems, which is experimentally accessible by spin-sensitive scanning probe methods, such as spin-polarized scanning-tunneling microscopy (SP-STM) [Loth et al., 2010; Morgenstern, 2010; Nunes and Freeman, 1993; Wiesendanger, 2009; Yan et al., 2015]. The STM method allows for accurate spatial manipulation and resolution of atomic-scale spin structures and the Kondo resonance can be measured via the current-versus-voltage characteristic. Moreover the detection of spin-dependent exchange and correlation forces, such as the Ruderman-Kittel-Kasuya-Yosida (RKKY) indirect magnetic exchange inter-

action [Kasuya, 1956; Ruderman and Kittel, 1954; Yosida, 1957] allows for the study of the competition between Kondo screening and magnetic ordering in multi-impurity systems. A minimal realization where this competition already appears is given by the two-impurity Kondo problem as studied by Jones et al. [1988]. The RKKY coupling is an indirect inter-impurity magnetic interaction: A magnetic impurity couples to the conduction electrons locally and leads to the modulation of the spin density of the conduction electron system, known as Friedel oscillation, which affects another impurity placed at a certain distance. This indirect magnetic interaction between the two localized impurity spins $\boldsymbol{S}_i$ and $\boldsymbol{S}_j$ mediated via an oscillatory spin polarization of the conduction band can be derived formally in second order perturbation theory [Nolting and Ramakanth, 2009] and results in the effective Hamiltonian:

$$H_{\mathrm{RKKY}} = -J_{ij}^{\mathrm{RKKY}} \boldsymbol{S}_i \cdot \boldsymbol{S}_j \,, \tag{2.6}$$

where the J^{RKKY} is essentially the non-local static spin-susceptibility of the conduction electrons $\chi_{i,j}$ at $J = 0$ and can be expressed as

$$J_{ij}^{\mathrm{RKKY}} = J^2 \chi_{ij} \propto J^2 \rho \frac{\cos(k_F r)}{|i-j|^d} \,, \tag{2.7}$$

with k_F being the absolute value of the Fermi wave vector. d is the dimension of the substrate and ρ denotes the conduction electron density of state. Doniach [1977] provided a qualitative understanding of the competition between Kondo screening and magnetic ordering via RKKY interaction by comparing the binding energy of the Kondo singlet $T_K \sim e^{-1/J}$ with that of the antiferromagnetic state $E_{\mathrm{RKKY}} \sim J^2$, resulting in the famous Doniach phase diagram: In the weak coupling limit below a certain critical value $J < J_D$, where $E_{\mathrm{RKKY}} \gg T_K$, the RKKY interaction dominates over the Kondo effect leading to magnetic ordering. In contrast if J is increased past a critical value J_D where ultimately $T_K \gg E_{\mathrm{RKKY}}$, the Kondo singlet binding dominates. The validity of the above arguments emerging from a mean-field calculation of a simplified one-dimensional "Kondo necklace" model was later confirmed via the renormalization group method for a Kondo-lattice model Hamiltonian by Jullien et al. [1977] showing that the transition between the Kondo and the RKKY regimes is a continuous quantum phase transition.

2.3 Nonequilibrium many-body theory

In this section we define the nonequilibrium problem for correlated many-body electrons in condensed matter systems, which for a typical experiment consists of two challenging tasks: Firstly, one has to describe the systems initial state in equilibrium, which is often achieved by deploying Green's-function approaches in the case of strongly correlated electron systems. To this end, the Matsubara [1955] Green's function and diagrammatic perturbation theory based on Wick's theorem provide a very convenient approach to describe the physics in solid state systems. Secondly, a description of the system's time evolution far from equilibrium due to a time-dependent and possibly strong perturbation is required. Here, an extension of the equilibrium Green's function based techniques to the nonequilibrium circumstance is a very promising approach. Originally nonequilibrium Green's function methods were developed by Baym and Kadanoff [1961a], Keldysh [1965] and others, assuming that the initial state of the system under consideration is not correlated, which is appropriate describing, e.g. scattering processes in high-energy physics. However, this requirement is a considerable limitation for condensed matter applications, as the initial state at $t_0 = 0$ in solid state systems is in general strongly correlated. Consequently, one needs a unified Green's function approach, which describes initial correlations and the subsequent time evolution by means of the same technique. A unified theory which combines Keldysh and Matsubara Green's functions, for a general initial state, was introduced finally by Danielewicz [1984] and later by Wagner [1991].

Before introducing the contour Green's function, we would like to define the nonequilibrium problem we are dealing with in this work: we study closed systems as well as open systems, such as effective classical spin dynamics, where the electron degrees of freedom are integrated out altogether. However, for this section we assume a closed quantum system which is entirely characterized via a time-dependent Hamiltonian $H(t)$. The second issue concerns the initialization of the dynamics, which can be achieved in general by changing the systems parameters slowly or quickly. In this work, we exclusively deal with local parameter quenches (a sudden change of the corresponding parameters), which include interaction or external field parameter quenches. As a result, all timescales are due to the intrinsic energy scales of the underlying model. However, the subsequent (quantum) dynamics can enforce new time scales and especially a separation of time scales (see Sec. 5.3)

In this setup, the equilibrium state of a typical experiment of a correlated many-particle system is characterized by a mixed state at a temperature T and chemical potential μ given by the grand-canonical statistical operator of the Hamiltonian $\mathcal{B}(t_0)$ at time $t = t_0$:

$$\rho(t_0) = \frac{e^{-(\beta\mathcal{B})}}{tr(e^{(-\beta\mathcal{B})})}, \tag{2.8}$$

with an many-body operator $\mathcal{B}(t_0) = B(t_0) - \mu N$. The inverse temperature of the initial state is given by β and N denotes the total particle number operator. Considering the zero

temperature limit $\beta \to \infty$, the density matrix reduces to a pure state $\rho = |\Psi\rangle\langle\Psi|$. Here, $|\psi\rangle$ is in general the (interacting) N-particle ground state of the Hamiltonian $B(t_0) = B_0(t_0) + B'(t_0)$, where B_0 is quadratic in the field operators and B' denotes the more complicated interacting part.

At times t larger than t_0 a perturbation described by a Hamiltonian $H(t) = H_0(t) + H'(t)$ fulfilling the condition $[H(t), B]_- \neq 0$, is applied to the system's initial state, which drives the system out of the initial equilibrium state and thereby initializes the nonequilibrium dynamic. Both Hamiltonians B and $H(t)$ are given in the second quantized form as introduced in Eq. (2.1). The explicit time-dependence in $H(t)$ arises from the interaction parameter, but also an additional external bilinear time-dependent magnetic field can be included in the non-interaction part given by H_0.

The central issue in nonequilibrium physics is how to calculate average values of observable quantities $\langle \mathcal{O}_{\mathcal{H}}(t)\rangle_0$ at times $t > t_0$, where operators $\mathcal{O}_{\mathcal{H}}(t)$ are given in the Heisenberg picture with respect to the Hamiltonian $\mathcal{H}(t) = H(t) - \mu N$. The time dependence of $\mathcal{O}_{\mathcal{H}}(t)$ is determined by the Heisenberg equation of motion:

$$i\frac{d}{dt}\mathcal{O}_{\mathcal{H}}(t) = [\mathcal{O}_{\mathcal{H}}(t), \mathcal{H}(t)] + i\frac{\partial}{\partial t}\mathcal{O}_{\mathcal{H}}(t) \ , \tag{2.9}$$

with the initial condition $\mathcal{O}_{\mathcal{H}}(t_0) = \mathcal{O}(t_0)$ which fixes the reference time at which Schrödinger and Heisenberg pictures coincide. The Heisenberg equation of motion (2.9) may be formally integrated as

$$\mathcal{O}_{\mathcal{H}}(t) = \mathcal{U}_{\mathcal{K}}(t_0, t)\mathcal{O}(t)\mathcal{U}_{\mathcal{K}}(t_0, t) \ , \tag{2.10}$$

where $\mathcal{U}_{\mathcal{K}}$ is the unitary time evolution operator obeying the Heisenberg equation with respect to the Hamiltonian $\mathcal{H}(t)$ with the formal solution:

$$\mathcal{U}_{\mathcal{K}}(t, t_0) = \begin{cases} \mathcal{T}_{\mathcal{K}} e^{-i\int_{t_0}^{t} dt'\, \mathcal{H}(t')} & \text{for} \quad t > t_0 \\ \overline{\mathcal{T}}_{\mathcal{K}} e^{i\int_{t_0}^{t} dt'\, \mathcal{H}(t')} & \text{for} \quad t < t_0 \end{cases} , \tag{2.11}$$

where $\mathcal{T}_{\mathcal{K}}$ ($\overline{\mathcal{T}}_{\mathcal{K}}$) is the chronological (anti-chronological) time-ordering operator, which implies $\mathcal{T}_{\mathcal{K}}(H(t_0)H(t)) = \theta(t_0 - t)H(t_0)H(t) + \theta(t - t_0)H(t)H(t_0)$ and $\overline{\mathcal{T}}_{\mathcal{K}}(H(t_0)H(t))$ $= \theta(t - t_0)H(t_0)H(t) + \theta(t_0 - t)H(t)H(t_0)$ and $\Theta(t)$ denotes the Heaviside step function.

Considering again the initial state, in analogy to Matsubara Green's functions the grand canonical statistical operator in Eq. (2.8) can be formally rewritten as a time evolution operator in imaginary time on the Matsubara branch:

$$e^{-(\beta\mathcal{B})} = e^{-i\int_0^{\beta} d\tau\, \mathcal{B}} = \mathcal{T}_{\mathcal{M}} e^{-i\int_{t_0}^{t_0 - i\beta} dz\, \mathcal{B}} = \mathcal{U}_{\mathcal{M}}(t_0 - i\beta, t_0) \tag{2.12}$$

with $z = t_0 - i\tau$ and $0 \leq \tau \leq \beta$. The chronological (anti-chronological) time-ordering operator on the Matsubara branch is denoted by $\mathcal{T}_{\mathcal{M}}$ ($\overline{\mathcal{T}}_{\mathcal{M}}$) and assuming $t_0 - i\beta$ to be

'later' in time than t_0, the time-dependent expectation value of the observable $\mathcal{O}(t)$ for a system in an initial state ρ can be formulated as:

$$\begin{aligned}\langle\mathcal{O}(t)\rangle &= tr[\rho(t_0)\mathcal{O}_{\mathcal{H}}(t)] \\ &= \frac{tr[\mathcal{U}_{\mathcal{M}}(t_0-i\beta,t_0)\,\mathcal{U}_{\mathcal{K}}(t_0,t)\,\mathcal{O}(t)\,\mathcal{U}_{\mathcal{K}}(t,t_0)]}{tr[\mathcal{U}_{\mathcal{M}}(t_0-i\beta,t_0)]} \\ &= \frac{tr[\mathcal{T}_{\mathcal{C}}\,\exp(-i\int_{\mathcal{C}}dt'\,\mathcal{K}(t'))\mathcal{O}(t)]}{tr[\mathcal{T}_{\mathcal{C}}\,\exp(-i\int_{\mathcal{C}}dt'\,\mathcal{K}(t'))]}\,,\end{aligned} \tag{2.13}$$

where the time integration is carried out on the Keldysh-Matsubara contour $\mathcal{C}$, which extends along the upper and lower Keldysh branch (real time axis) from $t'=t_0$ to $t'=\infty$, subsequently back to $t'=t_0$ and finally from $t'=t_0$ to $t'=t_0-i\beta$ along the Matsubara branch (imaginary time axis). The contour ordering operator $\mathcal{T}_{\mathcal{C}}$ merges the ordering operators $\mathcal{T}_{\mathcal{K}}$,$\overline{\mathcal{T}}_{\mathcal{K}}$ and $\mathcal{T}_{\mathcal{M}}$ and operates on the Keldysh-Matsubara contour $\mathcal{C}$ after expanding the exponential as follows: $\mathcal{T}_{\mathcal{C}}\mathcal{K}(t)\mathcal{K}(t')=\theta_{\mathcal{C}}(t,t')\mathcal{K}(t)\mathcal{K}(t')-\theta_{\mathcal{C}}(t,t')\mathcal{K}(t')\mathcal{K}(t)$, where the Heaviside function $\theta_{\mathcal{C}}(t,t')=1$ on the contour $\mathcal{C}$ if t is later on $\mathcal{C}$ than t' and otherwise zero. Finally, $\mathcal{K}(t)=\mathcal{K}_0(t)+\mathcal{K}'(t)$ replaces $\mathcal{H}(t)$ on the Keldysh branch $\mathcal{C}_{\mathcal{K}}$ and $\mathcal{B}$ on the Matsubara branch $\mathcal{C}_{\mathcal{M}}$. Apart from that, $\mathcal{T}_{\mathcal{C}}$ also acts on $\mathcal{O}(t)$, where the time argument of $\mathcal{O}(t)$ is the time at which the observable is located and evaluated on the contour $\mathcal{C}$. The integration along the Keldysh branch in the enumerator can be limited to $t'<t$, as the results of integrating along the upper and lower Keldysh branches cancel out each other within the interval $t<t'<\infty$. For the denominator, only the Matsubara branch contributes to the integration, resulting in $tr[\exp(-\beta\mathcal{B})]$.

2.3.1 Nonequilibrium Green's function

So far we have considered expectation values of single operators with single time arguments $\langle\mathcal{O}(t)\rangle$. In this section, we extend this to time-dependent correlation function of observables with different time arguments, e.g. $\langle\mathcal{O}_1(t)\mathcal{O}_2(t')\rangle$, where in general a single time-ordering operator is not sufficient and an extra ordering operator has to be introduced [Wagner, 1991]. As a consequence standard perturbation theory is not applicable, as Wick's theorem requires a single time-ordering principle. A convenient way to resolve this problem, is to focus on the contour-ordered Green's function:

$$iG_{\alpha,\alpha'}(t,t')=\langle\mathcal{T}_{\mathcal{C}}c_{\mathcal{K},\alpha}(t)c^{\dagger}_{\mathcal{K},\alpha}(t')\rangle\,, \tag{2.14}$$

which according to Wagner [1991] and the notation being inline with Balzer and Potthoff [2011] can be formulated as follows:

$$iG_{\alpha,\alpha'}(t,t')=\frac{\langle\mathcal{T}_{\mathcal{C}}e^{-i\int_{\mathcal{C}}d\tilde{t}\mathcal{K}'_{\mathcal{K}_0}(\tilde{t})}c_{\mathcal{K}_0,\alpha}(t)c^{\dagger}_{\mathcal{K}_0,\alpha}(t')\rangle_{(0)}}{\langle\mathcal{T}_{\mathcal{C}}e^{-i\int_{\mathcal{C}}d\tilde{t}\mathcal{K}'_{\mathcal{K}_0}(\tilde{t})}\rangle_{(0)}}\,. \tag{2.15}$$

In expression (2.15), all operators are given in the Dirac picture, thus evolving in time according to $\mathcal{K}_0$ only. The expectation value $\langle \cdots \rangle_{(0)} \equiv tr(\rho_0 \cdots)$ is defined with respect to the 'free' density operator $\rho_0 = e^{-\beta \mathcal{B}_0}/Z_0$ only, which is a fundamental requirement for applying Wick's theorem and standard perturbation theory. The expression (2.15) is valid for all times t and t' on the contour $\mathcal{C}$. However, if the Hamiltonian $\mathcal{K}$ is entirely time-independent, the Keldysh-Matsubara contour $\mathcal{C}$ reduces to the Matsubara branch $\mathcal{M}$ and thereby the contour Green's function reduces to the Matsubara Green's function $G(t,t') = iG^{\mathcal{M}}(\tau - \tau')$. The most important advantage is that time-dependent expectation values of any one-particle observable quantity $\mathcal{O}(t) = -i \sum_{\alpha\beta} \mathcal{O}_{\alpha\beta}(t) c^\dagger_\alpha c_\beta$ are directly connected to the contour-ordered Green's function in the equal time-limit:

$$\langle \mathcal{O} \rangle(t) = -i \sum_{\alpha,\beta} \mathcal{O}_{\alpha,\beta}(t) G_{\beta\alpha}(t, t^+) \,, \tag{2.16}$$

where t^+ is infinitesimally later than t on the contour $\mathcal{C}$. But also a few two-particle observables, such as the interaction energy and the double occupancy can be obtained from the one-particle Green's function with the aid of the self-energy, which we will introduce in the subsequent section.

2.3.2 Equation of motion and perturbation theory

The aim of this section is to derive a time-dependent equation for the reduced one-particle density matrix. To this end we introduce the equation of motion for the contour Green's function and discuss the Hartree-Fock approximation. The Green's function as expressed in Eq. (2.15) meets all prerequisites for applying Wick's theorem, a general proof of which was given by Danielewicz [1984]. We briefly summarize the requirements of Wick's theorem: (i) A single time-ordering principle is ensured. (ii) The expectation values are taken with respect to some one-particle density matrix ρ_0. (iii) Finally, all operators are given in the Dirac picture.

Applying n-th order perturbation theory directly to the Green's function may result in approximations that do not guarantee basic conservation laws of the underlying Hamiltonian. In order to avoid this problem, it is convenient to set up perturbation theory for the self-energy, which we introduce in the context of the Kadanoff and Baym [1962] equation.

The equation of motion for contour Green's function is refereed to as the Kadanoff and Baym [1962] equation (KB) and can be obtained by the differentiation of Eq. (2.14) or deduced from the Heisenberg equation (2.9) for the construction operators.

$$\begin{aligned} i\frac{\partial}{\partial t} G_{\alpha\beta}(t,t') &= \left\langle \mathcal{T}_{\mathcal{C}} \Big(\frac{\partial}{\partial t} c_{\mathcal{K},\alpha}(t) \Big) c^\dagger_{\mathcal{K},\alpha}(t') \right\rangle + \delta_{\mathcal{C}}(t,t') \delta_{\alpha,\beta} \\ &= -i \Big\langle \mathcal{T}_{\mathcal{C}} \Big([c_{\mathcal{K},\alpha}(t), \mathcal{K}(t)]_- \Big) c^\dagger_{\mathcal{K},\alpha}(t') \Big\rangle + \delta_{\mathcal{C}}(t,t') \delta_{\alpha,\beta} \,, \end{aligned} \tag{2.17}$$

where $\int_{\mathcal{C}} dt' \delta_{\mathcal{C}}(t,t') f(t') = f(t)$ defines the delta-function on the contour for an arbitrary contour function $f(t)$. As mentioned earlier, $\mathcal{K} = \mathcal{K}_0(t) + \mathcal{K}'(t)$ consists of a quadratic term $\mathcal{K}_0(t)$ and a quartic term $\mathcal{K}'(t)$ describing the interaction. Whereas the former only results in a one particle Green's function again the latter term generates higher-order Green's function in Eq. (2.17). An analogous equation of motion for the higher-order Green's function leads to an infinite hierarchy of coupled equations for the Green's function, which is known as Martin-Schwinger-hierarchy. Formally, the Martin-Schwinger-hierarchy is decoupled via the self-energy Σ, defined as:

$$\sum_{\gamma} \int_{\mathcal{C}} dt'' \, \Sigma_{\alpha\gamma}(t,t'') G_{\gamma\beta}(t'',t') = -i \Big\langle \mathcal{T}_{\mathcal{C}} \Big([c_{\mathcal{K},\alpha}(t), \mathcal{K}'(t)]_- \Big) c^{\dagger}_{\mathcal{K},\alpha}(t') \Big\rangle \, . \tag{2.18}$$

The self-energy is a functional of the one-particle Green's function and includes all interaction effects. By inserting the expression (2.18) in Eq. (2.17), we obtain:

$$\begin{aligned} i \frac{\partial}{\partial t} G_{\alpha\beta}(t,t') &= \sum_{\gamma} T^{(\mathcal{K}_0)}_{\alpha\gamma}(t) G_{\gamma\beta}(t,t') \\ &\quad + \sum_{\gamma} \int_{\mathcal{C}} dt'' \, \Sigma_{\alpha\gamma}(t,t'') G_{\gamma\beta}(t'',t') + \delta_{\alpha,\beta} \, \delta_{\mathcal{C}}(t,t') \, , \end{aligned} \tag{2.19}$$

where $T^{(\mathcal{K}_0)}$ denotes the hopping matrix of the one-particle contribution $\mathcal{K}_0$. Applying diagrammatic perturbation theory to the self-energy Σ, which is defined as a sum over all distinct proper self-energy diagrams, provides a systematic expansion of the contour Green's function. Here, essentially the same diagram techniques as for Matsubara Green's function, see e.g. Negele and Orland [1998], can be applied to the non-equilibrium situation. The first order contribution to the self-energy Σ is called Hartree-Fock and contains two diagrams, which are local in time $-i\Sigma^{\mathrm{HF}}_{\alpha\beta}(t)\delta(t-t')$ and replace an interacting many-body problem by an effective one-particle problem. Note that on the Matsubara branch the Hartree-Fock term is given by a static field $i\Sigma^{\mathrm{HF}}_{\alpha\beta}\delta(\tau)$ and must be calculated in a self-consistent way. The Hartree-Fock approximation treats interactions in a many-body system at a mean-field level and neglects all correlation effects, which, however, are included in diagrams of higher order. Hence, it is convenient to subdivide the self-energy Σ into Hartree-Fock $\Sigma^{\mathrm{HF}}_{\alpha\beta}(t)$ and all higher order self-energy expressions, referred to as $\Sigma^{\mathrm{CORR}}_{\alpha\beta}(t)$. To this end, Eq. (2.19) can be recast as

$$\begin{aligned} i \frac{\partial}{\partial t} G_{\alpha\beta}(t,t') &= \sum_{\gamma} (T^{(\mathcal{K}_0)}_{\alpha\gamma}(t) + \Sigma^{\mathrm{HF}}_{\alpha\gamma}(t)) G_{\gamma\beta}(t,t') \\ &\quad + \sum_{\gamma} \int_{\mathcal{C}} dt'' \, \Sigma^{\mathrm{CORR}}_{\alpha\gamma}(t,t'') G_{\gamma\beta}(t'',t') + \delta_{\alpha,\beta} \, \delta_{\mathcal{C}}(t,t') \, . \end{aligned} \tag{2.20}$$

However, it is advantageous with respect to computational cost to neglect all higher order self-energy contributions Σ^{CORR} altogether and consider the Hartree-Fock contribution

Σ^{HF} only, which is time-local and therefore the corresponding Green's function is much easier accessible in equilibrium as well as in nonequilibrium case. Moreover, from a physical perspective the Hartree-Fock approach is considered as a reasonable approximation, e.g., in the case of small interactions.

Neglecting the self-energy contribution Σ^{corr}, subtracting from Eq. (2.20) the complex conjugate of Eq. (2.20) and considering only time-diagonal components of the Green's function, which is the reduced one-particle density-matrix $\rho_{\alpha\beta}(t) \equiv G_{\alpha\beta}(t, t^+)$, leads to a time-dependent mean-field equation:

$$i\frac{d}{dt}\varrho_{\alpha\beta}(t) = \left[\mathcal{T}^{(\mathcal{K})}(\varrho(t)), \varrho(t)\right]_{-,\alpha\beta} \ , \tag{2.21}$$

where, $\mathcal{T}^{(\mathcal{K})}(t)$ is an effective hopping matrix, which is replaced by $\mathcal{T}^{(\mathcal{B})}_{\alpha\gamma} = T^{\mathcal{B}}_{\alpha\gamma} + \Sigma^{\text{HF}}_{\alpha\gamma}$ at time $t = t_0$ and by $\mathcal{T}^{(\mathcal{H})}_{\alpha\gamma}(t) = T^{\mathcal{H}}_{\alpha\gamma} + \Sigma^{\text{HF}}_{\alpha\gamma}(t)$ at times $t > t_0$. Here, Σ^{HF} and $\Sigma^{\text{HF}}(t)$ are the static and time-dependent self-energy contributions to the interaction part of the underlying Hamiltonian $\mathcal{B}$ and $\mathcal{H}(t)$, respectively.

The time-dependent mean-field equation provides two important advantages: (i) The equilibrium and nonequilibrium self-energy contributions $\Sigma^{\text{HF}}(t)$ are functional derivatives of a truncated Luttinger-Ward function $\Phi(G)$ consisting of Hartree and Fock diagrams. Consequently, the Hartree-Fock mean-field approach is a conserving approximation in the sense of Baym and Kadanoff [1961b], i.e. macroscopic conservation laws stemming from the continuous symmetries of the underlying Hamiltonian are respected. (ii) The equation of motion (2.21) is a system of non-linear differential equation of first order and can be solved efficiently by standard Runge-Kutta methods, see e.g. Verner [2010], thus long-time propagation of quite large systems is accessible.

In the following chapter, using the nonequilibrium perturbation theory, we calculate the Hartree-Fock self-energy contributions to the multi-impurity Kondo model and derive a time-dependent hybridization mean-field theory for quantum-impurity models.

3 Static and time-dependent mean-field approach

Our basic concern in this chapter is to derive a time-dependent mean-field theory for quantum-impurity problems, which we refer to as the "time-dependent hybridization mean-field" approach (tHybMF). As a limiting case, for a time-independent Hamiltonian, the previously known static hybridization mean-field approach [Lacroix and Cyrot, 1979] is recovered. To this end, we use the aforementioned equation of motion for the reduced one-particle density matrix (2.21) derived from the non-equilibrium Green's function perturbation method, which requires the Hartree-Fock self-energy contribution of the underlying problem. Therefore we need to determine the Hartree-Fock self-energy contribution of the quantum-impurity model.

However, before proceeding, we introduce the multi-impurity Kondo Hamiltonian and specify the numerical setup as used in this study. Even though we study exclusively single-impurity Kondo model numerically later on, for the sake of generality, within this chapter a multi-impurity Kondo model on a lattice of finite size is considered:

$$\mathcal{H} = -\sum_{\langle i,j\rangle,\sigma} T_{ij} c^\dagger_{i\sigma} c_{j\sigma} + \sum_{m=1}^{M} \boldsymbol{s}_{i_m} \cdot \underline{\boldsymbol{J}} \cdot \boldsymbol{S}_m - \sum_{m=1}^{M} \boldsymbol{B}_m \boldsymbol{S}_m \,, \tag{3.1}$$

where the first term corresponds to the uncorrelated system of N itinerant conduction-electrons hoping with amplitude $T_{ij} = T = 1$ between non-degenerate orbitals on nearest-neighboring sites i, j of a lattice. Here, $c^\dagger_{i\sigma}$ ($c_{i\sigma}$) creates (annihilates) an electron at site $i = 1, ..., L$ with spin projection $\sigma = \uparrow, \downarrow$, and $\boldsymbol{s}_i = \frac{1}{2}\sum_{\sigma\sigma'} c^\dagger_{i\sigma} \boldsymbol{\sigma}_{\sigma\sigma'} c_{i\sigma'}$ is the local conduction-electron spin at site i, where $\boldsymbol{\sigma} = \sum_\alpha \sigma^\alpha \boldsymbol{e}_\alpha$ is the vector of Pauli matrices and $\alpha = x, y, z$. The second term consists of M spins $\boldsymbol{S}_m$ with spin-quantum numbers $1/2$, which are coupled via an antiferromagnetic exchange to the local spins $\boldsymbol{s}_i$ of the conduction electron system. Impurity spins couple to the local conduction-electron spins at the sites i_m where $m = 1, ..., M$. The tensor of coupling strengths $\underline{\boldsymbol{J}}$ is assumed to be diagonal $J_{\alpha\beta} = \delta_{\alpha\beta} J_\alpha$ with $J_x = J_y = J_\perp \geq 0$ and $J_z = J_\parallel \geq 0$. Finally, a local magnetic field $\boldsymbol{B}_m$ coupling to the m-th impurity spin is introduced to prepare the system's initial magnetic state.

For the sake of simplicity and in order to benchmark the mean field results with the time-dependent density matrix renormalization group (tDMRG) calculations, we investigate one-dimensional systems with open boundaries at zero temperature only. If not stated otherwise, systems are studied at half-filling.

In order to take advantage of the diagrammatic perturbation expansion, we express the Hamiltonian Eq. (3.1) in the "fermionized" form, as the Wick theorem can only be applied to fermions. By introducing Fermi operators $f_m = (f_{m\uparrow}, f_{m\downarrow})^{\mathrm{T}}$, $f_m^\dagger = (f_{m\uparrow}^\dagger, f_{m\downarrow}^\dagger)$ on the impurity sites, the impurity spins can be represented as $\boldsymbol{S}_m = \frac{1}{2} f_m^\dagger \boldsymbol{\sigma} f_m$. However, the constraint $f_m^\dagger f_m = \sum_\sigma f_{m\sigma}^\dagger f_{m\sigma} \equiv 1$ must be complied to suppress f-charge fluctuations and thereby ensure the conservation of the total particle number at each site m. The spinor notation is also used for the conduction-electron system, $c_i = (c_{i\uparrow}, c_{i\downarrow})^{\mathrm{T}}$. This results in

$$\mathcal{H} = -\sum_{\langle i,j\rangle,\sigma} T_{ij} c_{i\sigma}^\dagger c_{j\sigma} - \frac{1}{2}\sum_{m=1}^{M} \boldsymbol{B}_m f_m^\dagger \boldsymbol{\sigma} f_m + \frac{1}{4}\sum_{m=1}^{M} c_{i_m}^\dagger \boldsymbol{\sigma} c_{i_m} \cdot \underline{\boldsymbol{J}} \cdot f_m^\dagger \boldsymbol{\sigma} f_m \,. \tag{3.2}$$

The Hamiltonian possesses global U(1) and SU(2) gauge invariance given by $c_{i\sigma} \mapsto e^{-i\varphi} c_{i\sigma}$, $f_{m\sigma} \mapsto e^{-i\varphi} f_{m\sigma}$ and $c_i \mapsto e^{-i\boldsymbol{\varphi}\boldsymbol{\sigma}/2} c_i$, $f_m \mapsto e^{-i\boldsymbol{\varphi}\boldsymbol{\sigma}/2} f_m$, respectively. This ensures conservation of the total particle number and the total spin. In addition, there is a local U(1) gauge symmetry, $f_{m\sigma} \mapsto e^{-i\varphi_m} f_{m\sigma}$ for each m, characterizing the conservation of the f-charge at each impurity site m, consistent with the aforementioned constraint $f_m^\dagger f_m \equiv 1$.

3.1 Time-dependent hybridization mean-field

As mentioned earlier, in this study we assume that the Hamiltonian (3.1) determines the system's time evolution and the Hamiltonian $\mathcal{B}$ characterizes the system's initial state given by the statistical operator $\varrho_{\mathrm{stat}}(t=0) = e^{-\beta\mathcal{B}}/\mathrm{tr}\, e^{-\beta\mathcal{B}}$. Here, $\mathcal{B}$ is the Hamiltonian (3.2) and just contains different model parameters [1] $\boldsymbol{J}_{ini}$ and $\boldsymbol{B}_{ini}$.

As discussed previously in chapter 2.3, the diagrammatic perturbation theory is a convenient method to treat interacting many-particle systems and thereby construct a conserving time-dependent mean-field approach to compute the thermal and the non-equilibrium self-energy of the c and the f electrons as the functional derivative of a truncated Luttinger-Ward functional consisting of the Hartree and of the Fock diagram. In this context the central object of interest is the reduced one-particle density matrix

$$\varrho(t) = \begin{pmatrix} \rho^{(\mathrm{cc})}(t) & \rho^{(\mathrm{cf})}(t) \\ \rho^{(\mathrm{fc})}(t) & \rho^{(\mathrm{ff})}(t) \end{pmatrix} , \tag{3.3}$$

which consists of the conduction-electron and the f-electron one-particle density matrix with elements

$$\rho^{(\mathrm{cc})}_{ii',\sigma\sigma'}(t) = \langle c_{i'\sigma'}^\dagger c_{i\sigma}\rangle_t \,, \quad \rho^{(\mathrm{ff})}_{mm',\tau\tau'}(t) = \langle f_{m'\tau'}^\dagger f_{m\tau}\rangle_t \tag{3.4}$$

[1] As we do not consider geometrical quenches, we set $T^{\mathcal{H}} = T^{\mathcal{B}} \equiv T$

and of the hybridizations

$$\rho^{(\mathrm{cf})}_{im,\sigma\tau}(t) = \langle f^\dagger_{m\tau} c_{i\sigma} \rangle_t = \rho^{(\mathrm{fc})}_{mi,\tau\sigma}(t)^* \,. \tag{3.5}$$

Within the framework of the Hartree-Fock approximation, the one-particle density matrix can be evaluated by solving an effective problem where the interaction term $H'(t)$ of the Hamiltonian (3.2) is approximated by an effective one-particle mean-field Hamiltonian

$$\begin{aligned} H'(t) \;&\approx\; \sum_m c^\dagger_{i_m} \Sigma^{(\mathrm{cc})}_m(t) c_{i_m} + \sum_m f^\dagger_m \Sigma^{(\mathrm{ff})}_m(t) f_m \\ &+\; \sum_m f^\dagger_m \Sigma^{(\mathrm{fc})}_m(t) c_{i_m} + \sum_m c^\dagger_{i_m} \Sigma^{(\mathrm{cf})}_m(t) f_m \,. \end{aligned} \tag{3.6}$$

The Hartree-Fock self-energy $\Sigma_m(t)$ arises from the decoupling scheme $f^\dagger f c^\dagger c \mapsto \langle f^\dagger f \rangle c^\dagger c + \langle c^\dagger c \rangle f^\dagger f + \langle f^\dagger c \rangle f c^\dagger + \langle f c^\dagger \rangle f^\dagger c$ (Wick's theorem) as

$$\Sigma_m(t) = \begin{pmatrix} \Sigma^{(\mathrm{cc})}_m(t) & \Sigma^{(\mathrm{cf})}_m(t) \\ \Sigma^{(\mathrm{fc})}_m(t) & \Sigma^{(\mathrm{ff})}_m(t) \end{pmatrix} \,, \tag{3.7}$$

where

$$\begin{aligned} \Sigma^{(\mathrm{cc})}_{m,\sigma\sigma'}(t) &= \frac{1}{2} \langle \boldsymbol{S}_m \rangle_t \cdot \underline{\boldsymbol{J}} \cdot \boldsymbol{\sigma}_{\sigma\sigma'} \,, \\ \Sigma^{(\mathrm{ff})}_{m,\sigma\sigma'}(t) &= \frac{1}{2} \langle \boldsymbol{s}_{i_m} \rangle_t \cdot \underline{\boldsymbol{J}} \cdot \boldsymbol{\sigma}_{\sigma\sigma'} \,, \\ \Sigma^{(\mathrm{cf})}_{m,\sigma\sigma'}(t) &= -\frac{1}{4} \sum_{\tau\tau'} \langle f^\dagger_{m\tau} c_{i_m\tau'} \rangle_t \, \boldsymbol{\sigma}_{\sigma\tau'} \cdot \underline{\boldsymbol{J}} \cdot \boldsymbol{\sigma}_{\tau\sigma'} \,, \\ \Sigma^{(\mathrm{fc})}_{m,\sigma\sigma'}(t) &= -\frac{1}{4} \sum_{\tau\tau'} \langle c^\dagger_{i_m\tau'} f_{m\tau} \rangle_t \, \boldsymbol{\sigma}_{\tau'\sigma'} \cdot \underline{\boldsymbol{J}} \cdot \boldsymbol{\sigma}_{\sigma\tau} \,. \end{aligned} \tag{3.8}$$

It is important to observe that the self-energy contributions $\Sigma_m(t)$ depend on the elements of the one-particle density matrix and thereby become time-dependent.

As mentioned before, the original interacting Hamiltonian (3.2) is invariant under a local $U(1)$ gauge symmetry, which implies the conservation of the impurity particle number at each site m consistent with the constraint $f^\dagger_m f_m \equiv 1$, and as demonstrated by Elitzur [1975], it is impossible to spontaneously break local symmetries. However, exceptions to the rule, such as infinite-dimensional systems and mean-field theories, were reported by Maślanka [1988]. Consequently, the hybridization mean-field spontaneously breaks local symmetries as well, e.g. the local $U(1)$ gauge symmetry. Hence, the f-charge at each site m is conserved only on average $\langle f^\dagger_m f_m \rangle = 1$, which can be ensured by introducing time-dependent local Lagrange parameters $\mu^{(\mathrm{f})}_m(t)$. With the effective hopping matrix $\mathcal{T}^{\mathcal{H}} = T + \Sigma^{\mathrm{HF}}$ defined as

$$\mathcal{T}^{\mathcal{H}}(t) = \begin{pmatrix} \mathcal{T}^{(\mathrm{cc})}(t) & \mathcal{T}^{(\mathrm{cf})}(t) \\ \mathcal{T}^{(\mathrm{fc})}(t) & \mathcal{T}^{(\mathrm{ff})}(t) \end{pmatrix} \,, \tag{3.9}$$

the mean-field Hamiltonian reads

$$\begin{aligned}\mathcal{H}^{\text{MF}}(t) &= \sum_{ii'} c_i^\dagger \mathcal{T}_{ii'}^{(\text{cc})}(t) c_{i'} + \sum_{mm'} f_m^\dagger \mathcal{T}_{mm'}^{(\text{ff})}(t) f_{m'} \\ &+ \sum_{mi'} f_m^\dagger \mathcal{T}_{mi'}^{(\text{fc})}(t) c_{i'} + \sum_{im'} c_i^\dagger \mathcal{T}_{im'}^{(\text{cf})}(t) f_{m'} \,, \end{aligned} \tag{3.10}$$

where the matrix elements are given by:

$$\begin{aligned}\mathcal{T}_{ii'\sigma\sigma'}^{(\text{cc})}(t) &= -T_{ii'} + \sum_m \delta_{ii_m}\delta_{i'i_m}\Sigma_{m,\sigma\sigma'}^{(\text{cc})}(t) \,, \\ \mathcal{T}_{mm'\sigma\sigma'}^{(\text{ff})}(t) &= \delta_{mm'}\left(\Sigma_{m,\sigma\sigma'}^{(\text{ff})}(t) - \frac{1}{2}\boldsymbol{B}_m\boldsymbol{\sigma} - \mu_m^{(\text{f})}(t)\right) \,, \\ \mathcal{T}_{mi'\sigma\sigma'}^{(\text{fc})}(t) &= \delta_{i'i_m}\Sigma_{m,\sigma\sigma'}^{(\text{fc})}(t) \,, \\ \mathcal{T}_{im'\sigma\sigma'}^{(\text{cf})}(t) &= \delta_{ii_{m'}}\Sigma_{m',\sigma\sigma'}^{(\text{cf})}(t) \,. \end{aligned} \tag{3.11}$$

Using Eqs. (3.8), (3.10) and (3.11), we can then rewrite the mean-field Hamiltonian as

$$\begin{aligned}\mathcal{H}^{\text{MF}}(t) &= \sum_m \langle \boldsymbol{S}_m\rangle_t \,\underline{\boldsymbol{J}}\, \boldsymbol{s}_{i_m} + \sum_m \langle \boldsymbol{s}_{i_m}\rangle_t \,\underline{\boldsymbol{J}}\, \boldsymbol{S}_m \\ &- \sum_m \boldsymbol{B}_m\boldsymbol{S}_m - \sum_{\langle i,j\rangle,\sigma} T_{ij} c_{i\sigma}^\dagger c_{j\sigma} \\ &- \frac{1}{4}\sum_{m,\sigma\sigma'\tau\tau'} c_{i_m\sigma}^\dagger f_{m\sigma'} \langle f_{m\tau}^\dagger c_{i_m\tau'}\rangle_t \,\boldsymbol{\sigma}_{\sigma\tau'}\,\underline{\boldsymbol{J}}\,\boldsymbol{\sigma}_{\tau\sigma'} + \text{H.c.} \,. \end{aligned} \tag{3.12}$$

Next, we introduce charge and spin hybridization operators as follows:

$$K_m^{(0)} = \frac{1}{2}\sum_\sigma c_{i_m\sigma}^\dagger f_{m\sigma} \,, \quad \boldsymbol{K}_m = \frac{1}{2}\sum_{\sigma\sigma'} c_{i_m\sigma}^\dagger \boldsymbol{\sigma}_{\sigma\sigma'} f_{m\sigma'} \,. \tag{3.13}$$

By employing the identities

$$c_{i_m\sigma}^\dagger f_{m\sigma'} = K_m^{(0)}\delta_{\sigma\sigma'} + \boldsymbol{K}_m\boldsymbol{\sigma}_{\sigma\sigma'} \tag{3.14}$$

and

$$\boldsymbol{\sigma}_{\sigma\tau'}\cdot\underline{\boldsymbol{J}}\cdot\boldsymbol{\sigma}_{\tau\sigma'} = J_\parallel\delta_{\sigma\tau'}\delta_{\tau\sigma'}z_\sigma z_\tau + 2J_\perp\delta_{\sigma-\tau'}\delta_{\tau-\sigma'}\delta_{\sigma-\tau} \,, \tag{3.15}$$

with $z_\uparrow = +1$ and $z_\downarrow = -1$, in the isotropic case $J_\parallel = J_\perp$, the mean-field Hamiltonian

can be expressed in terms of the hybridization and spin operators:

$$\begin{aligned}\mathcal{H}^{\text{MF}}(t) \;=\; & \sum_m \langle \boldsymbol{S}_m \rangle_t \, \underline{\boldsymbol{J}} \, \boldsymbol{s}_{i_m} + \sum_m \langle \boldsymbol{s}_{i_m} \rangle_t \, \underline{\boldsymbol{J}} \, \boldsymbol{S}_m \\ & - \sum_m \boldsymbol{B}_m \boldsymbol{S}_m - \sum_{\langle i,j \rangle, \sigma} T_{ij} c^\dagger_{i\sigma} c_{j\sigma} \\ & - \frac{3}{2} \sum_m \left(J \langle K^{(0)\dagger}_m \rangle_t K^{(0)}_m + \text{H.c} \right) \\ & + \frac{1}{2} \sum_m \left(J \langle \boldsymbol{K}^\dagger_m \rangle_t \boldsymbol{K}_m + \text{H.c} \right) \; . \end{aligned} \tag{3.16}$$

Notice that the time dependence of the Hartree-Fock Hamiltonian arises as a result of the time dependence of the self-energy. Further properties of the Hamiltonian will be discussed in the subsequent sections.

But for now, returning to the system's dynamics, with the aid of the equation of motion of the one-particle density matrix (2.21) as derived in chapter 2.3.2 and the effective hopping matrix $\mathcal{T}^{\mathcal{H}}$ given in expressions (3.9) and (3.11), we obtain a time-dependent hybridization mean-field (tHybMF) equation:

$$i \frac{d}{dt} \varrho(t) = [\mathcal{T}^{\mathcal{H}}(\varrho(t)), \varrho(t)]_- \tag{3.17}$$

with the initial condition

$$\varrho(0) = \frac{1}{e^{\beta(\mathcal{T}^{\mathcal{B}})} + 1} \, , \tag{3.18}$$

where $\mathcal{T}^{\mathcal{B}}$ is the effective hopping matrix (3.11), but again with different model parameters $\underline{\boldsymbol{J}}_{\text{ini}}$ and $\boldsymbol{B}_{\text{ini}}$ stemming from the Hamiltonian $\mathcal{B}$ describing the system's initial thermal state. It must be emphasized that $\mathcal{T}^{\mathcal{B}}$ depends on the initial one-particle density matrix $\varrho(0)$ as can be seen from Eq. (3.11). Consequently, Eq. (3.18) presents a non-linear system of equations that must be solved self-consistently for $\varrho(0)$, which will be discussed in detail in the subsequent section concerning the static hybridization mean-field approach.

3.2 Static hybridization mean-field

In this section we present the static hybridization mean-field approach (HybMf), originally introduced by Lacroix and Cyrot [1979], generalizing a method of functional integration to the Kondo lattice first reported by Yoshimori and Sakurai [1970] for the single impurity case. Later on, it was reformulated as a large-N approximation by Coleman [1983] and Read et al. [1984] in an adaptation to particular impurity systems, see for e.g.,

Coqblin and Schrieffer [1969] (rare-earth compounds), where N is the degeneracy of the localized spins. However, magnetic interactions are included only at $1/N^2$ order and vanish in large-N limit. In contrast, the HybMF approach treats the Kondo effect and magnetic interactions on an equal footing and has been used to study the metamagnetic transition in heavy fermions by, e.g., Beach [2005] and Viola Kusminskiy et al. [2008]. Even the so-called Kondo box problem, systems with a discrete energy spectrum resulting in an energy-level spacing as a new energy scale which competes with the Kondo scale, has been studied within the HybMF approach as reported by Bedrich et al. [2010].

Here, we use the standard diagram perturbation techniques for the Matsubara Green's function, see, e.g., Negele and Orland [1998], to calculate the Hartree and Fock self-energy diagrams and replace an interacting many-body problem in Eq. (3.2) by an effective hybridization mean-field Hamiltonian:

$$\begin{aligned}\mathcal{B}^{\mathrm{MF}} \;=\; & \sum_m \langle \boldsymbol{S}_m \rangle \, \underline{\boldsymbol{J}}_{ini} \, \boldsymbol{s}_{i_m} + \sum_m \langle \boldsymbol{s}_{i_m} \rangle \, \underline{\boldsymbol{J}}_{ini} \, \boldsymbol{S}_m \\ & - \sum_m \boldsymbol{B}_{m,ini} \boldsymbol{S}_m - \sum_{ij,\sigma} (T_{ij} + \mu \delta_{ij}) c^\dagger_{i\sigma} c_{j\sigma} \\ & - \frac{3}{2} \sum_m \left(J_{ini} \langle K^{(0)\dagger}_m \rangle K^{(0)}_m + \mathrm{H.c} \right) \\ & + \frac{1}{2} \sum_m \left(J_{ini} \langle \boldsymbol{K}^\dagger_m \rangle \boldsymbol{K}_m + \mathrm{H.c} \right) \; . \end{aligned} \tag{3.19}$$

As mentioned previously, we assume that initially, the system is in a thermal state given by the statistical operator $\rho_{\mathrm{stat}}(0) = e^{-\beta \mathcal{B}^{\mathrm{MF}}} / \mathrm{tr}\, e^{-\beta \mathcal{B}^{\mathrm{MF}}}$ and characterized by the inverse temperature β and the chemical potential μ. However, here again the central object of interest remains the reduced one-particle density matrix as this is the initial condition for the time-dependent hybridization mean-field equation (3.17) and is given by:

$$\varrho(0) = \frac{1}{e^{\beta(\mathcal{T}^{\mathcal{B}})} + 1} \, , \tag{3.20}$$

where $\mathcal{T}^{\mathcal{B}}$ is the effective hopping matrix (see Eq. (3.9) and Eq. (3.11)), but again with different model parameters $\underline{\boldsymbol{J}}_{\mathrm{ini}}$ and $\boldsymbol{B}_{\mathrm{ini}}$ stemming from the Hamiltonian $\mathcal{B}$ describing the system's initial thermal state.

As already mentioned in the last section, $\mathcal{T}^{\mathcal{B}}$ depends on the initial one-particle density matrix $\varrho(0)$, as evident from Eq. (3.11). It is apparent that in general both the effective hopping $\mathcal{T}^{\mathcal{B}}$ and the reduced one-particle density matrix $\varrho(0)$ are not known a priori.
As a result, the non-linear system of equations (3.20) must be solved self-consistently for $\varrho(0)$, as detailed in Fig. 3.1. The numerical procedure is as follows: Starting from an initial guess for the hybridization functions $\langle K^{(0)}_m \rangle$ and $\langle \boldsymbol{K}_m \rangle$ and the impurity and conduction electron spins $\langle \boldsymbol{S}_m \rangle$ and $\langle \boldsymbol{s}_{i_m} \rangle$, which can be incorporated into the self-energy

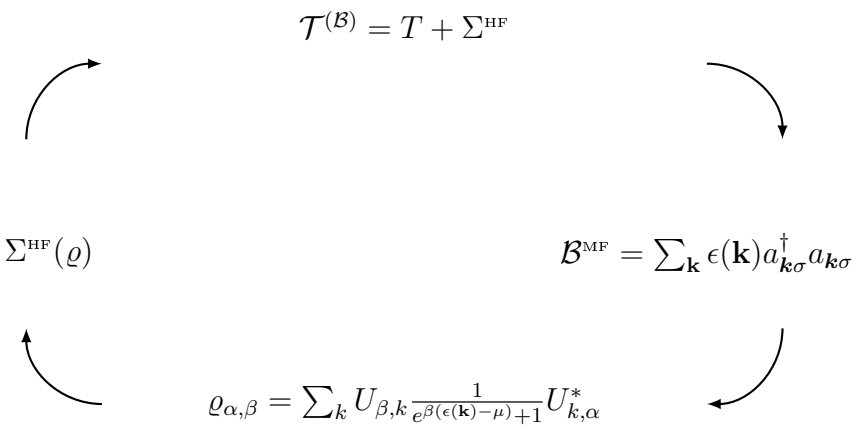

Figure 3.1: Hybridization mean-field self-consistency loop using the self-energy $\Sigma^{\text{HF}}(\varrho)$ as the adjustable quantity.

Σ_m in Eq. (3.8), the effective hopping matrix is obtained from Eq. (3.11). Notice that the self-energy in the initial state is the same as in Eq. (3.8), but time-independent and with different parameters $\underline{\boldsymbol{J}}_{\text{ini}}$ and $\boldsymbol{B}_{\text{ini}}$. Next, the effective hopping $\mathcal{T}^{\mathcal{B}}$ can be diagonalized $\mathcal{T}^{\mathcal{B}} = U\epsilon U^{\dagger}$ resulting in the diagonal correlation functions:

$$\langle a^{\dagger}_{\boldsymbol{k}\sigma} a_{\boldsymbol{k}\sigma} \rangle = \frac{1}{e^{\beta(\epsilon(\boldsymbol{k})-\mu)}+1} \,, \tag{3.21}$$

where the new operator $a_{\boldsymbol{k}\sigma}$ is a linear combination of the original operators $c_{\boldsymbol{k}\sigma}$ and $f_{\boldsymbol{k}\sigma}$. The diagonal correlation function (3.21) can be transformed back via the matrix U, resulting in the one-particle density matrix, which is simply a correlation function in real space.

$$\varrho_{\alpha,\beta} = \sum_k U_{\beta,k} \frac{1}{e^{\beta(\epsilon(\mathbf{k})-\mu)}+1} U^*_{k,\alpha} \,, \tag{3.22}$$

where the indices α and β label sites, spins and the location of the density matrix element $\rho_{ii',\sigma\sigma'}$ within the matrix ϱ in Eq. (3.3). Finally, the self-energy can be calculated from ϱ using Eq. (3.8). The self-consistency loop is iterated until the convergence measure $\delta = ||\mathcal{T}^{\mathcal{B}}_{old} - \mathcal{T}^{\mathcal{B}}_{new}||$ becomes smaller than a prescribed value. In the majority of cases the self-consistency loop converges after few iterations. However, in a few cases linear mixing is required to enforce convergence, e.g., in order to stabilize a self-consistent solution with finite $\langle K^{(0)}_m \rangle \neq 0$ and $\langle \boldsymbol{K}_m \rangle \neq 0$. It should also be noted that from the numerical study it seems that an induced magnetic state $\langle \boldsymbol{S}_m \rangle \neq 0$ and $\langle \boldsymbol{s}_{i_m} \rangle \neq 0$ does coexist with a finite $\langle K^{(0)}_m \rangle \neq 0$. In contrast, $\langle \boldsymbol{K}_m \rangle$ vanishes in presence of any finite magnetic field $\boldsymbol{B} \neq 0$.

Kondo effect. The equilibrium hybridization mean-field theory provides a simple but very tempting picture to describe the Kondo effect and captures the two key characteristics

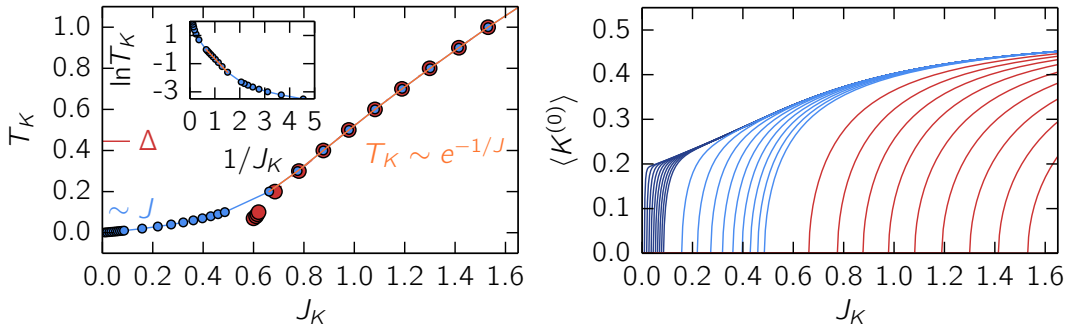

Figure 3.2: *Left panel:* The Kondo scale obtained from the self-consistent HybMF calculation for a one-dimensional chain of length $L = 13$ at half-filling with open boundaries and a single impurity at site $i_0 = 6$ (red dots) and $i_0 = 7$ (blue dots), respectively. In a system of finite size, a competition between the energy-level spacing Δ of the conduction electron system and the Kondo scale T_K arises if the bulk T_K becomes comparable to Δ. In this case, logarithmic Kondo correlations are cut off, resulting in an unconventional spatially dependent linear-in-J Kondo effect for odd sites ($i_0 = 7$) and in free magnetic moments (absence of Kondo effect) for even sites ($i_0 = 6$) below the critical value $J < J_\Delta$ with J_Δ being approximately the point where $T_K = \Delta$. However, for $J > J_\Delta \sim 0.7$, the conventional picture, namely the bulk $T_K \sim e^{-1/J}$, is reconstructed. The inset shows $\ln(T_K)$ versus $1/J$ to visualize the exponential behavior marked by the orange line. *Right Panel:* The charge hybridization $\langle K^{(0)} \rangle$ corresponding to the system with the single impurity placed at site $i_0 = 7$ is shown for different temperatures in ascending order from left to right. The dark blue lines indicate the temperature range $T \in [0.001, 0.01]$ in steps of 0.001, the light blue lines correspond to $T \in [0.02 - 0.1]$ in steps of 0.01. Finally, the red lines comply with the temperature range $T \in [0.2, 1.0]$ in steps of 0.1. For each temperature, the hybridization $\langle K^{(0)} \rangle$ is calculated as a function of the exchange coupling J. The onset of $\langle K^{(0)} \rangle \neq 0$ defines the corresponding value of J to the preassigned temperature T.

of the Kondo physics: At temperatures lower than the Kondo scale $T < T_K$: a finite $\langle K_m^{(0)} \rangle$ indicates screening of the impurity spin and the formation of a Kondo singlet, i.e. the charge hybridization plays the role of an order parameter and the Kondo temperature T_K is defined as the temperature for which a charge hybridization $\langle K_m^{(0)} \rangle \neq 0$ sets in (as detailed in Fig. 3.2, right panel). Only in the case of antiferromagnetic exchange $J > 0$, there is an exponentially small energy scale $T_K \propto e^{-1/\rho_0 J}$ below which a finite $\langle K_m^{(0)} \rangle$ can be stabilized self-consistently for the single-impurity model as shown by fig. 3.2. For temperatures above the Kondo scale $T > T_K$, the hybridization vanishes, $\langle K_m^{(0)} \rangle = 0$, thus the two subsystems, conduction electrons and spins, are decoupled completely at the mean-field level (see Eq. (3.16)). The Kondo effect is thus described as a spontaneous symmetry breaking ("singlet condensation") of the the mean-field Hamiltonian, and T_K plays the role of a critical temperature. However, this strongly simplified description neglects fluctuations which turn the phase transition into a smooth crossover.

Kondo effect in a quantum box. As mentioned before, we study an one-dimensional lattice of conduction electrons of size L with open boundaries at half-filling to which the impurity spins couple, as described by the Hamiltonian (3.1). The finite-size tight-binding part can be analytically diagonalized resulting in nondegenerate conductionband energies $\epsilon_k = -2t\cos(k)$ with discrete values $k = {}^{n\pi}/_{(L+1)}$ with integers $n = 1, \ldots, L$. At half-filling ($N = L$), the finite nature of the system results in an energy-level spacing $\Delta = 2t\sin[{}^{\pi}/_{(L+1)}]$ and a discrete local density of states consisting of finite delta-peaks given by $\rho_{ii}(\omega) = \sum_k U_{ik}^2 \delta[\omega - (\epsilon_k - \epsilon_F)]$ at site i, where $U_{ik} = \sqrt{{}^{2}/_{(L+1)}}\sin(ik)$. According to Schwabe et al. [2012], if the level-spacing Δ becomes comparable to the bulk Kondo temperature T_K, two effects must be considered: (i) An even/odd effect in the number of conduction electrons is observed: if N is even, ϵ_F is located in a finite-size gap of the single-conduction-electron spectrum ("off-resonant"). For $J < J_\Delta$, the Kondo effect is absent, as the Fermi sea is nondegenerate and thus a finite energy Δ would be required to screen the spin. In contrast, if N is odd, the highest one-particle eigenenergy ϵ_{k_F} is singly occupied at the Fermi level resulting in a twofold spin degeneracy of the ground state. Thus the impurity can be screened even for $J \to 0$ ("on-resonant").

(ii) In the "on-resonant" case and for an energy-level spacing Δ being comparable to the bulk Kondo temperature T_K, second-order perturbation theory for the Kondo problem is regularized due to the finite-size gap Δ and results in an effective Hamiltonian:

$$\mathcal{H}^{eff} = \sum_{m=1}^{M} (J_m^{(1)} + J_m^{(2)}) \boldsymbol{S}_m \boldsymbol{s}_F - \sum_{m,n=1}^{M} J_{mn} \boldsymbol{S}_m \boldsymbol{s}_n \,, \tag{3.23}$$

where $\boldsymbol{s}_F$ denotes the spin of the entirely delocalized k_F-electron and $J_{mn} \propto (-)^{|m-n|} J^2/|m-n|$ is the RKKY coupling constant. At $k_F = {}^{\pi}/_{2}$, the effective coupling constants in first and second order $J_m^{(1)} = J|U_{i_m k_F}|^2$ and $J_m^{(2)} = 2J^2|U_{i_m k_F}|^2 \times \sum_{p>k_F} {}^{|U_{i_m k_F}|^2}/_{\epsilon_p - \epsilon_{k_F}}$ vanish for even sites ($i = 2, 4, \ldots, L-1$), for which $|U_{i_m k_F}|^2 = 0$. In contrast $|U_{i_m k_F}|^2 \neq 0$ for odd sites ($i = 1, 3, \ldots, L-2$), which results in a linear-in-J Kondo effect.

We found the aforementioned finite-size effects studied previously by Schwabe et al. [2012] using exact diagonalization, perturbation theory and density matrix renormalization group (DMRG) within the hybridization mean-field approach as can be observed from Fig. 3.2 (left panel). Here, the "on-resonant" case $L = 13$ is considered. If the impurity is placed on an even site $i_0 = 6$, the Kondo effect is absent for $J < J_\Delta$. On the other hand, for the impurity being located at an odd site $i_0 = 7$, a linear-in-J Kondo effect is observed for small but finite $J \to 0$.

Kondo versus RKKY. As mentioned above, in contrast to the large-N approach, the hybridization mean-field is an appropriate method to describe the competition between Kondo screening and indirect magnetic exchange interaction. Although it is beyond the scope of this study to enter the debate on this topic, we would like to discuss briefly how the Doniach picture changes in the presence of finite-size effects: As discussed in

chapter (2.2.2), the conventional Doniach picture [Doniach, 1977] states that in the weak-coupling limit below a certain critical value J_D the RKKY interaction dominates over the Kondo effect, which also remains unchanged for a system of finite size in the "off-resonant" case. In contrast, the perturbation theory by Schwabe et al. [2012] resulting in Eq. (3.23) reveals that the finite-size gap Δ in the "on-resonant" case leads to a modified Doniach phase diagram: The Kondo effect for impurities located at odd sites results in a linear-in-J Kondo scale dominating over the RKKY scale $\sim J^2$ in the weak-coupling limit and $J < J_\Delta$. The remaining impurities located on even sites are coupled via the RKKY interaction. We would like to point out that both the conventional and the modified Doniach phase diagram due to finite-size effects are accessible to the hybridization mean-field approach.

3.3 Spin and charge dynamics

Spin dynamics. We now derive equations for spin (and charge) dynamics via the Heisenberg equation of motion by evaluating the commutator of spin (and charge) with the mean-field Hamiltonian (3.16), which we repeat here:

$$\begin{aligned}\mathcal{H}^{\text{MF}}(t) &= \sum_m \langle \boldsymbol{S}_m \rangle_t \, \underline{\boldsymbol{J}} \, \boldsymbol{s}_{i_m} + \sum_m \langle \boldsymbol{s}_{i_m} \rangle_t \, \underline{\boldsymbol{J}} \, \boldsymbol{S}_m \\ &\quad - \sum_m \boldsymbol{B}_m \boldsymbol{S}_m - \sum_{ij,\sigma} T_{ij} c^\dagger_{i\sigma} c_{j\sigma} \\ &\quad - \frac{3}{2} \sum_m \Big(J \langle K^{(0)\dagger}_m \rangle_t K^{(0)}_m + \text{H.c} \Big) \\ &\quad + \frac{1}{2} \sum_m \Big(J \langle \boldsymbol{K}^\dagger_m \rangle_t \boldsymbol{K}_m + \text{H.c} \Big) \ . \end{aligned} \tag{3.24}$$

The first two terms on the right-hand side generate torques on the conduction-electron and on the impurity spins at sites i_m, respectively, resulting in classical spin dynamics. The Zeeman term causes an external torque exerted on the impurity spins (if $\boldsymbol{B}_m \neq 0$ is assumed). The fourth term induces charge and spin currents in the conduction-electron system which dissipate local excitations. Finally, the last term leads to a spin current between the two subsystems at sites i_m. The resulting spin dynamics for the impurity and conduction electron spins reads:

$$\begin{aligned}\frac{d}{dt} \langle \boldsymbol{S}_m \rangle_t &= J \langle \boldsymbol{s}_{i_m} \rangle_t \times \langle \boldsymbol{S}_m \rangle_t - \boldsymbol{B}_m \times \langle \boldsymbol{S}_m \rangle_t \\ &\quad - \ i \, J \Big(\langle K^{(0)\dagger}_m \rangle_t \langle \boldsymbol{K}_m \rangle_t \ - \text{c.c.} \Big) \end{aligned} \tag{3.25}$$

and

$$\begin{aligned}\frac{d}{dt} \langle \boldsymbol{s}_i \rangle_t &= \sum_m \delta_{i i_m} J \langle \boldsymbol{S}_m \rangle_t \times \langle \boldsymbol{s}_{i_m} \rangle_t \\ &\quad - \ i \sum_j T_{ij} \frac{1}{2} \sum_{\sigma\sigma'} \Big(\langle c^\dagger_{i\sigma} \boldsymbol{\sigma}_{\sigma\sigma'} c_{j\sigma'} \rangle_t - \text{c.c.} \Big) \\ &\quad - \ i \, J \sum_m \delta_{i i_m} \left(\langle \boldsymbol{K}^\dagger_m \rangle_t \, \langle K^{(0)}_m \rangle_t - \text{c.c.} \right) \ . \end{aligned} \tag{3.26}$$

Next we turn to the physical interpretation of the above equations. To this end, it is reasonable to distinguish between transversal (classical) and longitudinal spin dynamics. Whereas the first is characterized by a constant spin length $|\langle \boldsymbol{S}_m \rangle_t| = \text{const.}$, the latter exhibits fluctuating spin length. Notice that in both cases, the length of conduction electron

spins $|\langle \boldsymbol{s}_{i_m}\rangle_t|$ fluctuates due to the electron hopping. However, the longitudinal fluctuation of the impurity spins $\boldsymbol{S}_m$ stems from the hybridization spin and charge ($\langle \boldsymbol{K}_m\rangle_t$ and $\langle K_m^{(0)}\rangle_t$) only.

The torque on $\boldsymbol{S}_m$ in Eq. (3.25) results from the external field $\boldsymbol{B}$, and the conduction-electron local moment at i_m acting as an effective time-dependent internal field $J\langle \boldsymbol{s}_{i_m}\rangle_t$, as well as the hybridization spin and charge current. Vice versa, this holds for $\langle \boldsymbol{s}_{i_m}\rangle_t$ as well, as can be observed from Eq. (3.26). In addition, the second term on the r.h.s. of Eq. (3.26) describes the coupling of the local conduction electron spin to its environment and the dissipation of spin and energy into the conduction-electron system.

For the sake of completeness, we specify the equations of motion for the charge and spin hybridization:

$$\begin{aligned} i\frac{d}{dt}\langle K_m^{(0)}\rangle_t &= -\frac{1}{2}\boldsymbol{B}_m\langle \boldsymbol{K}_m\rangle_t - \sum_i T_{ii_m}\,\frac{1}{2}\sum_\sigma \langle c_{i\sigma}^\dagger f_{m\sigma}\rangle_t \\ &- \frac{3}{4}J\langle \boldsymbol{K}_m\rangle_t\Big(\langle \boldsymbol{S}_m\rangle_t - \langle \boldsymbol{s}_{i_m}\rangle_t\Big) \\ &+ \frac{3}{4}J\langle K_m^{(0)}\rangle_t\frac{1}{2}\sum_\sigma(\langle f_{m\sigma}^\dagger f_{m\sigma}\rangle_t - \langle c_{i_m\sigma}^\dagger c_{i_m\sigma}\rangle_t)\,. \end{aligned} \tag{3.27}$$

Furthermore, for the spin hybridization we find

$$\begin{aligned} i\frac{d}{dt}\langle \boldsymbol{K}_m\rangle_t &= -\frac{1}{2}\boldsymbol{B}_m\langle K^{(0)}\rangle_t - i\,\frac{1}{2}\boldsymbol{B}_m\times\langle \boldsymbol{K}_m\rangle_t \\ &- \sum_i T_{ii_m}\,\frac{1}{2}\sum_{\sigma\sigma'}\langle c_{i\sigma}^\dagger \boldsymbol{\sigma}_{\sigma\sigma'} f_{m\sigma'}\rangle_t \\ &+ \frac{1}{4}J\langle K_m^{(0)}\rangle_t\Big(\langle \boldsymbol{S}_m\rangle_t - \langle \boldsymbol{s}_{i_m}\rangle_t\Big) \\ &- i\,\frac{1}{4}J\langle \boldsymbol{K}_m\rangle_t\times\Big(\langle \boldsymbol{S}_m\rangle_t + \langle \boldsymbol{s}_{i_m}\rangle_t\Big)\,. \end{aligned} \tag{3.28}$$

Apparently, the possible couplings of the charge and spin hybridizations among each other, to the impurity-spin and to the conduction-electron charge and spin degrees of freedom are highly constrained by the rotational invariance of the mean-field Hamiltonian.

As already described, the f-charge is conserved at each site on average $\sum_\sigma\langle f_{m\sigma}^\dagger f_{m\sigma}\rangle = 1$. In addition, the average c-charge is also $\sum_\sigma\langle c_{i_m\sigma}^\dagger c_{i_m\sigma}\rangle = 1$ in the particle-hole-symmetric case at half-filling, thus the last term in Eq. (3.27) vanishes identically. Moreover Eq. (3.27) and Eq. (3.28) can be used to study the spatiotemporal formation of the Kondo effect on a lattice at mean-field level. However, in the more general case, the time-dependent competition of the Kondo effect with the RKKY interaction is also accessible to the tHybMF approach.

Finally, three more points should be mentioned. Firstly, the conservation of total spin (for $\boldsymbol{B} = 0$) is easily verified from the equations above. Secondly, by omitting the

hybridization terms $\langle \boldsymbol{K}_m \rangle_t = 0$ and $\langle K_m^{(0)} \rangle_t = 0$ in Eqs. (3.25) and (3.26), we can relate our approach to theories with classical impurity spins, which we will discuss in chapter (4). Thirdly, the system of equations of motion (3.25) and (3.26) as well as the Eqs. (3.27) and (3.28) can only be closed by considering the complete one-particle density matrix equation (3.17).

Charge dynamics. For the dynamics of the conduction-electron charge density $\langle n_i \rangle_t = \sum_\sigma \langle n_{i\sigma} \rangle_t$ and the charge density on the impurity sites, the Heisenberg equation of motion results in:

$$\frac{d}{dt} \Big\langle \sum_\sigma f_{m\sigma}^\dagger f_{m\sigma} \Big\rangle_t = 0 \,, \tag{3.29}$$

$$\frac{d}{dt} \langle n_i \rangle_t = i \sum_{j,\sigma}^{n.n.} T_{ij} \left(\langle c_{i\sigma}^\dagger c_{j\sigma} \rangle_t - \text{c.c.} \right) \,. \tag{3.30}$$

Here, we observe that neither the local spin-spin coupling, nor the hybridization terms of the Hamiltonian (3.24) contribute, i.e. there is a charge current in the conduction-electron system only, and the conservation of total particle number is easily verified from the above equations. In particular, though $[\sum_\sigma f_{m\sigma}^\dagger f_{m\sigma}, \mathcal{H}^{\text{MF}}(t)] \neq 0$ due to the hybridization terms, the impurity charge density is conserved *on average*. As a result, we can set the Lagrange multiplier $\mu_m^{(\text{f})}(t) = 0$ for the final-state dynamics, while a time-independent Lagrange multiplier $\mu_m^{(\text{f})}$ is sufficient to impose the constraint on the initial state. In conclusion, while there is a complex spin dynamics, the charge dynamics is entirely trivial in hybridization mean-field theory.

3.4 Conclusions

In this chapter, we have proposed a generalization of the hybridization mean-field theory [Lacroix and Cyrot, 1979; Yoshimori and Sakurai, 1970] to Kondo systems far from thermal equilibrium. To this end, we have used the equation of motion for the reduced one-particle density matrix derived in chapter 2.3.2 and have calculated the corresponding Hartree-Fock self-energy contributions of the underlying multi-impurity Kondo model.

As a limiting case, for a time-independent Hamiltonian the static hybridization mean-field approach is recovered and the self-consistent scheme for the resulting non-linear equation of motion for the equilibrium one-particle density matrix is discussed in detail. In addition, the Kondo effect for a single impurity is studied in terms of the hybridization mean-field theory, which provides a very simple picture. However, key characteristics of the Kondo effect are captured on a mean-field level. While a finite hybridization implies the formation of the Kondo effect at temperatures lower than the Kondo scale $T < T_K$, for temperatures above the Kondo scale, $T > T_K$, the hybridization vanishes and the

impurity decouples from the conduction-electron system. Thus, the Kondo effect is characterized as a spontaneous symmetry breaking of the the mean-field Hamiltonian, and the hybridization plays the role of an order parameter, while T_{K} can be seen as a critical temperature. However, this strongly simplified picture neglects fluctuations which turn the phase transition into a smooth crossover.

Furthermore, we derived equations of motion for the charge, hybridization and spin dynamics. It became apparent that the charge dynamics is completely trivial in the hybridization mean-field approach. While the impurity charge density is conserved *on average*, there is a charge current in the conduction-electron system only.

However, the hybridization and the spin dynamics remain still complex. From the equations of motion for the impurity and conduction electron spins it is evident that the real-time dynamics of a spin in an external magnetic field exhibits not only a spin precession, but also spin relaxation due to the coupling of the local conduction-electron spin to its environment and the dissipation of spin and energy into the bulk of the electronic system. In addition to the transversal spin dynamics, which appears as a more classical phenomenon, also the longitudinal spin dynamics, such as arising from the time-dependent Kondo screening is captured by the hybridization spin and charge terms.

To conclude this chapter, we give a brief overview of the various applications of the time-dependent hybridization mean-field approach. Firstly, the spatial and temporal formation or breaking of on a Kondo singlet [Lechtenberg and Anders, 2014; Medvedyeva et al., 2013; Nuss et al., 2015a] can be studied on mean-field level. To this end, the impurity spin is initially fully polarized by an external magnetic field $B > T_K$ and subsequently the polarizing external field is switched off suddenly. Another possibility comprises an interaction quench through the phase boundary of the finite-temperature equilibrium phase diagram of the Kondo impurity Hamiltonian (see Fig. 3.2).

Secondly, details of the spatial and temporal formation of the Kondo screening are also of basic importance for the understanding of the competition of the Kondo effect with the RKKY interaction for systems with many magnetic impurities, which has not yet been studied on the time domain. This scenario can be realized by interaction or external field quenches across the phase boundary of the Doniach diagram [Doniach, 1977].

Finally, the Kondo model is the prototypical system to study the real-time dynamics of a spin coupled to a Fermi sea. Thus another line of research comprises spin dynamics on an atomistic level. For the remainder of this thesis, we concentrate on the transversal spin dynamics, which is apparently a more classical phenomenon. We relate our approach to previous methods in current literature. Subsequently, a comprehensive numerical study of the real-time dynamics of a classical spin coupled to a Fermi sea is performed in order to study the microscopic cause of relaxation and inertia effects beyond phenomenological LLG-type approaches [Evans et al., 2014]. Moreover, we identify quantum effects by a systematic comparison of the classical spin dynamics with the exact quantum spin dynamics for different spin quantum numbers S. Finally, we study the effect of electronic

correlations on the real-time dynamics of a classical spin coupled to a correlated electron system by means of a combination of linear-response spin dynamics [Bhattacharjee et al., 2012; Onoda and Nagaosa, 2006] for the spin dynamics with time-dependent density-matrix renormalization group [Haegeman et al., 2011, 2016; Schollwöck, 2011] for the correlated electronic subsystem.

4 Relation to theories with classical impurity spins

In the previous chapter we introduced the time-dependent hybridization mean-field approach and derived equations of motion for charge, hybridization and spin dynamic. The purpose of this chapter is to focus exclusively on spin dynamics and relate our approach to previous ones.[2] To this end, firstly, we neglect longitudinal fluctuations altogether and point out that the remaining equation of motion is equivalent to that of a quantum-classical hybrid spin dynamics (QCH-SD) [Elze, 2012] obtained from the classical-spin multi-impurity Kondo model. Secondly, in the weak-coupling limit, the conduction-electron degrees of freedom can be integrated out altogether by applying linear-response-theory which results in an equation for the classical spins only [Bhattacharjee et al., 2012; Onoda and Nagaosa, 2006]. Finally, assuming separation of time scales, i.e., the classical spin dynamics is slow as compared to the electron dynamics, the linear-response spin dynamics (LR-SD) can be simplified further by applying the Markov approximation which results in the Landau-Lifshitz-Gilbert equation [Gilbert, 2004; Landau and Lifshitz, 1935].

4.1 Exact quantum-classical hybrid dynamics

In this section we demonstrate that the transversal spin dynamic in Eqs. (3.25) and (3.26), i.e. without the hybridization terms $\langle K_m^{(0)}\rangle_t = 0$ and $\langle \boldsymbol{K}_m\rangle_t = 0$, which results from the mean-field treatment of the quantum-model in Eq. (3.1), can be related to the classical spin dynamics resulting from a hybrid quantum-classical Kondo model. To this end, consider the quantum-classical variant of the multi-impurity Kondo model, Eq. (3.1), where the quantum spins $\boldsymbol{S}_m$ are replaced by classical spins $\boldsymbol{S}_m^{(\mathrm{cl.})}$ resulting in:

$$\mathcal{H}^{(\mathrm{cl.})} = -\sum_{\langle i,j\rangle,\sigma} T_{ij} c_{i\sigma}^\dagger c_{j\sigma} + \sum_{m=1}^{M} \boldsymbol{s}_{i_m} \cdot \underline{\boldsymbol{J}} \cdot \boldsymbol{S}_m^{(\mathrm{cl.})} - \sum_{m=1}^{M} \boldsymbol{B}_m \boldsymbol{S}_m^{(\mathrm{cl.})} , \tag{4.1}$$

[2] Some of the results obtained in this chapter are applied to the classical-spin Kondo-impurity model and published as M. Sayad and M. Potthoff: *Spin dynamics and relaxation in the classical-spin Kondo-impurity model beyond the Landau-Lifschitz-Gilbert equation*, New J. Phys. 17, 113058 (2015) - Copyright © 2015 IOP Publishing Ltd and Deutsche Physikalische Gesellschaft.

which is a quantum-classical hybrid model, as classical degrees of freedom are coupled directly to quantum-mechanical degrees of freedom. Here, the conduction-electron and the impurity-spin systems are completely decoupled on the operator level, while only parametrical coupling is retained, which, however, induces a non-trivial quantum-classical hybrid dynamics, which is determined via the Liouville-equation by the Hamiltonian function $\mathcal{H}_{\mathcal{F}} \equiv \langle \mathcal{H}^{(\mathrm{cl.})} \rangle$:

$$\frac{d}{dt}\boldsymbol{S}_m^{(\mathrm{cl.})}(t) = \{\boldsymbol{S}_m^{(\mathrm{cl.})}, \mathcal{H}_{\mathcal{F}}\} \; . \tag{4.2}$$

This is the only known way to consistently describe the dynamics of a quantum-classical hybrids as previously studied by, e.g, Heslot [1985], Hall [2008] and Elze [2012].

For this purpose, the classical Poisson bracket on the r.h.s. of Eq. (4.2) must be generalized to include classical spins[3] [Lakshmanan and Daniel, 1983; Yang and Hirschfelder, 1980], which then satisfies the following algebraic relations between arbitrary functions A and B of the spin components :

$$\{A, B\} = \sum_{m,\alpha=x,y,z} \varepsilon_{\alpha\beta\gamma} \frac{\partial A}{\partial S_{m\alpha}} \frac{\partial B}{\partial S_{m\beta}} S_{m\gamma} \; , \tag{4.3}$$

where $\varepsilon_{\alpha\beta\gamma}$ is the antisymmetric ε-tensor. With this in mind, the r.h.s. of Eq. (4.2) yields:

$$\frac{d}{dt}\boldsymbol{S}_m(t) = J\langle \boldsymbol{s}_{i_m} \rangle_t \times \boldsymbol{S}_m(t) - \boldsymbol{B}_m \times \boldsymbol{S}_m(t) \; , \tag{4.4}$$

which has the same structure as the Landau-Lifshitz equation, but the classical spin is coupled to the conduction-electron spin $\langle \boldsymbol{s}_{i_m} \rangle_t$ which is again time-dependent. The equation of motion of the conduction-electron spins obeys the Heisenberg equation of motion with respect to the Hamiltonian $\mathcal{H}^{(cl)}$ in Eq. (4.1) and reads as:

$$\frac{d}{dt}\langle \boldsymbol{s}_i \rangle_t = \delta_{ii_m} J\boldsymbol{S}(t) \times \langle \boldsymbol{s}_{i_m} \rangle_t - T \sum_j^{n.n.} \frac{1}{2i} \sum_{\sigma\sigma'} (\langle c_{i\sigma}^\dagger \boldsymbol{\sigma}_{\sigma\sigma'} c_{j\sigma'} \rangle_t - \text{c.c.}) \; , \tag{4.5}$$

Apparently, the system of equations of motion can only be closed by considering the complete one-particle density matrix equation of motion given in Eq. (3.17), which was derived in chapter (2.3.2) using nonequilibrium diagrammatic perturbation theory. However, the reduced one-particle density matrix equation of motion can be also easily derived from the Heisenberg equation of motion for the annihilators and creators, which leads to a closed set of equations of motion, since the quantum-classical hybrid Hamiltonian (4.1) is quadratic on the operator level. As is evident from the equations of motion, the real-time dynamics of the quantum-classical multi-impurity Kondo model on a lattice with a

[3] In the following we omit the index "(cl)" and denote the classical spin vector by $\boldsymbol{S}$.

finite but large number of sites L can be treated numerically exactly. However, the model implies highly nontrivial physics as the electron dynamics becomes effectively correlated due to the interaction with the classical spin. Apart from that, the effective electron-electron interaction mediated by the classical spin is retarded: electrons scattered from the spin at time t will experience the effects of the spin torque exerted by electrons that have been scattered from the spin at earlier times $t' < t$. Furthermore, the conservation of the total energy, total spin and total conduction-electron number is easily verified for the hybrid system. We also note that Eq. (4.4) implies $\|\boldsymbol{S}_m(t)\| = \text{const.}$ while the length of $\langle \boldsymbol{s}_{i_m} \rangle$ is not fixed but fluctuates due to electron hopping. Finally, as we exactly recover Eqs. (3.25) and (3.26), we can conclude that the mean-field treatment of the quantum model is equivalent with the classical-spin case if the charge or spin hybridization $\langle K_m^{(0)} \rangle_t = 0$ or $\langle \boldsymbol{K}_m \rangle_t = 0$ vanishes.

4.2 Linear-response spin dynamics

As already mentioned, Eqs. (4.4) and (4.5) do not form a closed set of equations of motion but must be supplemented by the full equation of motion for the reduced one-particle conduction-electron density matrix. As a consequence, the fast electron dynamics must be propagated in real-time with small time steps explicitly, even if the spin dynamics is much slower and could be resolved with much larger time steps within a corresponding spin-only time-propagation method. It is therefore advantageous with respect to computational costs to integrate out the conduction-electron degrees of freedom altogether. Recently, this has been done by expressing the partition function of the system as a path-integral over the fermionic degrees of freedom and of a classical action for the classical spins on the Keldysh contour, which includes the Wess-Zumino-Witten-Novikov term describing the Berry phase of the classical spins, see, e.g., Onoda and Nagaosa [2006] and Bhattacharjee et al. [2012]. Unfortunately, a tractable effective spin-only action can be obtained in the weak-coupling (small-J) limit only. This weak-coupling approximation is also implicit to all effective spin-only approaches that consider the effect of conduction electrons on the spin dynamics [Zhang and Li, 2004].

However, in the weak-coupling limit, the electron degrees of freedom can also be eliminated in a more straightforward way which is completely equivalent with the path-integral approach, namely using standard linear-response theory [Negele and Orland, 1998]. We assume that the initial state at $t = 0$ is given by the conduction-electron system in thermal equilibrium and some arbitrary configuration of the classical spins. This may be realized by suddenly switching on the interaction $J(t)$ at time $t = 0$, i.e. $J(t) = J\Theta(t)$ and by switching the configuration of the local fields $\boldsymbol{B}_m(t)$ from some initial values, realizing a certain initial state of the classical spins, to final values for $t > 0$. The response of the conduction-electron spin at i_m and time $t > 0$ ($\langle \boldsymbol{s}_{i_m} \rangle_t = 0$ for $t = 0$) due to the

time-dependent perturbation $J(t)\boldsymbol{S}_{m'}(t)$ coupling to the spin, is

$$\langle \boldsymbol{s}_{i_m} \rangle_t = J \int_0^t dt' \sum_{m'} \chi^{(\mathrm{ret})}_{mm'}(t,t') \cdot \boldsymbol{S}_{m'}(t') \tag{4.6}$$

up to linear order in J for the final-state dynamics. Here, the free ($J = 0$) retarded spin susceptibility of the conduction electrons $\chi^{(\mathrm{ret})}_{mm'}(t,t')$ is a tensor with elements

$$\chi^{(\mathrm{ret})}_{mm',\alpha\alpha'}(t,t') = -i\Theta(t-t')\langle [s^{\alpha}_{i_m}(t), s^{\beta}_{i_{m'}}(t')] \rangle \,, \tag{4.7}$$

where $\alpha, \beta = x, y, z$. Using this in Eq. (4.4), we obtain an equation of motion for the classical spins only,

$$\frac{d}{dt}\boldsymbol{S}_m(t) = \boldsymbol{S}_m(t) \times \boldsymbol{B}_m - \boldsymbol{S}_m(t) \times \int_0^t dt' \sum_{m'} J^{\mathrm{RKKY}}_{mm'}(t-t') \cdot \boldsymbol{S}_{m'}(t') \,, \tag{4.8}$$

where the time-dependent coupling of the indirect magnetic interaction is given by $J^{\mathrm{RKKY}} = J^2 \chi^{(\mathrm{ret})}_{mm'}(t,t')$, as previously discussed in chapter (2.2.2). The Eq. (4.8) represents an integro-differential equation for the classical spin only and possesses a spatially and temporally non-local structure, as a spin at site m and time t is coupled via the equilibrium and homogeneous-in-time conduction-electron spin susceptibility $\underline{\chi}^{(\mathrm{ret})}(t-t')$ to an spin at site m' and earlier time t'. Compared with the results of the full quantum-classical theory, we expect that the perturbative spin-only theory breaks down after a propagation time $t \sim 1/J$ at the latest. However, if the spin dynamic is nearly adiabatic, it will produces rather a very weak torque $\propto \boldsymbol{S}_m(t) \times \boldsymbol{S}_m(t')$ and the first-order perturbation theory could become reliable on much larger time scales $t \gg 1/J$.

The integro-differential equation (4.8) can be solved numerically by a combination of Runge-Kutta method [Verner, 2010] and Newton–Cotes quadrature rule (required for the evaluation of the integral [Press et al., 2007]). To this end, the time-dependent RKKY indirect magnetic interaction must be calculated in advance, as this fixes the kernel in the integro-differential equation (4.8). Using Wick's theorem the time-dependent parameters of the retarded RKKY interaction can be formulated in terms of the greater and the lesser one-particle Green's function, $G^{>}_{ii',\sigma\sigma'}(t,t') = -i\langle c_{i\sigma}(t) c^{\dagger}_{i'\sigma'}(t') \rangle$ and $G^{<}_{ii',\sigma\sigma'}(t,t') = i\langle c^{\dagger}_{i'\sigma'}(t') c_{i\sigma}(t) \rangle$, respectively, in thermal equilibrium at inverse temperature β and chemical potential μ:

$$J^{\mathrm{RKKY}}_{mm',\alpha\alpha'}(t-t') = \frac{J^2}{2}\Theta(t-t') \times \mathrm{Im}\,\mathrm{tr}_{2\times 2}\Big[\sigma^{\alpha} G^{>}_{i_m i_{m'}}(t,t') \sigma^{\alpha'} G^{<}_{i_{m'} i_m}(t',t)\Big] \,. \tag{4.9}$$

Assuming that the conduction electrons are characterized by a real, symmetric and spin-independent hopping matrix T_{ij} (as given by the first term of Eq. (4.1)). This implies that $G^{>/<}$ are unit matrices with respect to the spin indices. With $\mathrm{tr}\,(\sigma^{\alpha}\sigma^{\alpha'}) = 2\delta_{\alpha\alpha'}$ and

with the explicit representations of $G^{>/<}$ as functions of $\boldsymbol{T}$ (see, e.g., Balzer and Potthoff [2011]) we find:

$$J^{\mathrm{RKKY}}_{mm',\alpha\alpha'}(t-t') = \Theta(t-t')J^2\delta_{\alpha\alpha'}\mathrm{Im}\times\left(\frac{e^{-i\boldsymbol{T}(t-t')}}{1+e^{-\beta(\boldsymbol{T}-\mu)}}\right)_{i_m i_{m'}}\left(\frac{e^{-i\boldsymbol{T}(t'-t)}}{e^{\beta(\boldsymbol{T}-\mu)}+1}\right)_{i_{m'} i_m} \tag{4.10}$$

Furthermore, taking advantage of time homogeneity and spatial translational symmetry, the hopping matrix $\boldsymbol{T}$ is diagonalized by Fourier transformation:

$$T_{ij} = \sum_{\boldsymbol{k}} U_{i\boldsymbol{k}}\varepsilon(\boldsymbol{k})U^{\dagger}_{\boldsymbol{k}j} \tag{4.11}$$

with $U_{i\boldsymbol{k}} = L^{-1/2}\exp(i\boldsymbol{k}\boldsymbol{R}_i)$ and the eigenvalues of $\boldsymbol{T}$ are given by the tight-binding dispersion relation $\varepsilon(\boldsymbol{k}) = 2T\sum_{\alpha=1}^{d}\cos k_\alpha$ of the conduction band. This leads to

$$J^{\mathrm{RKKY}}_{mm',\alpha\alpha'}(t) = \Theta(t)\frac{J^2}{L^2}\times \tag{4.12}$$
$$\mathrm{Im}\left\{\left(\sum_{\boldsymbol{k}} e^{i\boldsymbol{k}(\boldsymbol{R}_{i_m}-\boldsymbol{R}_{i_{m'}})}\frac{e^{-i\varepsilon(\boldsymbol{k})t}}{1+e^{-\beta(\varepsilon(\boldsymbol{k})-\mu)}}\right)\left(\sum_{\boldsymbol{p}} e^{-i\boldsymbol{p}(\boldsymbol{R}_{i_m}-\boldsymbol{R}_{i_{m'}})}\frac{e^{i\varepsilon(\boldsymbol{p})t}}{e^{\beta(\varepsilon(\boldsymbol{p})-\mu)}+1}\right)\right\}$$

where the components of the wave vectors are given as $k_\alpha, q_\alpha \in \{-\pi/a + 2\pi z/aL\,|1 \le z \le L, z \in \mathrm{N}\}$ with the lattice constant $a = 1$. The Eq. (4.12) can be evaluated numerically and an example for the time-dependence of the RKKY interaction in various dimensions is presented in Fig. (4.1). The calculations have been done at half-filling and at finite temperature $\beta = 10^3$. We find that the susceptibility is in fact peaked around $t = 0$ and decays as $1/t^d$ for long times, where d is the dimension of the system. In the following, we analyze the physical origin of the asymptotic behavior of the RKKY interaction for $t \to \infty$, as this is of great importance for the estimation of the Gilbert-damping constant later on. For simplicity, we discuss its local part $j(t) \equiv J^{\mathrm{RKKY}}_{m=m',\alpha\alpha}(t)/J^2$:

$$j(t) = \Theta(t)\mathrm{Im}\frac{1}{L^2}\sum_{\boldsymbol{k}}\frac{e^{-i\varepsilon(\boldsymbol{k})t}}{1+e^{-\beta(\varepsilon(\boldsymbol{k})-\mu)}}\sum_{\boldsymbol{p}}\frac{e^{i\varepsilon(\boldsymbol{p})t}}{e^{\beta(\varepsilon(\boldsymbol{p})-\mu)}+1}\,. \tag{4.13}$$

With the Fermi function $f(\omega) = 1/(e^{\beta\omega}+1)$ and the noninteracting conduction-electron one-particle spectral density

$$\rho(\omega) = \frac{1}{L}\sum_{\boldsymbol{k}}\delta(\omega+\mu-\varepsilon(\boldsymbol{k})) \tag{4.14}$$

we obtain

$$\begin{aligned} j(t) &= \Theta(t)\mathrm{Im}\int dx\,\rho(x)e^{-ixt}(1-f(x))\int d\omega\,\rho(\omega)e^{i\omega t}f(\omega) \\ &= \Theta(t)\mathrm{Im}[\rho_{\mathrm{unocc}}(-t)\rho_{\mathrm{occ}}(t)]\,. \end{aligned} \tag{4.15}$$

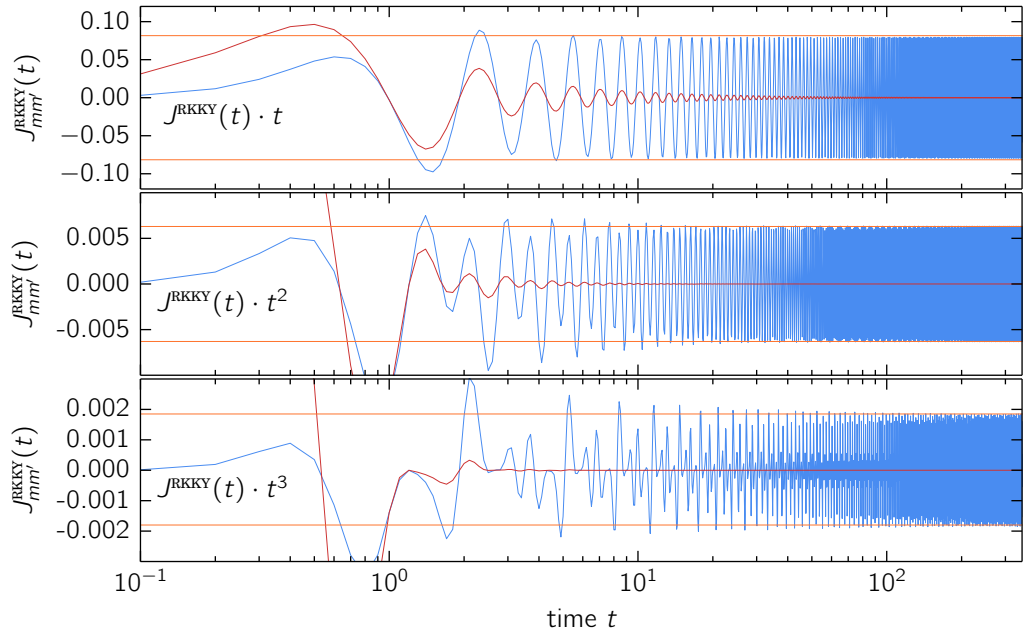

Figure 4.1: RKKY indirect magnetic interaction $J^{\mathrm{RKKY}}(t)$ (red line) and $t^d\, J^{\mathrm{RKKY}}(t)_{mm'}$ (blue) as obtained from Eq. (4.12) for $\beta = 10^3$ in various dimensions d for a conduction-electron system with $L = 10000$ ($d = 1$), $L = 1000 \times 1000$ ($d = 2$) and $L = 800 \times 800 \times 800$ (d=3) sites and periodic boundary conditions. The two impurities located at sites m and m' in Eq. (4.12) are chosen to be nearest neighbours in all cases.

Its long-time behavior is governed by the long-time behavior of the Fourier transform

$$\rho_{\mathrm{occ,unocc.}}(t) = \int d\omega\, e^{i\omega t} \rho_{\mathrm{occ,unocc.}}(\omega) \tag{4.16}$$

of the occupied, $\rho_{\mathrm{occ}}(\omega) = f(\omega)\rho(\omega)$, and of the unoccupied, $\rho_{\mathrm{unocc}}(\omega) = (1-f(\omega))\rho(\omega)$, part of the spectral density. For functions with a smooth ω-dependence, the Fourier transform generically drops to zero exponentially fast if $t \to \infty$. A power-law decay, however, is obtained if there are singularities of $\rho_{\mathrm{occ,unocc.}}(\omega)$. We can distinguish between van Hove singularities, which are, e.g., of the form $\propto \Theta(\omega - \omega_0)(\omega - \omega_0)^k$ (with $k > -1$), and the step-like singularity $\propto \Theta(\omega - \omega_0)$ (i.e. $k = 0$), arising in the zero-temperature limit at $\omega_0 = 0$ due to the Fermi function. These give rise to the asymptotic behavior $\rho_{\mathrm{occ,unocc.}}(t) \propto t^{-1-k}$, apart from a purely oscillatory factor $e^{i\omega_0 t}$. Generally, the location of the van Hove singularity on the frequency axis, i.e. ω_0, determines the oscillation period while the decay of $j(t)$ is governed by the strength of the singularity.

Consider, as an example, the zero-temperature case and assume that there are no van Hove singularities. The sharp Fermi edge implies $\rho_{\mathrm{loc}}^{(\mathrm{occ,unocc})}(t) \propto t^{-1}$, and thus $j(t) \propto t^{-2}$. However, in general, van Hove singularities are unavoidable and their strength depends on the lattice dimension d [Ashcroft and Mermin, 1976]:

- *One-dimensional lattice ($d = 1$):*
  The van Hove singularities with $k = -1/2$ leads to $j(t) \propto t^{-1}$. The strong van Hove singularity dominates the long-time asymptotic behavior as compared to the weak Fermi-edge singularity with a more rapid and thus negligible decay $j(t) \propto t^{-2}$.
- *Two-dimensional lattice ($d = 2$):*
  The logarithmic van Hove singularity $\propto \ln|\omega|$ leads to $j(t) \propto t^{-2}$. This, however, applies to cases off half-filling only. At half-filling the van Hove and the Fermi-edge singularity combine to a singularity $\propto \Theta(\omega)\ln|\omega|$ which gives $j(t) \propto \ln^2(t)/t^2$. For finite temperatures, we again have $j(t) \propto t^{-2}$. We like to mention that $j(t) \propto t^{-3}$ in models where its Fourier transform is given by $j(\omega) \propto \omega e^{-|\omega|/\lambda}$ with some cutoff parameter λ. In this case the singularity is of the order of $k = 2$.
- *Three-dimensional lattice ($d = 3$):*
  Here, we have $k = 1/2$ and $j(t) \propto t^{-3}$ if $T > 0$, while for $T = 0$ the Fermi-edge singularity dominates and $j(t) \propto t^{-2}$.

We conclude that the numerical results at finite temperature ($\beta = 10^3$) in figure (4.1) with $j(t) \propto 1/t^d$ are in line with the analytical consideration from above. The $t \to \infty$ behavior is important for static quantities like $\int_{\text{const.}}^{\infty} dt\, j(t)$ and $\int_{\text{const.}}^{\infty} dt\, t\, j(t)$. The latter is related to the Gilbert damping constant, which we will discuss in the subsequent section.

4.3 Derivation of the Landau-Lifshitz-Gilbert equation

In the preceding sec. 4.2, the linear-response approach to integrate out the electron degrees of freedom is carefully examined. Here, we go one step further by including a discussion of the additional approximations that are necessary to re-derive the LLG equation and the damping term in particular. Moreover, we show that the damping constant is sensitively dependent on the low-energy electronic structure and as a result even ill-defined in some cases.

We begin our discussion with a brief introduction to the Landau-Lifshitz-Gilbert [Gilbert, 2004; Landau and Lifshitz, 1935] equation, which for a suitable choice of units and for several spins $\boldsymbol{S}_m(t)$ at lattice sites m, has the following structure:

$$\begin{aligned} \frac{d\boldsymbol{S}_m(t)}{dt} &= \boldsymbol{S}_m(t) \times \boldsymbol{B} + \sum_{m'} J_{mm'} \boldsymbol{S}_m(t) \times \boldsymbol{S}_{m'}(t) \\ &- \sum_{m'} \alpha^{\mathrm{G}}_{mm'} \boldsymbol{S}_m(t) \times \dot{\boldsymbol{S}}_{m'}(t)\,. \end{aligned} \tag{4.17}$$

It consists of precession terms coupling the spin at site m to an external magnetic field $\boldsymbol{B}$ and, via exchange couplings $J_{mm'}$, to the spins at sites m'. Those precession terms typi-

cally have a clear atomistic origin, such as the Ruderman-Kittel-Kasuya-Yoshida (RKKY) interaction which is mediated by the magnetic polarization of conduction electrons. The non-local RKKY couplings $J_{mm'} = J^2\chi_{mm'}$ are given in terms of the elements $\chi_{mm'}$ of the static conduction-electron spin susceptibility and the local exchange J between the spins and the local magnetic moments of the conduction electrons. Other possibilities comprise direct (Heisenberg) exchange interactions, intra-atomic (Hund's) couplings as well as the spin-orbit and other anisotropic interactions. The relaxation term, on the other hand, is often assumed as local, $\alpha_{mm'} = \delta_{mm'}\alpha$, and is represented by purely phenomenological Gilbert damping constant α only. It describes the angular-momentum transfer between the spins and a usually unspecified heat bath. On the atomistic level, the Gilbert damping must be seen as originating from microscopic couplings of the spins to the conduction-electron system (as well as to lattice degrees of freedom which, however, will not be considered here). As prevoiusly mentioned in the introductory chapter 1, there are numerous studies where the damping constant, or tensor, α has been computed numerically from a more fundamental model including electron degrees of freedom explicitly [Bhattacharjee et al., 2012; Onoda and Nagaosa, 2006; Umetsu et al., 2012] or even from first principles. [Antropov et al., 1995; Capelle and Gyorffy, 2003; Ebert et al., 2011; Kuneš and Kamberský, 2002a; Sakuma, 2012]. All these studies rely on two, partially related, assumptions: Firstly, the spin-electron coupling J is weak and can be treated perturbatively to lowest order, i.e., the Kubo formula or linear-response theory can be employed, as already discussed at the derivation of Eq. (4.8). Secondly, he weak-coupling approach can be simplified further by applying a Markov approximation and may lead eventually to the LLG equation. Assuming a separation of time scales, i.e., the electron dynamics is much faster than the spin dynamics, [Bhattacharjee et al., 2012; Fransson, 2008] the RKKY interaction takes place almost instantaneously on the time scale of the spin system, i.e. the memory kernel in Eq. (4.8) is peaked at $t' \approx t$, and we can replace $\boldsymbol{S}(t')$ by its Taylor expansion $\boldsymbol{S}(t') \approx \boldsymbol{S}(t) + (t'-t)\dot{\boldsymbol{S}}(t) + (t'-t)^2\ddot{\boldsymbol{S}}(t)/2$ in the integrand. Sending the upper bound of the integral to infinity as an additional approximation, which is a necessary step to yield constant coupling parameters and which can be justified by noting that $J^{\mathrm{RKKY}}(t)$ is peaked around $t = 0$, we obtain:

$$\begin{aligned}\frac{d}{dt}\boldsymbol{S}_m(t) &= \boldsymbol{S}_m(t) \times \boldsymbol{B}_m \\ &- \boldsymbol{S}_m(t) \times \sum_{m'} J^{\mathrm{RKKY}}_{mm'} \cdot \boldsymbol{S}_{m'}(t) \\ &- \boldsymbol{S}_m(t) \times \sum_{m'} \alpha^{\mathrm{G}}_{mm'} \cdot \dot{\boldsymbol{S}}_{m'}(t) \\ &+ \boldsymbol{S}_m(t) \times \sum_{m'} \mathcal{I}_{mm'} \cdot \ddot{\boldsymbol{S}}_{m'}(t) \; . \end{aligned} \tag{4.18}$$

Static RKKY interaction. The first two terms in the r.h.s. of Eq. (4.18) can also be

derived from the classical Heisenberg model

$$H_{\text{eff}} = \frac{1}{2}\sum_{mm'} \boldsymbol{S}_m J^{\text{RKKY}}_{mm'} \boldsymbol{S}_{m'} - \sum_m \boldsymbol{B}_m \boldsymbol{S}_m \,, \tag{4.19}$$

where the *static* RKKY interaction is defined as

$$\begin{aligned} J^{\text{RKKY}}_{mm'} &= J^2 \lim_{t\to\infty} \int_{-\infty}^{t} dt' \theta(t')\, \chi^{(\text{ret})}_{mm'}(t-t') \\ &= J^2 \int_{-\infty}^{\infty} d\tau\, \chi^{(\text{ret})}_{mm'}(\tau) e^{-i\omega\tau} \mid_{\omega=0} \\ &= J^2\, \chi^{(\text{ret})}_{mm'}(\omega=0) \,, \end{aligned} \tag{4.20}$$

which can be computed by expressing the static conduction-electron spin susceptibility as $\chi^{(\text{ret})}_{mm',\alpha\alpha'}(\omega=0) = \int_{-\infty}^{\infty} dt\, \Pi^{(\text{ret})}_{mm',\alpha\alpha'}(t) = \partial\langle s^{\alpha}_{i_m}\rangle/\partial b^{\alpha'}_{i_{m'}}|_{\boldsymbol{b}=0} = \int_0^{\beta}\langle s^{\alpha}_{i_m}(\tau) s^{\alpha'}_{i_{m'}}(0)\rangle d\tau - \beta\langle s^{\alpha}_{i_m}\rangle\langle s^{\alpha'}_{i_{m'}}\rangle$, where $\boldsymbol{b}_i = \sum_\alpha b^{\alpha}_i \boldsymbol{e}_\alpha$ is a local field coupling to the conduction-electron spins via $H \mapsto H - \sum_m \boldsymbol{b}_{i_m}\boldsymbol{s}_{i_m}$ and $s^{\alpha}_{i_m}(\tau) = e^{H\tau} s^{\alpha}_{i_m} e^{-H\tau}$. Applying Wick's theorem, we find (see, e.g., Ref. Antropov et al. [1995]):

$$J^{\text{RKKY}}_{mm',\alpha\alpha'} = \frac{1}{\pi}\frac{J^2}{4}\int_{-\infty}^{\infty} d\omega f(\omega) \times \text{Im}\,\text{tr}_{2\times 2}\left(\sigma^{\alpha} G^{\text{ret}}_{i_m i_{m'}}(\omega)\sigma^{\alpha'} G^{\text{ret}}_{i_{m'} i_m}(\omega)\right) \tag{4.21}$$

where $f(\omega) = 1/(e^{\beta\omega}+1)$ is the Fermi function at inverse temperature β of the free conduction-electron in thermal equilibrium and $G^{\text{ret}}_{ii'}(\omega)$ is the free single-electron retarded Green's function, a 2×2 matrix with elements $G^{\text{ret}}_{ii',\sigma\sigma'}(\omega)$. An alternative approach to calculate the static RKKY interaction would be the evaluation of the time integral over the static conduction-electron spin susceptibility $\underline{\chi}^{(\text{ret})}(t)$ in Eq. (4.20).

Gilbert damping and moment of inertia. The first- and second-order Taylor expansion included this microscopic approach yield a spatially non-local Gilbert damping and a non-local moment of inertia:

$$\alpha^{\text{G}}_{mm'} = -\int_0^{\infty} dt\, t\, J^{\text{RKKY}}_{mm'}(t) \,, \tag{4.22}$$

$$\mathcal{I}_{mm'} = -\int_0^{\infty} dt\, t^2\, J^{\text{RKKY}}_{mm'}(t) \,. \tag{4.23}$$

The Eq. (4.22) represents the fundamental definition of the Gilbert damping constant ($\alpha^{\text{G}} > 0$) and the limit $t\to\infty$ is crucial to recover the LLG equation in its standard form as given in Eq. (4.18). The existence of the integral Eq. (4.22) decisively depends on the $t\to\infty$ behavior and either requires a decay as $J^{\text{RKKY}}(t) \propto t^{-s}$ with $s > 2$, or

an asymptotic form $J^{\mathrm{RKKY}}(t) \propto e^{i\omega_0 t}/t^s$ (and $s \geq 2$) with an oscillating factor resulting from a non-zero position $\omega_0 \neq 0$ of the van Hove singularity. As previously discussed in section (4.2), for the one-dimensional case the RKKY scales as $J^{\mathrm{RKKY}} \propto 1/t$ due to the van Hove singularity, hence we conclude that the LLG equation (with a time-independent damping constant) is based on an ill-defined concept. The same applies to the inertia term in (4.23), which requires a decay as $J^{\mathrm{RKKY}}(t) \propto t^{-s}$ with $s > 3$, consequently the inertia term is even ill-defined for two-dimensional systems. This conclusion might change for the case of *interacting* conduction electrons, as one would expect a regularization of van Hove singularities due to a finite imaginary part of the conduction-electron self-energy.

Scaling properties. Finally, we analyze the scaling properties of the equation of motion (4.18). To this end, we rescale the length of the classical spin $\widetilde{\boldsymbol{S}}_m = \lambda \boldsymbol{S}_m$ and see immediately that if $\boldsymbol{S}_m$ solves the equation for parameters $\boldsymbol{B}, \alpha^{\mathrm{G}}$ and $\mathcal{I}$, then $\widetilde{\boldsymbol{S}}_m$ solves the same equation with rescaled parameters $\alpha^{\mathrm{G}}/\lambda$ and $\mathcal{I}/\lambda$. Hence, the damping parameter α^{G} and the inertia constant $\mathcal{I}$ have a stronger impact on the dynamics of an elongated spin ($S_{\mathrm{cl.}} \equiv |\boldsymbol{S}| > 1$), i.e. smaller effective parameters

$$\widetilde{\alpha}^{\mathrm{G}} = \alpha^{\mathrm{G}}/S_{\mathrm{cl.}} \,, \qquad \mathcal{I}' = \mathcal{I}/S_{\mathrm{cl.}} \,, \tag{4.24}$$

result in the same dynamics as for a spin of unit length.

As is evident from the defining equations (4.22) and (4.23), the parameters $\alpha^{\mathrm{G}}, \mathcal{I}$ are properties of the conduction-electron system only and do not depend on the length of the classical spin $S_{\mathrm{cl.}}$. As a result, the equation of motion (4.18) for a given system is therefore independent of $S_{\mathrm{cl.}}$. It is worth adding, that this scaling property also applies to the integro-differential equation (4.8).

Furthermore, for a single spin and fixed α, the relaxation time can be determined analytically [Kikuchi, 1956] and results in $\tau_{\mathrm{rel}} \propto (1 + \alpha^2 S_{\mathrm{cl.}}^2)/(\alpha S_{\mathrm{cl.}} B)$. Hence in the large-$S_{\mathrm{cl.}}$ limit, the relaxation time scales linearly in $S_{\mathrm{cl.}}$:

$$\tau_{\mathrm{rel}} \propto S_{\mathrm{cl.}} \,. \tag{4.25}$$

Finally, we identify $S_{\mathrm{cl.}}$ with the modulus of the angular momentum L of a fast-spinning gyroscope. From elementary theory (see, e.g., Ref. Butikov [2006]) it is well known that $L \sim \omega_{\mathrm{N}}$, and thus we find

$$\omega_{\mathrm{N}} \propto S_{\mathrm{cl.}} \,, \tag{4.26}$$

which is consistent with results obtained by Kikuchi and Tatara [2015]. In 5.2.3 we will check the scaling behavior found in terms of the perturbative LLG-approach in Eqs. (4.25) and (4.26) with numerical results obtained from the quantum-classical hybrid theory (QCH-SD) and from the full quantum dynamics (tDMRG method).

4.4 Conclusions

In this Chapter, we have focused on the transversal spin dynamics which is a classical phenomenon and compared our method to existing approaches to classical spin dynamics. Firstly, we have found that the transversal spin dynamics yield from the mean-field treatment of the quantum model is equivalent to the quantum-classical hybrid spin dynamics (QCH-SD) obtained from the classical-spin multi-impurity Kondo model.

Secondly, in the weak-coupling limit, we recover an equation of motion for the classical spins only [Bhattacharjee et al., 2012; Onoda and Nagaosa, 2006]. To this end, the electronic degrees of freedom explicitly included in the quantum-classical hybrid spin dynamics are integrated out altogether by applying standard linear-response theory [Negele and Orland, 1998]. The resulting linear-response spin dynamics (LR-SD) is an integro-differential equation for the classical spins only with a spatially and temporally non-local structure and is numerically solvable by means of a combination of Runge-Kutta method [Verner, 2010] and Newton–Cotes quadrature rule [Press et al., 2007]. On the one hand, this weak-coupling approach is expected to break down after a propagation time $t \sim 1/J$ as the dimensionless small parameter is given by Jt. However, on the other hand, if the spin dynamics is nearly adiabatic the perturbation will produce a rather weak torque $\boldsymbol{S}_m \times \boldsymbol{S}_m(t')$ and the weak-coupling approach becomes reliable on rather large time-scales $t \gg 1/J$. These assumptions will be checked numerically by a comparison of the LR-SD with the exact QCH-SD in Sec. 5.1.4.

Thirdly, the Landau-Lifshitz-Gilbert equation [Gilbert, 2004; Landau and Lifshitz, 1935] and in particular the Gilbert-damping and the moment of inertia are re-derived. Assuming separation of time-scales, i.e., the classical spin dynamics is slow as compared to the electron dynamics, the LR-SD is simplified further by applying a Markov approximation which results in the Landau-Lifshitz-Gilbert equation. Moreover, it has been demonstrated that the Gilbert damping constant and the moment of inertia are sensitively dependent on the low-energy electronic structure. In particular, the van Hove singularities have the result that the Gilbert damping is ill-defined in the case of an uncorrelated one-dimensional lattice. The same is true for the moment of inertia, which is *not* well-defined in the case of an uncorrelated one- and two-dimensional lattices. However, this conclusion may change for systems where the classical spin is coupled to a correlated electron system. Here the van Hove singularities could be lifted by the finite imaginary part of the conduction-electron self-energy.

Finally, the scaling property of the LLG equation is analyzed. It has been found that the relaxation time scales linearly in S in the large-S limit. The Landau-Lifshitz-Gilbert theory also predicts a linear behavior for the nutation frequency as a function of S.

5 Dynamics of a single impurity coupled to an electron system

In this chapter, we study the real-time dynamics of a single quantum and classical-spin $\boldsymbol{S}$ coupled via an antiferromagnetic local exchange interaction to the local quantum spin of an one-dimensional conduction electron system with open boundary conditions at zero temperatures ($\beta = \infty$). The spin dynamics initiated by suddenly switching the direction of a local magnetic field, is studied by means of the time-dependent density-matrix renormalization group (tDMRG)[4], exact quantum-classical hybrid spin dynamics (QCH-SD) and the linear-response spin dynamics (LR-SD).

In section 5.1, we discuss spin dynamics and relaxation in the classical-spin Kondo-impurity model in terms of the QCH-SD approach [Sayad and Potthoff, 2015]. Section 5.2 is devoted to the study of inertia effects in the real-time dynamics of a classical as well as a quantum spin coupled to a noninteracting conduction electron system [Sayad et al., 2016a]. Here, quantum effects are identified by systematic tDMRG study for different spin quantum numbers S and by comparing with the QCH-SD approach for the classical-spin Kondo model. Finally, in section 5.3, we focus on the relaxation of a classical spin coupled to a Hubbard system as a function of the local Coulomb interaction U [Sayad et al., 2016b]. To this end, we combine the LR-SD approach for the spin dynamics with the tDMRG method for the correlated electron system.

5.1 Relaxation of a classical spin coupled to a Fermi sea

The purpose of the present section[5] is to explore the physics beyond the LR-SD approach and the LLG theory presented in chapter 4.2 and 4.3. To this end, we use the QCH-SD method introduced in chapter 4.1 by which the dynamics of classical spins coupled to a system of noninteracting conduction electrons can be treated numerically exactly.

[4] The time-dependent density-matrix renormalization group code was provided by Roman Rausch.

[5] Major parts of this section have been published as M. Sayad and M. Potthoff: *Spin dynamics and relaxation in the classical-spin Kondo-impurity model beyond the Landau-Lifschitz-Gilbert equation*, New J. Phys. 17, 113058 (2015) -

The theory applies to arbitrary coupling strengths and does not assume a separation of electron and spin time scales. As previously discussed in chapter 4.1, this approach is a quantum-classical hybrid theory [Elze, 2012] which may be characterized as Ehrenfest dynamics, similar to exact numerical treatments of the dynamics of nuclei, treated as classical objects, coupled to a quantum system of electrons (see, e.g., Ref. Marx and Hutter [2009] for an overview). Moreover, the quantum-classical hybrid theory of spin and electron dynamics reveals a precise microscopic picture of the electron dynamics, which can be used to discuss the precession and relaxation dynamics of the spin from another, namely from the electronic perspective. This information is in principle experimentally accessible to spin-resolved scanning-tunnelling microscope techniques [Loth et al., 2010; Morgenstern, 2010; Nunes and Freeman, 1993; Wiesendanger, 2009] and important for an atomistic understanding of nano-spintronics devices [Khajetoorians et al., 2011; Wolf et al., 2001]. Here, we are particularly interested in the physics of the system in the strong-J regime or for a strong field $\boldsymbol{B}$ where the time scales of the spin and the electron dynamics become comparable. This has not yet been explored but could become relevant to understand real-time dynamics in realizations of strong-J Kondo-lattice models by means of ultracold fermionic Yb quantum gases trapped in optical lattices [Cappellini et al., 2014; Scazza et al., 2014].

The obvious numerical advantage of an effective spin-only theory, as given by LLG equations of the form (4.17), is that in solving the equations of motion there is only the time scale of the spins that must be taken care of. As compared to our hybrid theory, much larger time steps and much longer propagation times can be achieved. Opposed to ab-initio approaches [Antropov et al., 1995; Kuneš and Kamberský, 2002b] we therefore consider a simple one-dimensional non-interacting tight-binding model for the conduction-electron degrees of freedom, i.e., electrons are hopping between the nearest-neighboring sites of a lattice. Within this model approach, systems consisting of about 1000 sites can be treated easily, and we can access sufficiently long time scales to study the spin relaxation. An equilibrium state with a half-filled conduction band is assumed as the initial state. The subsequent dynamics is initiated by a sudden switch of a magnetic field coupled to the classical spin. Here, we study a *single* spin, i.e., we consider a classical-spin Kondo-impurity model with antiferromagnetic local exchange coupling J, while the theory itself, as formulated in chapter (3) and (4.1), is general and can be applied to more than a single or even to a large number of spins as well. As compared to the conventional (quantum-spin) Kondo model [Kondo, 1964], the model considered here does not account for the Kondo effect and therefore applies to situations where this is absent or less important, such as for systems with large spin quantum numbers S, strongly anisotropic systems or, as considered here, systems in a strong magnetic field. To estimate the quality of the classical-spin approximation *a priori* is difficult [Delgado et al., 2015; Gauyacq and Lorente, 2014; Sayad et al., 2012]. For one-dimensional systems, however, a quantitative study is possible by comparing with full quantum calculations and will be

discussed in section 5.2.

This section is organized as follows: We first repeat the Hamiltonian and the equations of motion for the exact quantum-classical hybrid dynamics as presented in chapter 3 (and 4.1) for a single classical-spin Kondo model and discuss the numerical setup and computational details in section 5.1.2. A comprehensive analysis of the relaxation of the classical spin after a sudden switch of a magnetic field is provided in section 5.1.3: There, the reversal time as a function of the interaction and the field strength is analyzed in detail. Subsequently, the focus is set on the conduction-electron system which induces the relaxation of the classical spin by dissipation of energy. Sec. 5.1.4 is devoted to the comparison of the LR-SD approach with the QCH-SD. Finally, section 5.1.5 summarizes the results and the main conclusions.

5.1.1 Single classical-spin Kondo model

For a single classical spin $\boldsymbol{S}$ with $|\boldsymbol{S}| = 1/2$, the quantum-classical hybrid Hamiltonian introduced in Eq. (4.1) reads as

$$\mathcal{H} = -T \sum_{\langle ij \rangle, \sigma} c_{i\sigma}^{\dagger} c_{j\sigma} + J \boldsymbol{s}_{i_0} \boldsymbol{S} - \boldsymbol{B} \boldsymbol{S} \,, \tag{5.1}$$

where the classical spin $\boldsymbol{S}$ is coupled via a local exchange interaction of strength J to the local quantum spin $\boldsymbol{s}_{i_0}$ at the site i_0 of a system of N itinerant and non-interacting conduction electrons. The conduction electrons hop with amplitude $-T$ between non-degenerate orbitals on nearest-neighboring sites of a one-dimensional lattice, see Fig. 5.1. Energy and time units are fixed by the nearest-neighbor hopping $T = 1$ throughout this this study. L is the number of lattice sites, and $n = N/L$ is the average conduction-electron density with $N = L$ (half-filling). As usual, $c_{i\sigma}$ annihilates an electron at site $i = 1, ..., L$ with spin projection $\sigma = \uparrow, \downarrow$, and $\boldsymbol{s}_i = \frac{1}{2} \sum_{\sigma\sigma'} c_{i\sigma}^{\dagger} \boldsymbol{\sigma}_{\sigma\sigma'} c_{i\sigma'}$ is the local conduction-electron spin at i, where $\boldsymbol{\sigma}$ denotes the vector of Pauli matrices. The sum runs over the different ordered pairs $\langle ij \rangle$ of nearest neighbors. $\boldsymbol{B}$ is an external magnetic field which couples to the classical spin.

To be definite, an antiferromagnetic exchange coupling $J > 0$ is assumed. If $\boldsymbol{S}$ was a quantum spin with $S = 1/2$, Eq. (5.1) would represent the single-impurity Kondo model [Kondo, 1964]. However, in the case of a classical spin considered here, there is no Kondo effect. The semiclassical single-impurity Kondo model thus applies to systems where a local spin is coupled to electronic degrees of freedom but where the Kondo effect is absent or suppressed. This comprises the case of large spin quantum numbers S, the case of temperatures well above the Kondo scale, or systems with a ferromagnetic Kondo coupling $J < 0$ where, for a classical spin, we expect a qualitatively similar dynamics as for $J > 0$.

We assume that initially, at time $t = 0$, the classical spin $\boldsymbol{S}(t = 0)$ has a certain direction and that the conduction-electron system is in the corresponding ground state,

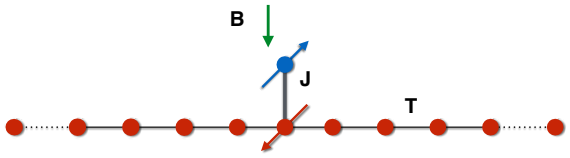

Figure 5.1: Classical spin $\boldsymbol{S}(t)$ coupled via an antiferromagnetic local exchange interaction of strength J to a system of conduction electrons tunneling with nearest-neighbor hopping amplitude T over the sites of a one-dimensional lattice with open boundaries. The spin couples to the central site i_0 of the system and is subjected to a local magnetic field of strength $\boldsymbol{B}$.

i.e., the conduction electrons occupy the lowest N one-particle eigenstates of the non-interacting Hamiltonian Eq. (5.1) for the given $\boldsymbol{S} = \boldsymbol{S}(t=0)$ up to the chemical potential μ. A non-trivial time evolution is initiated if the initial direction of the classical spin and the direction of the field $\boldsymbol{B}$ are non-collinear. In order to analyze the spin dynamics, we revisit the equations of motion for the real-time dynamics of the classical spin and the conduction electron spin as discussed in section 4.1 (or 3.3 with $\langle K_m^{(0)\dagger}\rangle_t = 0$ and $\langle \boldsymbol{K}_m\rangle_t = 0$), which do not change much for the single impurity case:

$$\frac{d}{dt}\boldsymbol{S}(t) = J\langle \boldsymbol{s}_{i_0}\rangle_t \times \boldsymbol{S}(t) - \boldsymbol{B}\times\boldsymbol{S}(t)\,. \tag{5.2}$$

This is the Landau-Lifschitz equation where the expectation value of the conduction-electron spin at i_0 is then again time-dependent, hence $J\langle \boldsymbol{s}_{i_0}\rangle_t$ acts as an effective time-dependent internal field in addition to the external field $\boldsymbol{B}$. The equation of motion for $\langle \boldsymbol{s}_i\rangle_t$ reads as

$$\frac{d}{dt}\langle \boldsymbol{s}_i\rangle_t = \delta_{ii_0} J\boldsymbol{S}(t)\times\langle \boldsymbol{s}_i\rangle_t - T\sum_j^{n.n.}\frac{1}{2i}\sum_{\sigma\sigma'}(\langle c_{i\sigma}^\dagger \boldsymbol{\sigma}_{\sigma\sigma'} c_{j\sigma'}\rangle_t - \text{c.c.})\,, \tag{5.3}$$

where the sum runs over the nearest neighbors of i. The second term on the right-hand side describes the coupling of the local conduction-electron spin to its environment and the dissipation of spin and energy into the bulk of the system (see below). Finally, the system of equations of motion can be closed by considering the complete one-particle density matrix $\varrho(t)$, which also determines the real-time dynamics of the electronic subsystem. As preliminary discussed in section 2.3.2, the one-particle density matrix obeys a von Neumann equation of motion,

$$i\frac{d}{dt}\varrho(t) = [\mathcal{T}^{\mathcal{H}}(\varrho(t)), \varrho(t)]_-\,, \tag{5.4}$$

where the initial condition $\varrho(0) = 1/(e^{\beta(\mathcal{T}^{\mathcal{B}})}+1)$ has to be determined in a self-consistent scheme as presented in section 3.2. Furthermore, the effective hopping matrix $\mathcal{T}^{\mathcal{H}} =$

$T + \Sigma^{\text{HF}}(t)$ as defined in Eq. (3.11) is simplified significantly for a classical spin:

$$\begin{aligned} \mathcal{T}^{(\text{cc})}_{ii'\sigma\sigma'}(t) &= -T\delta_{\langle ii'\rangle}\delta_{\sigma\sigma'} + \delta_{ii_0}\delta_{i'i_0}\frac{J}{2}(\boldsymbol{S}(t)\boldsymbol{\sigma})_{\sigma\sigma'} \,, \\ \mathcal{T}^{(\text{ff})}_{\sigma\sigma'}(t) &= \frac{J}{2}\big((\langle \boldsymbol{s}_{i_0}\rangle_t - \boldsymbol{B})\boldsymbol{\sigma}\big)_{\sigma\sigma'} \,. \end{aligned} \tag{5.5}$$

Note that the effective hopping matrix for the initial state given by $\mathcal{T}^{\mathcal{B}} = T + \Sigma^{\text{HF}}$ is the same matrix as $\mathcal{T}^{\mathcal{H}}$, but with time-independent self-energy contribution Σ^{HF} and different parameters J_{ini} and $\boldsymbol{B}_{ini}$ stemming from the Hamiltonian $\mathcal{B}$ describing the systems initial state. As previously mentioned in section 4.1, for the classical spin Kondo model, the charge and spin hybridization terms $\langle K^{(0)}_m\rangle_t = 0$ and $\langle \boldsymbol{K}_m\rangle_t = 0$ vanish, consequently $\mathcal{T}^{(\text{cf})} = 0$ is also zero, as evident from Eqs. (3.11) and (3.8).

As is obvious from the equations of motion, the real-time dynamics of the quantum-classical Kondo-impurity model on a lattice with a finite but large number of sites L can be treated numerically exactly. In the following we will discuss in detail the numerical setup and some computational details.

5.1.2 Numerical setup and computational details

Eqs. (5.2), (5.3) and (5.4) represent a coupled non-linear system of first-order ordinary differential equations which can be solved numerically. By blocking up the von Neumann equation (5.4), the differential equations are written in a standard form $\dot{\boldsymbol{y}} = \boldsymbol{f}(\boldsymbol{y}(t), t)$, where $\boldsymbol{y}(t)$ is a high-dimensional vector, such that an explicit Runge-Kutta method can be applied. A high-order propagation technique is used [Verner, 2010] which provides the numerically exact solution up to 6-th order in the time step Δt. For a typical system consisting of about $L = 10^3$ sites, about $\sim 10^6$ coupled equations must be solved for each time step.

We consider a one-dimensional system with open boundaries consisting of $L = 1001$ sites and a local perturbation at the central site i_0 of the system, see Fig. 5.1. For a half-filled tight-binding conduction band, the Fermi velocity $v_{\text{F}} = 2T$ roughly determines the maximum speed of the excitations and defines a "light cone" [Bravyi et al., 2006; Lieb and Robinson, 1972]. This means that finite-size effects due to scattering at the system boundaries become relevant after a propagation time $t_{\max} \sim 500$ (in units of $1/T$). A time step $\Delta t = 0.1$ is usually sufficient for reliable numerical results up to $t_{\max}$, i.e., about 5000 time steps are performed. The computational cost is moderate, and calculations can be performed in a few hours on a standard desktop computer.

Assuming, for example, that $\boldsymbol{B} = (0, 0, B)$, the Hamiltonian is invariant under rotations around the z axis. It is then easily verified that not only is the length of the spin $|\boldsymbol{S}| = 1/2$ conserved, but also the total number of conduction electrons,

$$N_{\text{tot}} = \sum_{i\sigma}\langle c^\dagger_{i\sigma}c_{i\sigma}\rangle \,, \tag{5.6}$$

the z-component of the total spin,

$$S_{\mathrm{tot,z}} = S_z + \sum_i \langle s_{iz} \rangle \,, \tag{5.7}$$

as well as the total energy,

$$E_{\mathrm{tot}} = \langle H \rangle = \mathrm{tr}\left(\boldsymbol{\rho}(t)\boldsymbol{T}(t)\right) - \boldsymbol{B}\boldsymbol{S}(t) \,. \tag{5.8}$$

The conservation of the above-mentioned global observables serves as a sensitive check for the accuracy of the numerical procedure.

5.1.3 Coupled spin and electron dynamics

Spin relaxation. Fig. 5.2 shows the real-time dynamics of the classical spin for $J = 1$. Initially, for $t = 0$, the spin is oriented (almost) *antiparallel* to the external local field $\boldsymbol{B} = (0, 0, B)$ with $B = 1$, i.e., initially $S_x(0) = \frac{1}{2}\sin\vartheta$, $S_y(0) = 0$, $S_z(0) = -\frac{1}{2}\cos\vartheta$ where a non-zero but small polar angle $\vartheta = \pi/50$ is necessary to slightly break the symmetry of the initial state and to initialize the dynamics.

For the same setup, the Landau-Lifschitz-Gilbert equation would essentially predict two effects: first, a precession of the classical spin around the field direction with Larmor frequency $\omega_L = B_z$, and second, a relaxation of the spin to the equilibrium state with $\boldsymbol{S}$ *parallel* to $\boldsymbol{B} \sim B\boldsymbol{e}_z$ for $t \to \infty$. Both effects are also found in the full dynamics of the quantum-classical hybrid model. The frequency of the oscillation of $S_x(t)$ that is seen in Fig. 5.2 is ω_L, and S_z is reversed after a few hundred time units. The precessional motion is easily explained by the torque on the spin exerted by the field according to Eq. (5.2). The explanation of the damping effect is more involved:

Even for the high field strength considered here, the spin dynamics is slow as compared to the characteristic electronic time scale such that it could be reasonable to assume the electronic system being in its instantaneous ground state at any instant of time and corresponding to the configuration of the classical spin. This, however, would imply that the expectation value $\langle \boldsymbol{s}_{i_0} \rangle_t$ of the local conduction-electron moment at i_0 is always strictly parallel to $\boldsymbol{S}(t)$ and, hence, there would not be any torque mediated by the exchange coupling J on $\boldsymbol{S}(t)$.

In fact, the direction of $\langle \boldsymbol{s}_{i_0} \rangle_t$ is always somewhat *behind* the "adiabatic direction", i.e., behind $-\boldsymbol{S}(t)$: This is shown in Fig. 5.3 for a field of strength $B = 0.1$ where the spin dynamics is by a factor 10 slower, compared to Fig. 5.2, and for different stronger exchange couplings J. Even in this case the process is by no means adiabatic, and the angle $\gamma(t)$ between $\boldsymbol{S}(t)$ and $\langle \boldsymbol{s}_{i_0} \rangle_t$ is close to but clearly smaller than $\gamma = \pi$ at any instant of time. This non-adiabaticity results from the fact that the motion of the classical spin affects the conduction electrons in a retarded way, i.e., it takes a finite time until the local conduction-electron spin $\langle \boldsymbol{s}_{i_0} \rangle_t$ at i_0 reacts to the motion of the classical spin.

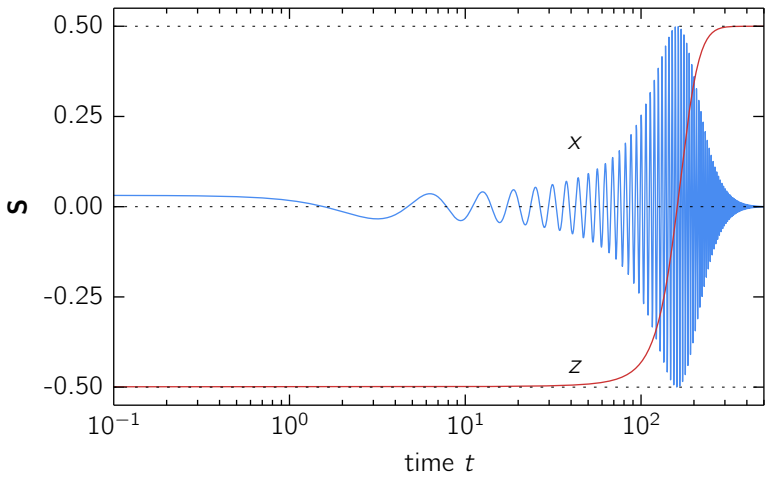

Figure 5.2: Real-time dynamics of the classical spin: x and z components of $\boldsymbol{S}(t)$ ($|\boldsymbol{S}| = 1/2$) are shown. Calculations for exchange coupling $J = 1$ and field strength $B = 1$ and for a system of $L = 1001$ sites. ($L = 1001$ is kept fixed for the rest of the section 5.1). Energy and time units are fixed by the nearest-neighbor hopping $T = 1$.

This retardation effect results in a torque $J\langle \boldsymbol{s}_{i_0}\rangle_t \times \boldsymbol{S}(t) \neq 0$ exerted on the classical $\boldsymbol{S}(t)$ in the $+z$ direction which adds to the torque due to $\boldsymbol{B}$ and which drives the spin to its new equilibrium direction. Hence, retardation is the physical origin of the Gilbert spin damping.

With increasing time, the deviation of $\gamma(t)$ from the instantaneous equilibrium value $\gamma = \pi$ increases in magnitude, i.e., the direction of $\langle \boldsymbol{s}_{i_0}\rangle_t$ is more and more behind the adiabatic direction, and the torque increases. Its magnitude is at a maximum at the same time when the oscillating x, y components of $\boldsymbol{S}(t)$ are at a maximum (see Fig. 5.2). The z-component of the torque does not vanish before the spin has reached its new equilibrium position $\boldsymbol{S}(t) \propto \boldsymbol{e}_z$.

Fig. 5.3 shows results for different J. Generally, non-adiabatic effects show up if the typical time scale of the dynamics is faster than the relaxation time, i.e., the time necessary to transport the excitation away from the location i_0 where it is created initially. Roughly, this time scale is set by the inverse hopping $1/T$. One therefore expects that for fixed $T = 1$, a stronger J implies a stronger retardation of the conduction-electron dynamics. The results for different J shown in Fig. 5.3 in fact show that the maximum deviation of $\gamma(t)$ from the adiabatic direction $\gamma = \pi$ increases with increasing J (for very strong J the dynamics becomes much more complicated, see below). This results in a stronger torque on $\boldsymbol{S}(t)$ in z direction and thus in a stronger damping. The picture is also qualitatively consistent with the LLG equation, as the Gilbert damping constant α increases with J.

The spin (almost) reverses its direction after a finite reversal time τ which is shown in Fig. 5.4 (left panel) as a function of J. Calculations have been performed for an initial

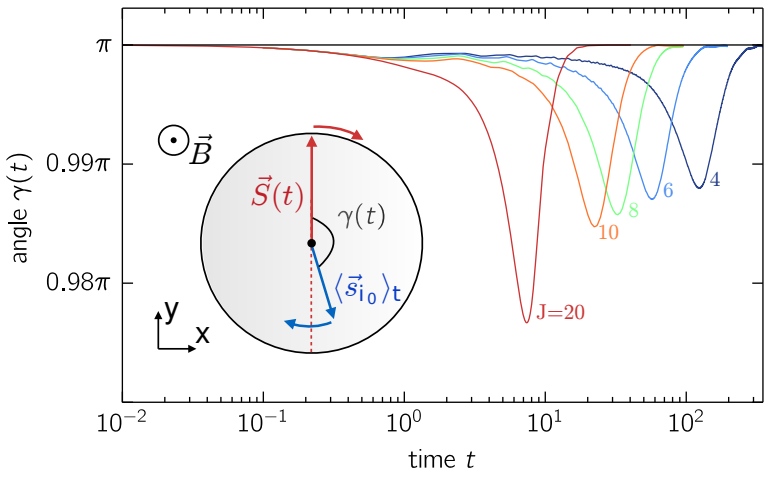

Figure 5.3: Time dependence of the angle $\gamma(t)$ enclosed by $\boldsymbol{S}(t)$ and $\langle \boldsymbol{s}_{i_0} \rangle_t$ for $B = 0.1$ and different J as indicated.

direction of the classical spin with $S_z(0) = -(1/2)\cos\vartheta$ with two different polar angles $\vartheta_{1,2}$. If ϑ is sufficiently small, the results for different ϑ are expected to differ by a J- and B- independent constant factor only. As Fig. 5.4 (left panel) demonstrates, the ratio τ_1/τ_2 is in fact nearly constant. For weak J and up to coupling strengths of about $J \lesssim 30$, we find that the reversal time decreases with increasing J. With increasing J, the retardation effect increases, as discussed above, and the stronger damping results in a shorter reversal time.

The prediction of the LLG equation for the reversal time of a single spin τ can be derived analytically [Kikuchi, 1956] and is given by

$$\tau \propto \frac{1+\alpha^2}{\alpha}\frac{1}{B}\ln\left|\frac{1/2 - S_z(0)}{1/2 + S_z(0)}\right| . \tag{5.9}$$

However, down to the smallest J for which τ can be calculated reliably, our results for the full spin dynamics do not scale as $\tau \propto 1/J^2$ as one would expect for weak J assuming that $\alpha \propto J^2$ (see discussion in Sec. 4.3).

The B dependence of the reversal time is shown in Fig. 5.4 (right panel). With increasing field strength, the classical spin $\boldsymbol{S}(t)$ precesses with a higher Larmor frequency $\omega_L \approx B$ around the z axis. Hence, non-adiabatic effects increase. The stronger the field, the more delayed is the precessional motion of the local conduction-electrons spin $\langle \boldsymbol{s}_{i_0} \rangle_t$. This results in a stronger torque in $+z$ direction exerted on the classical spin. Therefore, the relaxation is faster and the reversal time τ smaller. For weak and intermediate field strengths, τ is roughly proportional to $1/B$. This is consistent with the prediction of the LLG equation, see Eq. (5.9).

In the limit of very strong fields one would expect an increase of the reversal time with increasing B since the field term will eventually dominate the dynamics, i.e., only the

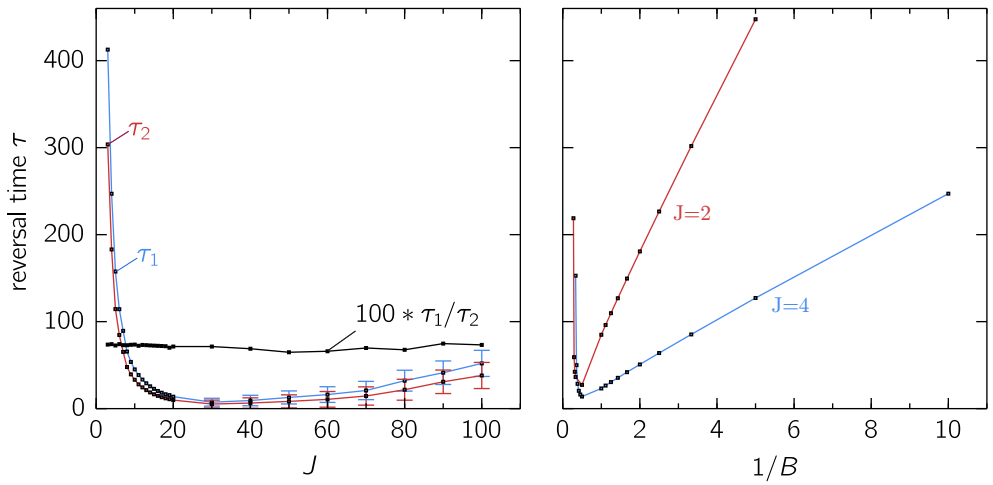

Figure 5.4: *Left panel:* Time for a spin reversal $S_z = \frac{1}{2}\cos(\pi - \vartheta) = -\frac{1}{2}\cos(\vartheta) \to S_z = \frac{1}{2}\cos(\vartheta)$ for $\vartheta = \vartheta_1 = \pi/50$ (reversal time τ_1) and for $\vartheta = \vartheta_2 = \pi/25$ (reversal time τ_2). Calculations as a function of J for fixed $B = 0.1$. *Right panel:* Reversal time τ_1 as function of $1/B$ for fixed $J = 2$ and $J = 4$ as indicated.

precessional motion survives which implies a diverging reversal time. In fact, for a field strength exceeding a critical strength B_c, which depends on J, there is no full relaxation any longer, and $\tau = \infty$. This strong-B regime cannot be captured by the LLG equation and deserves further studies.

The strong-J regime is interesting as well. For coupling strengths exceeding $J \approx 30$ the reversal time *increases* with J (see Fig. 5.4, left panel). Eventually, the reversal time must even diverge. This is obvious, as the dynamics is described by a simple two-spin model in the limit $J = \infty$ which cannot show spin relaxation. The corresponding equations of motion are obtained from Eqs. (5.2) and (5.3) by setting $T = 0$ and $\boldsymbol{B} = 0$:

$$\begin{aligned} \frac{d}{dt}\boldsymbol{S}(t) &= J\langle \boldsymbol{s}_{i_0}\rangle_t \times \boldsymbol{S}(t)\,, \\ \frac{d}{dt}\langle \boldsymbol{s}_{i_0}\rangle_t &= J\boldsymbol{S}(t) \times \langle \boldsymbol{s}_{i_0}\rangle_t\,. \end{aligned} \tag{5.10}$$

Note that we have $|\langle \boldsymbol{s}_{i_0}\rangle_t| = 1/2$ for $J \to \infty$. The equations are easily solved by exploiting the conservation of the total spin $\boldsymbol{S}_{\rm tot} = \boldsymbol{S}(t) + \langle \boldsymbol{s}_{i_0}\rangle_t$. Both spins precess with constant frequency $\omega_0 = JS_{\rm tot}$ around $\boldsymbol{S}_{\rm tot}$. Their components parallel to $\boldsymbol{S}_{\rm tot}$ are equal, and their components perpendicular to $\boldsymbol{S}_{\rm tot}$ are anti-parallel and of equal length.

However, the two-spin dynamics of the $J = \infty$ limit is not stable against small perturbations. Fig. 5.5 shows the classical spin dynamics of the full model (with $T = 1$ and $B = 0.1$) for a very strong but finite coupling $J = 100$. Here, the motion of the classical spin gets very complicated as compared with the highly regular behavior in the weak-J regime (cf. Fig. 5.2). In particular, the z-component of $\boldsymbol{S}(t)$ is oscillating on nearly the

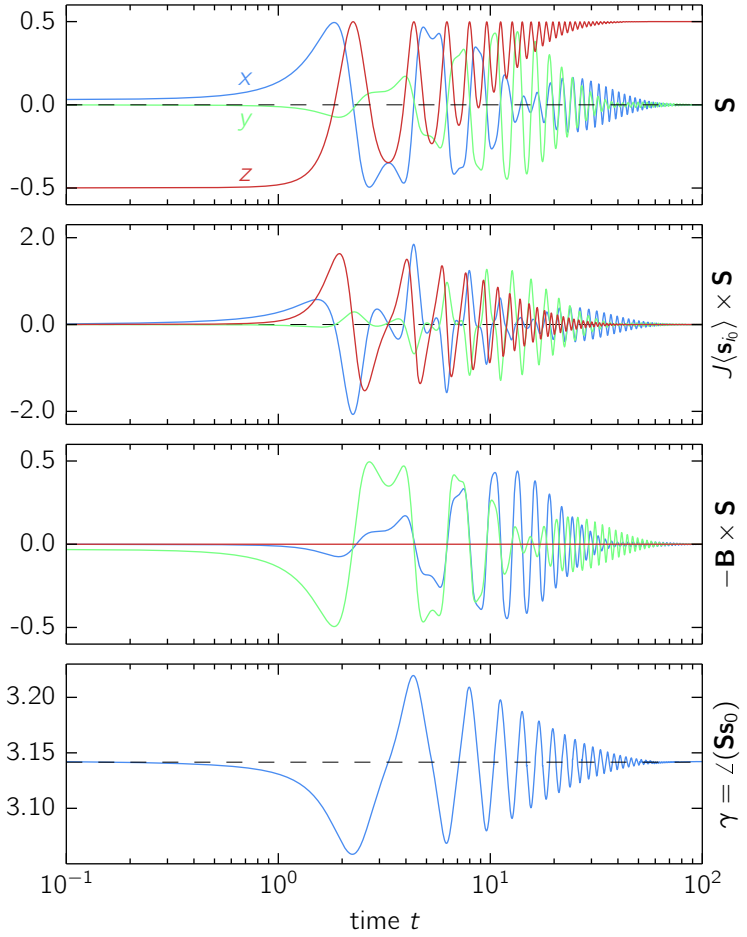

Figure 5.5: Real-time dynamics in the strong-J regime: $J = 100$ and $B = 0.1$. *First panel:* Classical spin $\boldsymbol{S}(t)$. *Second panel:* Torque on $\boldsymbol{S}(t)$ due to the exchange interaction. *Third panel:* Torque on $\boldsymbol{S}(t)$ due to the field term. *Fourth panel:* Angle enclosed by $\boldsymbol{S}(t)$ and $\langle \boldsymbol{s}_{i_0} \rangle_t$.

same scale as the x and y components. This characteristic time scale $\Delta t \approx 4$ of the oscillation corresponds to a frequency $\omega \approx 1.5$ which differs by more than an order of magnitude from both, the Larmor frequency $B = 0.1$ and from the exchange-coupling strength $J = 100$. Note that the oscillation of $S_z(t)$ is actually the reason for the ambiguity in the determination of the precise reversal time and gives rise to the error bars in Fig. 5.4 (left panel) for strong J.

We attribute the complexity of the dynamics to the fact that the torque due to the field term and the torque due to the exchange coupling are of comparable magnitudes, see second and third panel in Fig. 5.5. It is interesting that even for strong J, where one would expect $\boldsymbol{S}(t)$ and $\langle \boldsymbol{s}_{i_0} \rangle_t$ to form a tightly bound local spin-zero state, there is actually

a small deviation from perfect antiparallel alignment, i.e., $\gamma(t) \neq \pi$, as can be seen in the fourth panel of Fig. 5.5. This results in a finite z-component of the torque on $\boldsymbol{S}(t)$ which leads to a very fast reversal with $S_z(t) \approx +0.5$ at time $t \approx 2.1$. Contrary to the weak-coupling limit, however, the z-component of the torque changes sign at this point and drives the spin back to the $-z$-direction. At $t \approx 3.2$, however, the z-component of $\boldsymbol{S}(t)$ once more reverses its direction. Here, the torque due to the exchange coupling vanishes completely as $\boldsymbol{S}(t)$ and $\langle \boldsymbol{s}_{i_0} \rangle_t$ are perfectly antiparallel (see the first zero of $\gamma(t)$ in the fourth panel). The motion continues due to the non-zero field-induced torque. This pattern repeats several times. $\boldsymbol{S}(t)$ mainly oscillates within a plane including and slowly rotating around the z-axis.

Eventually, there is a perfect relaxation of the classical spin for large t but in a very different way as compared to the weak-coupling limit. While the deviation from $\gamma = \pi$ is small at any instant of time as for weak J, the most apparent difference is perhaps that the new ground state is approached with an oscillating behavior of $\gamma(t)$ around $\gamma = \pi$, i.e., $\langle \boldsymbol{s}_{i_0} \rangle_t$ may run behind or *ahead of* $\boldsymbol{S}(t)$ as well. This behavior is identified as an inertia effect, which is well known in classical spin dynamics [Kikuchi and Tatara, 2015] and can be described by an additional term to the standard LLG equation with second-order time-derivative of the spin (see, e.g., Bhattacharjee et al. [2012]). Inertia effects will be discussed in depth in Sec. 5.2.

At this point, we summarize the main differences between the quantum-classical hybrid and the effective LLG dynamics of the classical spin: For weak J and B, the qualitative behavior, precessional motion and relaxation, is the same in both approaches. Quantitatively, however, the LLG equation is inconsistent with the observed J dependence of the reversal time when assuming $\alpha \propto J^2$. The B dependence of $1/\tau$ is linear as expected from the LLG approach. For strong J, the spin dynamics qualitatively differs from standard LLG dynamics and gets more complicated with a new time scale emerging. Absence of complete relaxation, as observed in the strong-B limit, is also not accessible to the LLG theory.

Energy dissipation. To complete the picture of the relaxation dynamics of the classical spin, the discussion should also comprise the dynamics of the electronic degrees of freedom. The spin relaxation must be accompanied by a dissipation of energy and spin into the bulk of the electronic system since the total energy and the total spin are conserved quantities, see Eqs. (5.7) and (5.8), while conservation of the total particle number, Eq. (5.6), is trivially ensured by the particle-hole symmetric setup considered here where the average conduction-electron number at every site is time-independent: $\sum_\sigma \langle n_{i\sigma} \rangle_t = 1$.

The total energy is given by $E_{\mathrm{tot}} = \langle H \rangle$, see Eq. (5.8), and is a sum over different contributions, $E_{\mathrm{tot}} = E_{\mathrm{B}}(t) + E_{\mathrm{hop}}(t) + E_{\mathrm{int}}(t)$, namely the interaction energy with the field

$$E_{\mathrm{B}}(t) = -\boldsymbol{B}\boldsymbol{S}(t)\,, \tag{5.11}$$

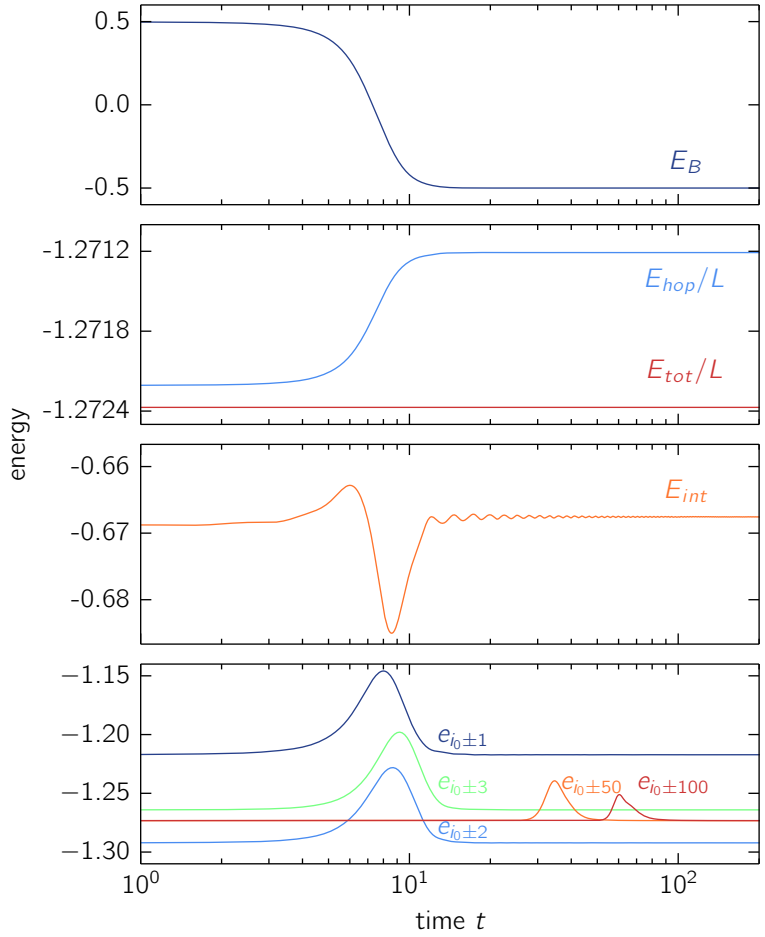

Figure 5.6: Different contributions to the total energy as functions of time for $J = 5$ and $B = 1$. *Top panel*: E_{B}, energy of the classical spin in the external field. *Second panel*: E_{hop}/L, kinetic (hopping) energy of the conduction-electron system per site, and E_{tot}/L, total energy per site. *Third panel*: E_{int}, exchange-interaction energy. The fourth panel shows the time-dependence of the total-energy density at different distances from the site i_0.

the kinetic (hopping) energy of the conduction-electron system

$$E_{\mathrm{hop}}(t) = -T \sum_{\langle ij \rangle} \sum_{\sigma} \langle c^{\dagger}_{i\sigma} c_{j\sigma} \rangle_t \ , \tag{5.12}$$

and the exchange-interaction energy

$$E_{\mathrm{int}}(t) = J \langle \boldsymbol{s}_{i_0} \rangle_t \boldsymbol{S}(t) \ . \tag{5.13}$$

The time dependence of those contributions is shown in Fig. 5.6 for $J = 5$ and $B = 1$. The top panel of Fig. 5.6 shows that the system releases the interaction energy $|2\boldsymbol{BS}|$

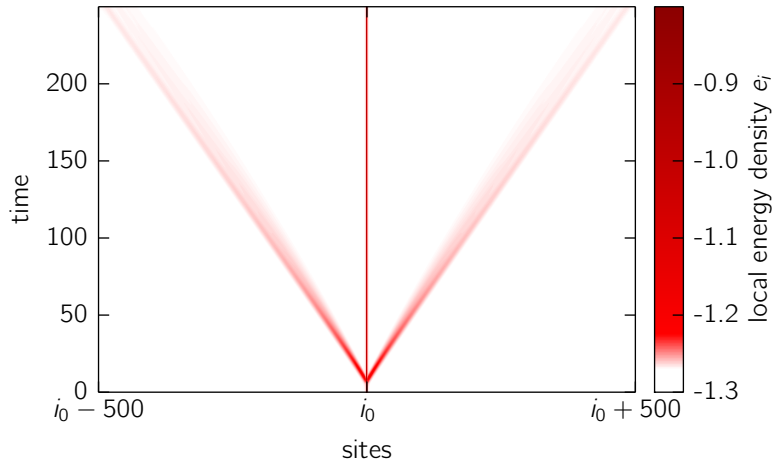

Figure 5.7: Spatiotemporal evolution of the total-energy density $e_i(t)$, as defined in Eq. (5.14). Calculation for $J = 5$, $B = 1$.

of the classical spin in the external field by aligning the spin to the field direction. In the long-time limit, this energy is stored in the conduction-electron system: The average kinetic energy per site ($L = 1001$) increases by the same amount as shown in the second panel (note the different scales). The exchange-interaction energy changes with time but is the same for $t = 0$ and $t \to \infty$ (see third panel). The total energy is constant as can be observed from the second panel.

The relaxation of the classical spin in the external field $\boldsymbol{B}$ implies an energy flow away from the site i_0 into the bulk of the conduction-electron system such that *locally*, in the vicinity of i_0 the system is in its new ground state. To discuss this energy flow, it is convenient to consider the total energy as a lattice sum $E_{\mathrm{tot}} = \sum_i e_i(t)$ over the total energy "density" defined as

$$e_i(t) = -T \sum_{j}^{\mathrm{n.n.}(i)} \sum_{\sigma} \langle c_{i\sigma}^{\dagger} c_{j\sigma} \rangle_t + \delta_{ii_0} (J \langle \boldsymbol{s}_{i_0} \rangle_t - \boldsymbol{B}) \boldsymbol{S}(t) \,, \tag{5.14}$$

where the sum over j runs over the nearest neighbors of site i. The time dependence of the energy density in the vicinity of i_0 and at distances 50 and 100 is shown in the fourth panel of Fig. 5.6.

At any site in the conduction-electron system, the energy density increases from its ground-state value, reaches a maximum and eventually relaxes to the energy density of the new ground state. Since the latter is just the ground state with the reversed classical spin, the new ground-state energy density is the same as in the initial state at $t = 0$. As can be seen in the fourth panel of Fig. 5.6, there is also a slight spatial oscillation of the ground-state energy density which just reflects the Friedel oscillations around the impurity at i_0.

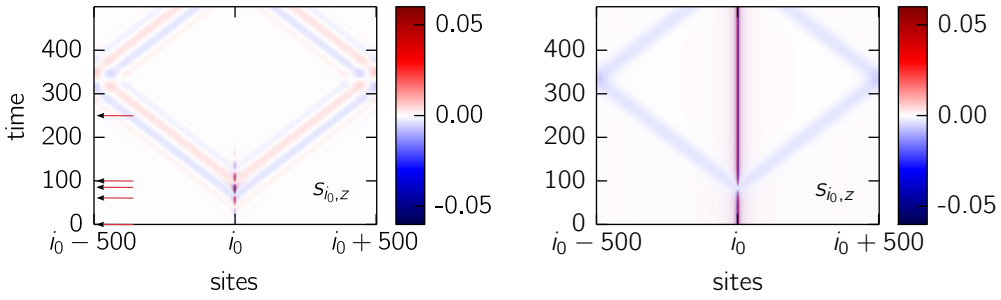

Figure 5.8: Spatiotemporal evolution of the total-spin density $\langle \boldsymbol{s}_i \rangle_t$ (left panel: x-component, right panel z-component) for $J = 5$ and $B = 0.1$. See Fig. 5.9 for snapshots at times indicated by the arrows.

Complete relaxation means that the excitation energy is completely removed from the vicinity of i_0 and transported into the bulk of the system. That this is in fact the case as can be seen by comparing the energy density at different distances from i_0. It is also demonstrated by Fig. 5.7 which visualizes the energy-current density which symmetrically points away from i_0: The total energy of the excitation flowing through each pair of sites $i_0 \pm \Delta i$ is constant, i.e., the time-integrated energy flux, $\int dt\, e_i(t)$ is the same for all lattice sites i.

As is seen in Fig. 5.6 (fourth panel) and Fig. 5.7, there is a considerable dispersion of the excitation wave packet carrying the energy. For example, at i_0+100 it takes more than four times longer, as compared to $i_0 + 1$, until most of the excitation has passed through (note the logarithmic time scale).

The broadening of the wave packet, due to dispersion, is asymmetric and bound by an upper limit for the speed of the excitation which is roughly set by the Fermi velocity $v_\mathrm{F} = 2T$. This Lieb-Robinson bound [Bravyi et al., 2006; Lieb and Robinson, 1972] determines the "light cone" seen in Fig. 5.7.

Spin dissipation. The same upper speed limit, given by the Fermi velocity of the conduction-electron system, is also seen in the spatiotemporal evolution of the conduction-electron spin density $\langle \boldsymbol{s}_i \rangle_t$. This is shown in Fig. 5.8 for a different magnetic field strength $B = 0.1$ where the classical spin dynamics is slower. Apparently, the wave packet of excitations emitted from the impurity not only carries energy but also spin. It symmetrically propagates away from i_0 and, at $t \approx 300$, reaches the system boundary where it is reflected perfectly. Up to $t = 500$ there is hardly any effect visible in the local observables close to i_0 that is affected by the finite system size.

Snapshots of the conduction-electron spin dynamics are shown in Fig. 5.9 for the initial state at $t = 0$ and for states at four later times $t > 0$ which are also indicated by the arrows in Fig. 5.8. At $t = 0$ the conduction-electron system is in its ground state for the given initial direction of the classical spin. The latter basically points into the $-z$ direction, apart

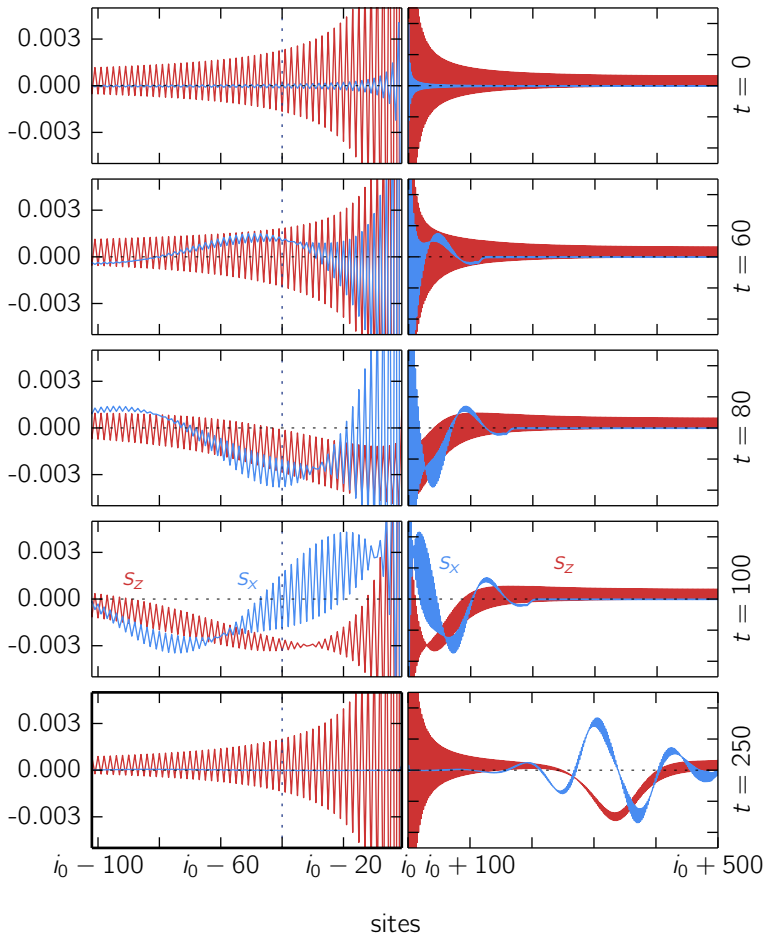

Figure 5.9: Snapshots of the conduction-electron magnetic moments $\langle \boldsymbol{s}_i \rangle_t$ at different times t as indicated on the right and by the corresponding arrows in Fig. 5.8. Red lines: z-components of $\langle \boldsymbol{s}_i \rangle_t$. Blue lines: x-components. The profiles are perfectly symmetric to the impurity site $i = i_0$ but displayed up to distances $|i - i_0| \leq 100$ on the left-hand side and up to the system boundary, $|i - i_0| \leq 500$, on the right-hand side. Parameters $J = 5, B = 0.1$.

from a small positive x-component ($\vartheta = \pi/50$) which is necessary to break the symmetry of the problem and to initiate the dynamics. This tiny effect will be disregarded in the following.

From the perspective of the conduction-electron system, the interaction term $J\boldsymbol{S}\boldsymbol{s}_{i_0}$ acts as a local external magnetic field $J\boldsymbol{S}$ which locally polarizes the conduction electrons at i_0. Since J is antiferromagnetic, the local moment $\langle \boldsymbol{s}_{i_0} \rangle$ points into the $+z$ direction. At half-filling, the conduction-electron system exhibits pronounced antiferromagnetic spin-spin correlations which give rise to an antiferromagnetic spin-density wave

structure aligned to the z axis at $t = 0$, see first panel of Fig. 5.9.

The total spin $\boldsymbol{S}_{\rm tot} = 0$ at $t = 0$, i.e., the classical spin $\boldsymbol{S}$ is exactly compensated by the total conduction-electron spin $\langle \boldsymbol{s}_{\rm tot} \rangle = \sum_i \langle \boldsymbol{s}_i \rangle = -\boldsymbol{S}$ in the ground state. This can be traced back to the fact that for a $D = 1$-dimensional tight-binding system with an odd number of sites L, with $N = L$ and with a single static magnetic impurity, there is exactly one localized state per spin projection σ, irrespective of the strength of the impurity potential (here given by $J\boldsymbol{S} = 0.5J\boldsymbol{e}_z$). The number of spin-up one-particle eigenstates therefore exceeds the number of spin-down states by exactly one.

Since the energy of the excitation induced by the external field $\boldsymbol{B}$ is completely dissipated into the bulk, the state of the conduction-electron system at large t (but shorter than $t \approx 500$ where finite-size effects appear) must locally, close to i_0, resemble the conduction-electron ground state for the reversed spin $\boldsymbol{S} = +0.5\boldsymbol{e}_z$. This implies that locally all magnetic moments $\langle \boldsymbol{s}_i \rangle_t$ must reverse their direction. In fact, the last panel in Fig. 5.9 (left) shows that the new spin configuration is reached for $t = 250$ at sites with distance $|i - i_0| \lesssim 100$, see dashed line, for example. For later times the spin configuration stays constant (until the wave packet reflected from the system boundaries reaches the vicinity of i_0). The reversal is almost perfect, e.g., $\langle \boldsymbol{s}_{i_0} \rangle_{t=0} = 0.2649 \rightarrow \langle \boldsymbol{s}_{i_0} \rangle_{t \geq 250} = -0.2645$. Deviations of the same order of magnitude are also found at larger distances, e.g., $i = i_0 - 100$. We attribute those tiny effects to a weak dependence of the local ground state on the non-equilibrium state far from the impurity at $t = 250$, see right part of the last panel in Fig. 5.9.

The other panels in Fig. 5.9 demonstrate the mechanism of the spin reversal. At short times (see $t = 60$, second panel) the perturbation of the initial equilibrium configuration of the conduction-electron moments is still weak. For $t = 80$ and $t = 100$ one clearly notices the emission of the wave packet starting. Locally, the antiferromagnetic structure is preserved (see left part) but superimposed on this, there is an additional spatial structure of much longer size developing. This finally forms the wave packet which is emitted from the central region. Its spatial extension is about $\Delta \approx 300$ as can be estimated for $t = 250$ (last panel on the right) where it covers the region $200 \lesssim i \lesssim 500$. The same can be read off from the upper part of Fig. 5.8. Assuming that the reversal of each of the conduction-electron moments takes about the same time as the reversal of the classical spin, Δ is roughly given by the reversal time times the Fermi velocity and therefore strongly depends on J and B. For the present case, we have $\tau_1 \approx 150/T$ which implies $\Delta \approx 150 \times 2 = 300$ in rough agreement with the data.

In the course of time, the long-wavelength structure superimposed on the short-range antiferromagnetic texture develops a node. This can be seen for $t = 100$ and $i \approx 40$ (fourth panel, see dashed line). The node marks the spatial border between the new (right of the node, closer to i_0) and the original antiferromagnetic structure of the moments and moves away from i_0 with increasing time.

At a fixed position i, the reversal of the conduction-electron moment $\langle \boldsymbol{s}_i \rangle_t$ takes place

in a similar way as the reversal of the classical spin (see both panels in Fig. 5.8 for a fixed i). During the reversal time, its x- and y-components undergo a precessional motion while the z-component changes sign. Note, however, that *during* the reversal $|\langle \boldsymbol{s}_i \rangle|$ gets much larger than its value in the initial and in the final equilibrium state.

5.1.4 Comparison with linear-response spin dynamics

As preliminary discussed in section 4.2, the Eqs. (5.2) and (5.3) do not form a closed set of equations of motion but must be supplemented by the full equation of motion for the one-particle conduction-electron density matrix (5.4). Moreover, under certain circumstances, e.g., separation of time scales (i.e. fast electron and much slower spin dynamics) it is advantageous with respect to computational cost to integrate out the conduction-electron degrees of freedom altogether by using standard linear-response theory in the weak-J limit [Negele and Orland, 1998]. For a single spin, the Eqs. (4.7) and (4.8) are simplified and read as:

$$\frac{d}{dt}\boldsymbol{S}(t) = \boldsymbol{S}(t) \times \boldsymbol{B} - J^2 \boldsymbol{S}(t) \times \int_0^t dt' \, \underline{\chi}^{(\mathrm{ret})}(t-t') \cdot \boldsymbol{S}(t') \, , \tag{5.15}$$

where the free ($J = 0$) local retarded spin susceptibility of the conduction electrons $\underline{\chi}^{(\mathrm{ret})}(t,t')$, which can be interpreted as an effective retarded self-interaction of the spin, is a tensor with elements

$$\chi^{(\mathrm{ret})}_{\alpha\beta}(t,t') = -i\Theta(t-t')\langle [s^{\alpha}_{i_0}(t), s^{\beta}_{i_0}(t')] \rangle \, , \tag{5.16}$$

with $\alpha, \beta = x, y, z$. The equation of motion for the classical spin Eq. (5.15) has a temporally nonlocal structure and includes an effective interaction of the classical spin at time $\boldsymbol{S}(t)$ with the same classical spin at earlier times $t' < t$. In the full quantum-classical theory where the electronic degrees of freedom are taken into account exactly, this retarded interaction is mediated by a non-equilibrium electron dynamics starting at site i_0 and time t' and returning back to the same site i_0 at time $t > t'$. Unfortunately, a simple effective spin-only action can be obtained in the weak-coupling (small-J) limit only [Zhang and Li, 2004]. Hence, we expect that the perturbative spin-only theory breaks down after a propagation time $t \sim 1/J$ at the latest, as Jt is the dimensionless small parameter. This implies that the fast electron dynamics must be taken into account explicitly even if the spin dynamics is much slower.

In the following, we study deviations of the perturbative LR-SD approach from the exact QCH-SD numerically. To this end, the integro-differential Eq. (5.15) that is obtained in first-order-in-J perturbation is solved numerically as described in section 4.2. We assume that the initial state at $t = 0$ is given by the conduction-electron system in its ground state or in thermal equilibrium and an arbitrary state of the classical spin. This

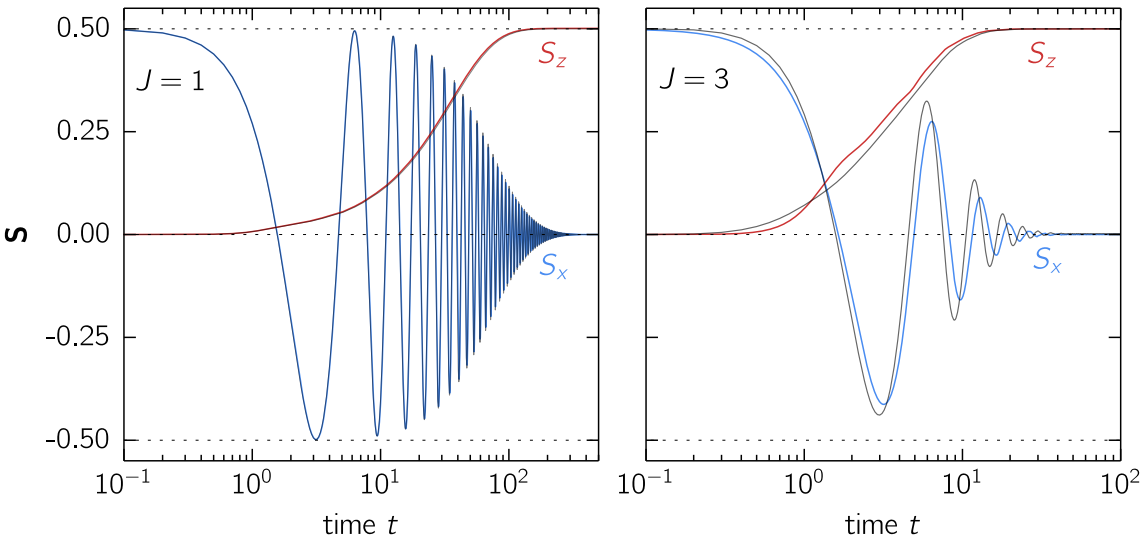

Figure 5.10: Left panel: Components $S_x(t)$ and $S_z(t)$ of the classical spin after a sudden switch of the field from x- to z-direction at $t = 0$. Calculations for $B = 1$ and $J = 1$ (left panel) and $J = 3$ (right panel). Colored lines: results of the LR-SD, Eq. (5.15). Black lines: results of the exact QCH-SD for $L = 1001$.

may be realized formally by suddenly switching on the interaction $J(t)$ at time $t = 0$, i.e., $J(t) = J\Theta(t)$ and by switching the local field from some initial value $\boldsymbol{B}_{\rm ini}$ at $t = 0$ to a final value $\boldsymbol{B}$ for $t > 0$. We again consider the system displayed in Fig. 5.1 with a single classical spin coupled via J to the central site i_0 of a chain consisting of $L = 1001$ sites. Finite-size artifacts do not show up before $t_{\rm max} = 500$.

Fig. 5.10 shows the resulting linear-response spin dynamics of the classical spin after preparing the initial state of the system with the classical spin pointing into the $+x$ direction while $\boldsymbol{B} = (0, 0, B)$. The external magnetic field induces a precessional motion of the classical spin: there is a rapid oscillation of its x-component (and of its y-component, not shown) with frequency $\omega \approx B$ (blue lines). Damping is induced by dissipation of energy and spin: for large times, the z-component aligns to the external field (red lines).

For weak coupling, up to $J = 1$ (Fig. 5.10, left panel), there is an almost perfect agreement between the results of the exact QCH-SD (black lines) and the LR-SD (colored lines) up to the maximum propagation time $t_{\rm max} = 500$. We note that, compared to the full theory, there is a tiny deviation of the linear-response result for the z component of $\boldsymbol{S}(t)$ visible in Fig. 5.10 (left panel) for times $t \gtrsim 10$. Hence, on this level of accuracy, $t_1 \approx 10$ sets the time scale up to which the linear-response theory is valid. This may appear surprising as this implies $t_1 J = 10$ for the "small" dimensionless parameter of the perturbation theory. One has to keep in mind, however, that even if the perturbation is "strong", its *effects* can be rather moderate since only non-adiabatic terms $\sim \boldsymbol{S}(t) \times \boldsymbol{S}(t')$ contribute in Eq. (5.15).

For $J = 3$, see Fig. 5.10 (right panel) , damping of the classical spin sets in much earlier. Visible deviations of the linear-response theory from the full dynamics already appear on a time scale that is almost two orders of magnitude smaller as compared to the case $J = 1$. A simple reasoning based on the argument that the dimensionless expansion parameter is $t_1 J$ fails as this disregards the strong enhancement of retardation effects with increasing J, which have been discussed in Sec. 5.1.3. These effects make the perturbation much more effective, i.e., lead to a torque, which is exerted by the conduction electrons on the classical spin, growing stronger than linear in J.

We conclude that the LR-SD approach is highly attractive formally, as it provides a tractable spin-only effective theory. On the other hand, substantial discrepancies compared to the (non-perturbative) QCH-SD method show up as soon as damping effects become stronger. Note that, with increasing time, these deviations must diminish and disappear eventually since both, the full and the effective theory, predict a fully relaxed spin state for $t \to \infty$ – see the right panel of Fig. 5.10, for example. At least for simple systems with a single classical spin, as considered here, this implies that the effective theory provides qualitatively reasonable results.

5.1.5 Conclusions

Hybrid systems consisting of classical spins coupled to a bath of non-interacting conduction electrons represent a class of model systems with a non-trivial real-time dynamics which is numerically accessible on long time scales. Here we have considered the simplest variant of this class, the Kondo-impurity model with a classical spin, and studied the relaxation dynamics of the spin in an external magnetic field. As a fundamental model this is interesting of its own but also makes contact with different fields, e.g., atomistic spin dynamics in magnetic samples, spin relaxation in spintronics devices, femto-second dynamics of highly excited electron systems where local magnetic moments are formed due to electron correlations, and artificial Kondo systems simulated with ultracold atoms in optical lattices.

We have compared the coupled spin and electron dynamics with the predictions of the widely used Landau-Lifshitz-Gilbert equation which is supposed to cover the regime of weak local exchange J and slow spin dynamics. For the studied setup, the LLG equation predicts a rather regular time evolution characterized by spin precession, spin relaxation and eventually reversal of the spin on a time scale τ depending on J (and the field strength B). We have demonstrated that this type of dynamics can be recovered and understood on a microscopic level in the more fundamental quantum-classical Kondo model. It is traced back to a non-adiabatic dynamics of the electron degrees of freedom and the feedback of the electronic subsystem on the spin. It turns out that the spin dynamics is essentially a consequence of the retarded effect of the local exchange. Namely, the classical spin can be seen as a perturbation exciting the conduction-electron system locally. This electronic excitation propagates and feeds back to the classical spin, but at a later time, and thereby

induces a spin torque.

We found that this mechanism drives the relaxation of the system to its local ground state irrespective of the strength of the local exchange J. As the microscopic dynamics is fully conserving, the energy and spin of the initial excitation which is locally stored in the vicinity of the classical spin, must be dissipated into the bulk of the system in the course of time. This dissipation could be uncovered by studying the relaxation process from the perspective of the electron degrees of freedom. Dissipation of energy and spin takes place through the emission of a dispersive spin-polarized wave packet propagating through the lattice with the Fermi velocity. In this process the local conduction-electron magnetic moment at any given distance to the impurity undergoes a reversal, characterized by precession and relaxation, similar to the motion of the classical spin.

The dynamics of the classical spin can be qualitatively very different from the predictions of the LLG equation for strong J. In this regime we found a complex motion characterized by oscillations of the angle between the classical spin $\boldsymbol{S}(t)$ and the local conduction-electron magnetic moment at the impurity site $\langle \boldsymbol{s}_{i_0} \rangle$ around the adiabatic value $\gamma = \pi$ which takes place on an emergent new time scale. However, we could identify this behavior as an inertia effect, which is well known in classical spin dynamics and can be described by an additional term to the standard LLG equation with second-order time-derivative of the spin.

In the weak-J limit, the classical spin dynamics is qualitatively predicted correctly by the LLG equation. At least partially, however, this must be attributed to the fact that the LLG approach, by construction, recovers the correct *final* state where the spin is parallel to the field. In fact, quantitative deviations are found *during* the relaxation process. The LLG approach is based on first-order perturbation theory in J and on the additional assumption that the classical spin is slow, as preliminary discussed in Sec. 4.3. To pinpoint the source of the deviations, we have numerically solved the integro-differential equation that is obtained in first-order-in-J perturbation theory, the LR-SD approach, and compared with the full hybrid dynamics (QCH-SD). The deviations of the perturbative approach from the exact dynamics are found to gradually increase with the propagation time (until the proximity to the final state enforces the correct long-time asymptotics). This is the expected result as the dimensionless small parameter is Jt. However, with increasing J the time scale on which perturbation theory is reliable decreases much stronger than $1/J$ due to a strong enhancement of retardation effects which make the perturbation more effective and produce a stronger torque.

Generally, the perturbation can be rather *ineffective* in the sense that it produces a torque $\propto \boldsymbol{S}(t) \times \boldsymbol{S}(t')$ which is very weak if the process is nearly adiabatic. This explains that first-order perturbation theory and the LLG equation is applicable at all for couplings of the order of hopping $J \sim T$. For the present study this can also be seen as a fortunate circumstance since the regime of very weak couplings $J \ll T$ is not accessible numerically. In this case the spin-reversal time scale gets so large that the propagation of excitations in

the conduction-electron subsystem would be affected by backscattering from the edges of the system which necessarily must be assumed as finite for the numerical treatment.

For the one-dimensional lattice studied here, a direct comparison between the LLG equation and the exact QCH-SD approach is not meaningful, as the damping constant α is ill-defined in this case. As discussed in detail in sections 4.2 and 4.3, this problem results from the strength of the van Hove singularities in the conduction-electron density of states which dictates the long-time behavior of the memory kernel of the integro-differential equation which is given by the equilibrium spin susceptibility. As the type of the van Hove singularity is characteristic for all systems of a given dimension, we can generally conclude that the LLG approach reduces to a purely phenomenological scheme in the one-dimensional case. However, this conclusion may change for systems where the Coulomb interaction among the conduction electrons is taken into account additionally, as a regularization of van Hove singularities could arise due to a finite imaginary part of the conduction-electron self-energy.

5.2 Inertia effects of a spin coupled to a Fermi see

In the previous section, we focused on transversal spin dynamics, which appears as a more *classical* phenomenon, in terms of the quantum-classical hybrid theory. Here[6], we explore whether there are quantum effects which are possibly overlooked by the semi-classical approach to transversal spin dynamics (i.e., apart from the Kondo effect). To this end we compare numerical results from the exact QCH-SD approach (see Sec. 4.1 and Sec. 5.1) with those of exact quantum theory, computed with the tDMRG method [Haegeman et al., 2011; Schollwöck, 2011], for different spin quantum numbers S. It turns out that even for $S = 1/2$ there is a surprisingly good qualitative agreement of quantum with semiclassical dynamics. However, we also identify a physical phenomenon, namely nutational motion, where remarkable differences are found between Classical and quantum nutation. Besides precession and damping, inertia effects are well known in classical spin dynamics [Butikov, 2006; Wegrowe and Ciornei, 2012] and can be described by an additional term to the LLG equation with a second-order time derivative of the spin. Similar as for the Gilbert damping term, the resulting nutation of the spin motion has been introduced and studied phenomenologically [Ciornei et al., 2011; Olive et al., 2012] and with realistic parameters taken from first-principles calculations [Böttcher and Henk, 2012; Thonig et al., 2016] but can also be derived on a microscopic level [Bhattacharjee et al., 2012; Fähnle et al., 2011; Kikuchi and Tatara, 2015] within the general framework of semiclassical spin dynamics [Evans et al., 2014; Fähnle and Illg, 2011; Tatara et al., 2008] (see also Sec. 4.3).

In case of a quantum spin, inertia effects have not yet been studied. As compared to spin precession and damping, nutation is a higher-order effect [Bhattacharjee et al., 2012], so that it is not *a priori* clear whether or not spin nutation is suppressed by quantum fluctuations. Here, by applying the tDMRG to the spin-S Kondo impurity model in a magnetic field, we are able to show for the first time that nutation also shows up in the full quantum spin dynamics. Remarkably, however, *quantum nutation* turns out to be strongly damped and shows up on a much shorter time scale as compared to the relaxation time. On a fundamental level, this pinpoints an unconventional new quantum effect in transversal spin dynamics, but is also relevant for experimental studies suggesting, e.g., inertia-driven spin switching [Kimel et al., 2009; Kirilyuk et al., 2010] opposed to standard precessional switching [Gerrits et al., 2002; Tudosa et al., 2004].

[6] Major parts of this section have been published as M. Sayad, R. Rausch and M. Potthoff: *Inertia effects in the real-time dynamics of a quantum spin coupled to a Fermi sea*, Europhys. Lett. 116, 17001 (2016) - Copyright © 2016 EPLA.

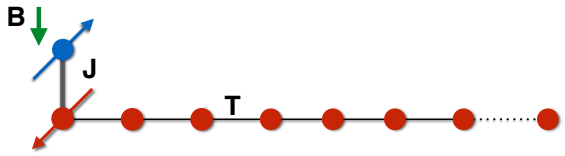

Figure 5.11: Classical spin $|\boldsymbol{S}| = S_{\text{cl.}}$ with $S_{\text{cl.}} = \sqrt{S(S+1)}$ or quantum spin $\boldsymbol{S}$ characterized by quantum number $S = \frac{1}{2}, 1, 2, 3...$, coupled via an antiferromagnetic local exchange interaction of strength J to a system of conduction electrons tunneling with nearest-neighbor hopping amplitude T over the sites of a one-dimensional lattice with open boundaries. The spin couples at the first site $i_0 = 1$ of the chain and is subject to a local magnetic field of strength $\boldsymbol{B}$.

5.2.1 Numerical setup and computational details

We once again consider the single impurity Kondo Hamiltonian, as a paradigmatic model of a spin coupled to a Fermi sea:

$$H = -T \sum_{i<j}^{n.n.} \sum_{\sigma=\uparrow,\downarrow} (c_{i\sigma}^\dagger c_{j\sigma} + \text{H.c.}) + J \boldsymbol{s}_{i_0} \boldsymbol{S} - \boldsymbol{B}\boldsymbol{S} \, . \tag{5.17}$$

Here, $c_{i\sigma}$ is the annihilator of an electron with spin projection $\sigma = \uparrow, \downarrow$ at site $i = 1, ..., L$ of an open one-dimensional chain of length L. The hopping $T = 1$ between nearest-neighboring (n.n.) sites defines the energy and the time scale ($\hbar \equiv 1$). We assume a half-filled band with $N = L$ conduction electrons. The impurity spin $\boldsymbol{S}$ is coupled antiferromagnetically with exchange coupling constant J to the local spin $\boldsymbol{s}_{i_0}$ of the itinerant conduction-electron system at the first site of the chain, $i_0 = 1$ (see Fig. 5.11). With the vector of Pauli matrices $\boldsymbol{\tau}$, we have $\boldsymbol{s}_i = \sum_{\sigma\sigma'} c_{i\sigma}^\dagger \boldsymbol{\sigma}_{\sigma\sigma'} c_{i\sigma'}/2$. $\boldsymbol{S}$ is a quantum spin characterized by quantum number $S = \frac{1}{2}, 1, 2, 3, ...$, and for $S > 1/2$, Eq. (5.17) is the underscreened Kondo model. Alternatively, $\boldsymbol{S}$ is considered as a classical spin with fixed length $|\boldsymbol{S}| = S_{\text{cl.}}$, as already discussed in Eq. (5.1), where $S_{\text{cl.}} = \sqrt{S(S+1)}$ for a meaningful comparison with results for a quantum spin.

Real-time dynamics. To initiate the spin dynamics we consider a local magnetic field $\boldsymbol{B}$ which, at time $t = 0$, is suddenly switched from $\boldsymbol{B} = (B_{\text{ini}}, 0, 0)$, forcing the spin to point in x direction, to $\boldsymbol{B} = (0, 0, B_{\text{fin}})$. This addresses, e.g., spin-resolved scanning-tunneling microscope experiments [Loth et al., 2010; Morgenstern, 2010; Nunes and Freeman, 1993; Wiesendanger, 2009; Yan et al., 2015]. We choose $B_{\text{ini}} = \infty$ to initially fully polarize the impurity spin. Note that the conduction-electron spin $\boldsymbol{s}_{i_0}$ in the initial state is also polarized, but typically much weaker, depending on the internal Weiss field $\boldsymbol{B}_{\text{eff}} \equiv J\boldsymbol{S}$ produced by the exchange interaction and the impurity spin. The dynamics is (predominantly) transversal if $B_{\text{fin}} \gg T_{\text{K}}$ which ensures that the Kondo singlet remains broken and that there are no (significant) longitudinal spin fluctuations.

For $t \to \infty$ we expect complete relaxation. This is achieved if the classical spin $\boldsymbol{S}(t)$ or, in the quantum case, $\boldsymbol{S}(t) \equiv \langle \boldsymbol{S} \rangle_t = \langle \Psi(t) | \boldsymbol{S} | \Psi(t) \rangle$ fully aligns with the z-axis. Likewise the expectation value $\boldsymbol{s}_{i_0}(t) \equiv \langle \boldsymbol{s}_{i_0} \rangle_t$ of the local conduction-electron spin at i_0 is expected to orient itself antiparallel to $\boldsymbol{S}(t)$ for $t \to \infty$.

Computational details. As regards the classical spin, the numerical method applied to study the real-time dynamics in terms of the quantum-classical hybrid theory remains the same as in Sec. 5.1.2. However, to study the quantum time-evolution of $\boldsymbol{S}(t)$ and $\boldsymbol{s}_{i_0}(t)$ after the sudden switch of the field, we employ the tDMRG method in the framework of matrix-product states and operators [Schollwöck, 2011]. The implementation of a quantum spin with arbitrary S is straightforward. For an impurity model with the spin attached to the first site of the chain, the numerical effort is essentially independent of S, as only the dimension of the local Hilbert space at i_0 scales with $2S + 1$. Due to the global $U(1) \times U(1)$ symmetry of H, the total particle number and the z component of the total spin are conserved. For a sudden field switch from $\hat{x}$ to $\hat{z}$ direction, however, only particle-number conservation can be exploited in the tDMRG calculation. As compared to a purely longitudinal dynamics, this implies an increased computational effort. The time evolution of matrix-product states is computed using the two-site version of the algorithm as suggested in Ref. [Haegeman et al., 2011, 2016], which is based on the time-dependent variational principle. The maximum bond dimension reached during the propagation is about 2000.

5.2.2 Quantum versus classical spin dynamics

Quantum-spin dynamics. We start the discussion with the tDMRG results, see the red lines in Fig. 5.12. The calculations have been performed for a chain with $L = 80$ sites. For a quantum spin $S = 1/2$ (Fig. 5.12, top panel), and for $J = 1$ and $B_{\mathrm{fin}} = 2$, the dynamics is sufficiently fast, i.e., the main physical effects take place on a time scale shorter than the time where finite-size artifacts show up. In the bulk of the noninteracting conduction-electron system, wave packets typically propagate with group velocity $v_{\mathrm{F}} = d\varepsilon(k)/dk|_{k_F} = \pm 2T$ at the Fermi wave vectors $k = k_{\mathrm{F}} = \pm\pi/2$ for half filling. This roughly determines the maximum speed of the excitations and defines a "light cone" [Bravyi et al., 2006; Lieb and Robinson, 1972]. Hence, a local perturbation at $i_0 = 1$ starts to show artificial interference with its reflection from the opposite boundary at $i = L$ after a time of about $t_{\mathrm{inter}} = 2L/v_{\mathrm{g}} = L/T$, i.e., after about 80 inverse hoppings – which is well beyond the time scale covered by Fig. 5.12.

The most obvious effect in the time dependence of $\boldsymbol{S}(t)$ (see upper part of the top panel) is the precessional motion around the $\hat{z}$-axis: $S_x(t)$ (and likewise of $S_y(t)$ which is not shown in the figure) oscillate with Larmor frequency $\omega_{\mathrm{L}} \approx B_{\mathrm{fin}}$. Note that $|\boldsymbol{S}(t)| = |\langle \Psi(t) | \boldsymbol{S} | \Psi(t) \rangle|$ is nearly constant, i.e., there are no substantial longitudinal fluctuations or Kondo screening. In addition to the spin precession, there is damping: The spin relaxes to its new equilibrium direction $\propto \hat{z}$ on the relaxation time scale $\tau_{\mathrm{rel}} \approx 50$. Despite the

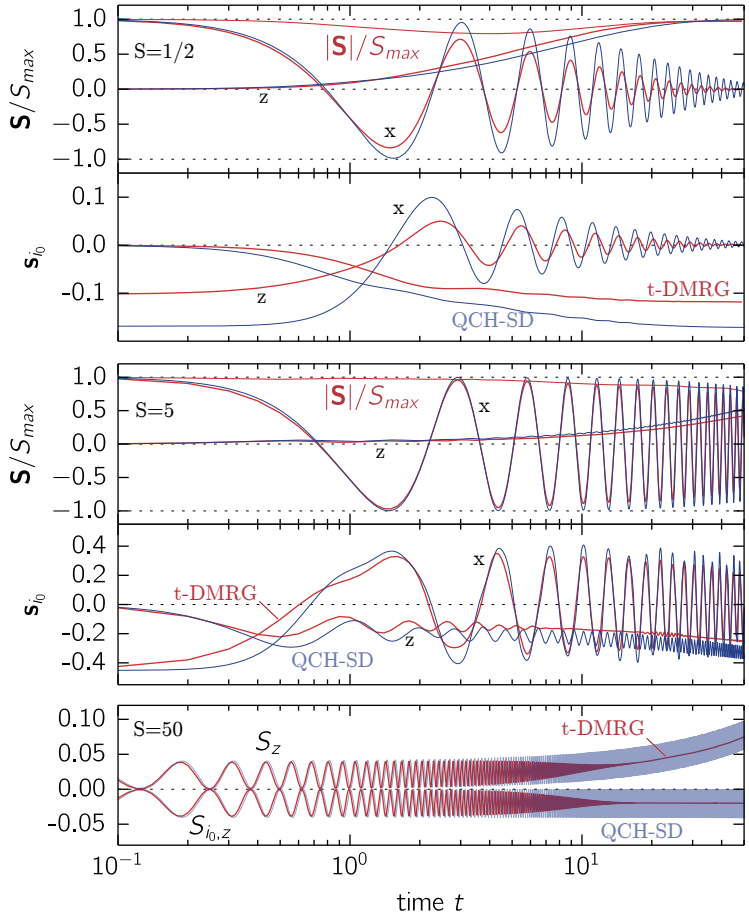

Figure 5.12: *Top panel, upper part:* Dynamics of $\boldsymbol{S}(t)/S_{\rm max}$ for the Kondo impurity model, Eq. (5.17), for $J = 1$ and $\boldsymbol{B} = B_{\rm fin}\hat{z}$ with $B_{\rm fin} = 2$. Only x and z components are shown. At $t = 0$, the system is prepared with $\boldsymbol{S}(0)/|\boldsymbol{S}(0)| = \hat{x}$. Time units are fixed by the inverse hopping $1/T \equiv 1$. Red lines: tDMRG calculations for a quantum spin, $\boldsymbol{S}(t) \equiv \langle\Psi(t)|\boldsymbol{S}|\Psi(t)\rangle$, and $S = 1/2$ ($S_{\rm max} = S$). Blue lines: QCH-SD approach with a classical spin $\boldsymbol{S}(t)$ of length $S_{\rm cl.} = \sqrt{S(S+1)} = \sqrt{3}/2$ ($S_{\rm max} = S_{\rm cl.}$). *Top panel, lower part:* Local conduction-electron moment $\boldsymbol{s}_{i_0}(t) \equiv \langle\boldsymbol{s}_{i_0}\rangle_t$. *Middle*: The same for $S = 5$. *Bottom*: z components of $\boldsymbol{S}(t)$ and $\boldsymbol{s}_{i_0}(t)$ for $S = 50$.

fact that the total energy and the z component of the total spin are conserved (as is also checked numerically), this is the expected result: At $t = 0$ the system is locally in an excited state; for large t, spin relaxation is achieved by dissipation of energy into the bulk of the chain. The dynamics does not stop until the excitation energy $\sim SB_{\rm fin}$ is fully dissipated into the bulk, and the system is – locally, close to i_0 – in its ground state. In the ground state of the system at time $t = 0$, the local conduction-electron spin at i_0 is partially polarized in $-x$ direction, i.e., antiparallel to $\boldsymbol{S}(t = 0)$ due to the internal magnetic field

$J\boldsymbol{S}(0)$ (see top panel of Fig. 5.12, lower part). For $t > 0$ we find that $\boldsymbol{s}_{i_0}(t)$ follows the dynamics of the impurity spin $\boldsymbol{S}(t)$ *almost* adiabatically, i.e., at a given instant of time t it is slightly behind the (instantaneous) ground-state expectation value $\langle \boldsymbol{s}_{i_0} \rangle_{\text{g.s.}} \uparrow\downarrow \boldsymbol{S}(t)$ for the conduction-electron system with a "given" Weiss field $J\boldsymbol{S}(t)$. This slight retardation effect is clearly visible in Fig. 5.12 (compare the location of the first minimum of $S_x(t)$ with the first maximum of $s_{i_0 x}(t)$, for instance). In the semiclassical picture retardation has been identified to drive the relaxation of $\boldsymbol{S}(t)$, as previously studied in-depth in Sec. 5.1.3.

Quantum nutation. In addition to the expected precessional motion and relaxation of $\boldsymbol{s}_{i_0}(t)$, there is a weak additional superimposed oscillation visible in $s_{i_0 z}(t)$. For $S = 1/2$ the frequency is close to the precession frequency. However, the results for higher spin quantum numbers (see lower part of the middle panel, $S = 5$) show that these oscillations have a characteristic frequency ω_{N} and hence a physical cause which may require but is independent of the precessional motion. The z component of the impurity spin actually shows oscillations with the same frequency and almost the same amplitude (which can hardly be seen in the first two panels of Fig. 5.12 due to the rescaling of $\boldsymbol{S}(t)$ by $S_{\max}$) but becomes obvious in the bottom panel (no rescaling, $S = 50$). By comparing with the semiclassical spin dynamics, we will argue that this is in fact nutation of the quantum spin.

Results of the semiclassical approach. Most (but not all) features of the transversal quantum dynamics are qualitatively captured by the numerically much cheaper quantum-classical hybrid spin dynamics (QCH-SD). The QCH-SD results are shown by light blue lines in Fig. 5.12. To make contact with the tDMRG data, we again consider $L = 80$ sites although much larger systems could be treated numerically (see Sec. 5.1). Overall, the semiclassical theory produces qualitatively very similar results as compared to the quantum dynamics. This concerns the precessional motion, the relaxation time scale and also the occurrence of nutation and the nutation frequency and amplitude.

However, we can identify basically three quantum effects which are different or even absent in the QCH-SD:

(i) Initially the local conduction-electron spin at i_0 is less polarized in the quantum case, and this has some quantitative consequences for the subsequent spin dynamics. The reason is that with $S_{\text{cl.}} = \sqrt{S(S+1)}$ the classical Weiss field is stronger: $JS_{\text{cl}} = J\sqrt{3}/2 > J/2 = JS$.

(ii) Opposed to the classical-spin case, which exclusively comprises transversal dynamics, we find $|\boldsymbol{S}(t)| \neq \text{const}$ in the quantum case, i.e., there are residual longitudinal fluctuations (see top panel, upper part). Due to the suppression of the Kondo effect by the magnetic field, these are moderate, such that the deviations from the QCH-SD are small. One should note, however, that nevertheless (weak) longitudinal fluctuations are *essential* for true quantum spin dynamics: Assuming the complete

absence of longitudinal fluctuations, we would have $\langle \boldsymbol{S} \rangle_t = S\,\hat{n}(t)$ with some unit vector $\hat{n}(t)$. Aligning the momentary quantization axis to $\hat{n}(t)$, the quantum state at time t is a product state with zero impurity-bath entanglement. For the impurity-spin equation of motion, $d\langle \boldsymbol{S} \rangle_t/dt = J\langle \boldsymbol{s}_{i_0} \times \boldsymbol{S} \rangle_t - \boldsymbol{B} \times \langle \boldsymbol{S} \rangle_t$, this implies the factorization $\langle \boldsymbol{s}_{i_0} \times \boldsymbol{S} \rangle_t = \boldsymbol{s}_{i_0}(t) \times \boldsymbol{S}(t)$, resulting in the equation:

$$\frac{d}{dt}\boldsymbol{S}(t) = J\boldsymbol{s}_{i_0} \times \boldsymbol{S}(t) - \boldsymbol{B} \times \boldsymbol{S}(t)\,. \tag{5.18}$$

With an analogous factorization in the equations of motion for the conduction-electron degrees of freedom, we obtain:

$$\frac{d}{dt}\boldsymbol{s}_{i_0}(t) = J\boldsymbol{S}(t) \times \boldsymbol{s}_{i_0}(t) - T\,\mathrm{Im}\sum_{\sigma\sigma'}\langle c^\dagger_{i_0\sigma}\boldsymbol{\sigma}_{\sigma\sigma'}c_{i_0+1\sigma'}\rangle_t\,. \tag{5.19}$$

The above equations imply classical-spin behavior as discusses in detail in Secs. 4.1 and 5.1 (cf. Eqs. (5.2) and (5.3)). Hence, longitudinal fluctuations produce entanglement and quantum effects.

(iii) The nutational motion is strongly damped in the quantum-spin case. Oscillations of $S_z(t)$ and of $s_{i_0 z}(t)$ with frequency ω_N decay on a finite time scale τ_N while there is no visible damping of the nutation for a classical spin on the scale displayed in Fig. 5.12. This is most obvious for $S = 50$ (bottom panel), but also for $S = 5$ (middle panel, lower part).

S-dependence. For large spin quantum numbers, one expects that the quantum-spin dynamics becomes equivalent with that of a classical spin of length $S_\mathrm{cl.} = \sqrt{S(S+1)}$ [Garanin et al., 2000; Garanin, 2008; Kladko et al., 1999; Lieb, 1973; Sayad et al., 2012]. Indeed, the agreement constantly improves with increasing S, see Fig. 5.12. The common trends found with increasing S are the following:

(i) There is a stronger and stronger initial polarization of the local conduction-electron spin at i_0 due to the increasing magnitude of the Weiss field $\boldsymbol{B}_\mathrm{eff} \equiv J\boldsymbol{S}$ coupling to $\boldsymbol{s}_{i_0}$. For $S = 5$ it is more than 80% polarized.

(ii) The relaxation time τ_rel increases with increasing S. For $S = 5$ (see Fig. 5.12, middle panel) $S_z(t)$ has reached only 50% of its final saturation value, and for $S = 50$ (bottom panel) there is hardly any damping visible on the time scale accessible to the tDMRG computations. Within weak-J perturbation theory and assuming that the spin dynamics is slow as compared to the electronic time scales (Markov approximation), we expect $\tau_\mathrm{rel} \propto S$ in the large-S limit, as is detailed in Sec. 4.3. However, for both the semiclassical and the quantum theory, we find $\tau_\mathrm{rel} \propto S^2$ from the data given in Fig. 5.13 (right panel). This indicates that the effective theory is of

limited use for reproducing the exact results of QCH-SD on the semiclassical level for large $S_{\mathrm{cl.}}$ and is furthermore inconsistent with the quantum dynamics as well. One may reject the Markov-type approximation (LLG equation (4.18)) and describe the spin dynamics with the linear-response theory and Eq. (4.8). The same scaling argument as above again tells us that an elongated ($\lambda > 1$) spin $\boldsymbol{S}'(t) \equiv \lambda \boldsymbol{S}(t)$ solves the same integro-differential equation,

$$\boldsymbol{S}'(t, \boldsymbol{B}, J') = \boldsymbol{S}(t, \boldsymbol{B}, J) \,, \tag{5.20}$$

but with a rescaled exchange coupling

$$J' = J/\sqrt{\lambda} \,. \tag{5.21}$$

Thus a weaker interaction $J' < J$ (for $\lambda > 1$) leads to the same dynamics.

Now, from the numerical evaluation of the linear-response equation (4.8) in Sec. 5.1.4, it is known that for fixed $S_{\mathrm{cl.}}$, the damping becomes stronger and the relaxation time shorter with increasing J. Hence, for fixed J, with the argument leading to Eq. (5.21), the dynamics of an elongated classical spin must therefore show a stronger damping, i.e., a shorter relaxation time. As this conflicts with our observations here (see Fig. 5.12 and Fig. 5.13, right panel), we must conclude that the linear-response approximation (4.8), is no longer valid for the parameter regime studied here. This furthermore implies that, besides damping, also the nutational motion of a spin exchange coupled to an unpolarized Fermi sea cannot be captured by the perturbative approach (despite the fact that the linear trend Eq. (4.26) is reproduced). This is not too surprising in view of the explanation for the inertia effect as will be described in Sec. 5.2.3, namely the formation of a bound state of the impurity spin with the exchange-coupled conduction-electron spin and the weak interaction of this bound state with the bulk of the system. Those details of the electronic structure are obviously not accounted for in a simple effective spin-only theory, such as Eq. (4.8), where the electron dynamics only enters via the $J = 0$ spin susceptibility.

(iii) For the nutation frequency we find $\omega_{\mathrm{N}} \propto S$ in the large-S limit (see also the discussion below). The amplitude of the nutation vanishes for $S \to \infty$ in both, the quantum- and the classical-spin case. In this way quantum- and classical-spin dynamics become equivalent in the large-S limit despite the absence of damping of the nutational motion in the classical case.

(iv) We finally note that $|\boldsymbol{S}(t)|/S_{\max}$ becomes constant in the quantum case as $S \to \infty$.

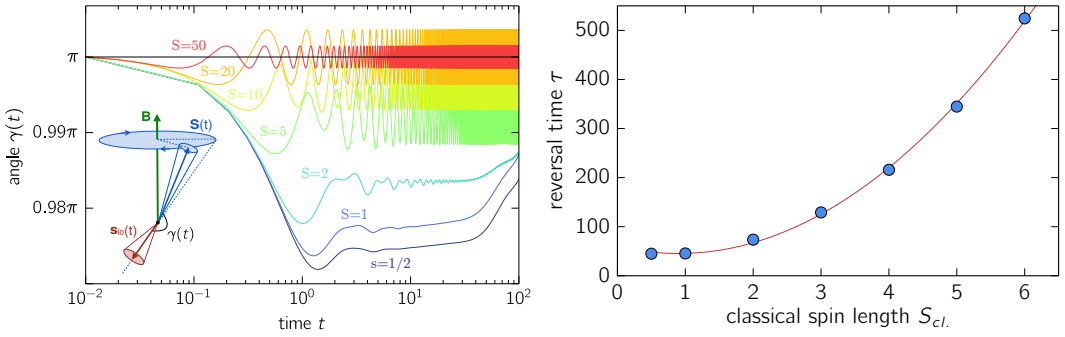

Figure 5.13: Left panel: Angle $\gamma(t)$ between $\boldsymbol{S}(t)$ and $\boldsymbol{s}_{i_0}(t)$ in the spin dynamics after the sudden switch of the field from x to z direction. QCH-SD results for $J = 1$, $L = 400$, $B_{\rm fin} = 0.1$ and different $S_{\rm cl.} = \sqrt{S(S+1)}$ as indicated. *Inset:* schematic illustration of the nutational motion, see text. Right panel: QCH-SD results, obtained for $J = 1$, $L = 600$ and $B_{\rm fin} = 1$, showing the reversal time τ as a function of the classical spin length $S_{\rm cl.}$ of a spin after the sudden switch of the field from x towards z direction.

5.2.3 Microscopic cause of the nutation

The nutational motion can be understood easily within the semiclassical approach (except for damping): Recall that the impurity spin precession with frequency $\omega_{\rm L} \approx B_{\rm fin}$ is mainly caused by the torque due to the magnetic field and note that the second term on the right-hand side of Eq. (5.18) is small if $\boldsymbol{s}_{i_0}(t)$ and $\boldsymbol{S}(t)$ are nearly collinear. In fact, in the instantaneous ground state at time t, the conduction-electron local moment $\boldsymbol{s}_{i_0}(t)$ would be perfectly aligned antiparallel to $\boldsymbol{S}(t)$ due to the antiferromagnetic exchange coupling J such that $\boldsymbol{s}_{i_0}(t)$ exhibits a precessional motion with the same frequency $\omega_{\rm L} \approx B_{\rm fin}$. Fig. 5.13 (left panel) demonstrates that the stronger the effective field JS, the smaller is the deviation of the angle $\gamma(t)$ between $\boldsymbol{S}(t)$ and $\boldsymbol{s}_{i_0}(t)$ from $\gamma = \pi$. Generally, however, $\gamma(t) < \pi$ (for all t) since, due to the damping, it takes a finite time for $\boldsymbol{s}_{i_0}(t)$ to react to the new position of $\boldsymbol{S}(t)$ (see the inset of Fig. 5.13, left panel). Note that for very large S only the time average $\overline{\gamma(t)}$ is smaller than π (for instance, see $S \geq 20$ in Fig. 5.13, left panel). This retardation effect results in a finite (average) torque $J\boldsymbol{S}(t) \times \boldsymbol{s}_{i_0}(t)$ acting on $\boldsymbol{s}_{i_0}(t)$, as can be seen from its equation of motion (5.19), where the second term on the right-hand side is important for energy and spin dissipation into the bulk of the system and causes the usual damping of the precession of $\boldsymbol{s}_{i_0}(t)$ (and of $\boldsymbol{S}(t)$) around $\boldsymbol{B}$. The first term in Eq. (5.19), however, leads to nutational motion.

This is most easily understood if there is a separation of time scales, i.e., if the nutation frequency $\omega_{\rm N}$ is large compared to the Larmor frequency $\omega_{\rm L} \approx B_{\rm fin}$. In this limit, Eq. (5.19) implies that $\boldsymbol{s}_{i_0}(t)$ precesses with frequency $\omega_N \approx JS_{\rm cl.}$ approximately around the momentary direction of $\boldsymbol{S}(t)$ (which itself slowly precesses around the field direction). Actually, however, due to the retardation, $\boldsymbol{s}_{i_0}$ precesses around an axis which is slightly tilted as compared to the momentary direction of $\boldsymbol{S}(t)$. This is nicely demonstrated by

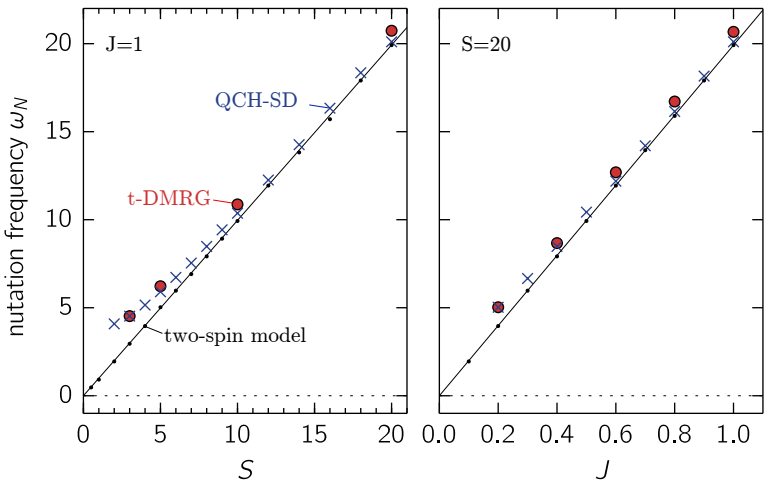

Figure 5.14: Nutation frequency ω_{N} as a function of S for $J = 1$ (left) and as a function of J for $S = 20$ (right). Dynamics initiated by a switch of the field from x to z direction with $B_{\mathrm{fin}} = 0.1$. Results for different $S_{\mathrm{cl.}}$ or S, respectively, as obtained by QCH-SD (crosses) and tDMRG (circles) in comparison with the classical two-spin model (filled dots).

the oscillations of $\gamma(t)$ with time-average $\overline{\gamma(t)} < \pi$ as displayed in Fig. 5.13, left panel. Furthermore, the equations of motion, Eq. (5.18) and Eq. (5.19), with the second term disregarded, imply that $S_z(t) + s_{i_0 z}(t) = \text{const}$ and, therefore, the impurity spin shows the same nutational motion, but with opposite amplitude.

In the middle panel of Fig. 5.12 we in fact observe a fast oscillation of $\boldsymbol{s}_{i_0}(t)$ with a frequency almost perfectly given by $JS_{\mathrm{cl.}}$ (with $J = 1$ and $S = 5$). Note that the nutation of $\boldsymbol{S}(t)$ is hardly visible due to the rescaling with $S_{\mathrm{max.}}$. The third panel for $S = 50$ nicely demonstrates the nutational motion of both, $\boldsymbol{s}_{i_0}(t)$ and $\boldsymbol{S}(t)$, with opposite amplitudes and common frequency $\omega_{\mathrm{N}} \gg \omega_{\mathrm{L}}$.

Fig. 5.14 displays the results of systematic QCH-SD calculations which demonstrate the linear dependence of ω_N on J and S for large JS. These calculations have been performed for a much weaker field $B_{\mathrm{fin}} = 0.1$ resulting in a much slower precession of $\boldsymbol{S}(t)$ around $\boldsymbol{B}$. Note the nearly perfect agreement between classical- and quantum-spin calculations also for smaller JS where there is a significant deviation from a linear behavior.

The mechanism described above also explains that the amplitudes of the nutational oscillations vanish in the limit $S \to \infty$: An increasing internal Weiss field JS more and more aligns $\boldsymbol{s}_{i_0}(t)$ to $\boldsymbol{S}(t)$, i.e., $\gamma(t) \to \pi$. Consequently, torque $J\boldsymbol{S}(t) \times \boldsymbol{s}_{i_0}(t)$ acting on $\boldsymbol{s}_{i_0}(t)$ vanishes in the large-S limit.

Two-spin model. Fig. 5.14 additionally presents the results for ω_{N} as obtained by a semiclassical two-spin model:

$$H_{2-\mathrm{spin}} = J\boldsymbol{s}\boldsymbol{S} - \boldsymbol{B}\boldsymbol{S}\,. \tag{5.22}$$

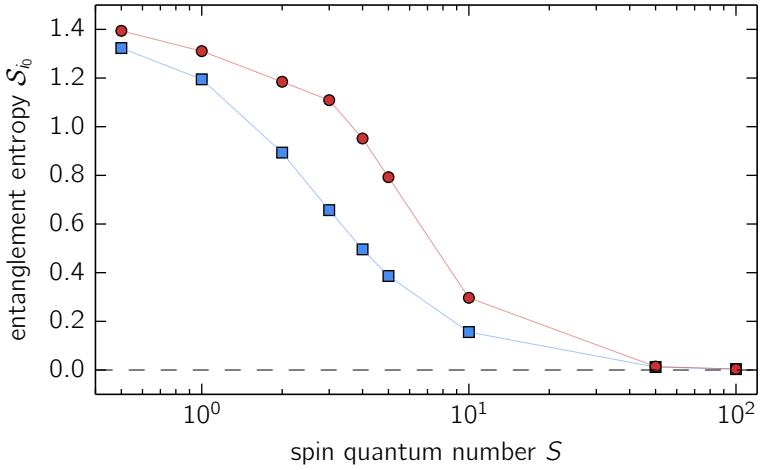

Figure 5.15: Entanglement entropy of the two-spin subsystem (impurity spin and site $i_0 = 1$) in the environment ($i = 2, ..., L$) as a function of S for $J = 1$ and at different times $t = 0$ and $t = 20$. tDMRG results for $B_{\text{fin}} = 2$ and $L = 50$.

This model disregards the coupling of the site i_0 to the bulk of the conduction-electron system and thus cannot describe the damping of the precessional motion. Due to the absence of damping, the time-averaged angle is $\overline{\gamma(t)} = \pi$.

From the numerical solution of Eq. (5.22) we also learn that it does not predict any damping of the nutational motion. The nutational oscillations themselves, however, are qualitatively captured by $H_{2-\text{spin}}$ and, in fact, the whole line of reasoning explaining the inertia effect also applies to this model. The nutation frequencies as computed from $H_{2-\text{spin}}$ fit the QCH-SD and tDMRG results rather well for strong effective fields $B_{\text{eff}} \equiv JS \gg T = 1$; stronger deviations are found for $JS \to 2$ (see Fig. 5.14). For $JS < 2$, there are clear nutational oscillations in the spin dynamics of the full model (5.17), as is seen in the top panel of Fig. 5.12, but ω_{N} cannot be defined accurately.

Bound states. $B_{\text{eff,cr}} = 2$ is actually the critical value of the local effective field $B_{\text{eff}} \equiv JS$ which couples to the local conduction-electron spin at i_0. For $B_{\text{eff}} > B_{\text{eff,cr}}$ there are two one-particle eigenenergies of the Hamiltonian (5.17) corresponding to bound states which symmetrically split off the continuum at the lower and at the upper band edge, respectively. Note that $B_{\text{eff,cr}}$ vanishes for a site i_0 in the bulk of an infinite chain as is well known for one-dimensional systems. Contrary, at the edge ($i_0 = 1$) there is a finite critical field, as is reminiscent of the physics in higher dimensions.

The sudden switch of the field excites the system locally at i_0. Consequently, if $JS > B_{\text{eff,cr}}$, the subsequent dynamics is predominantly local since the excitation is mainly carried by a state whose amplitude is exponentially suppressed with increasing distance from i_0. The dynamics should be understood in this case as a weak perturbation of the dynamics of the two-spin model Eq. (5.22).

That this also applies to the quantum-spin case is demonstrated with Fig. 5.15 which shows the entanglement entropy $\mathcal{S}_{i_0}$ of the subsystem consisting of the quantum impurity spin and the conduction-electron site i_0. In the ground state at $t = 0$, the entropy decreases with increasing effective field JS. For $JS = 50$ it nearly vanishes which implies that ground-state expectation values of local observables at i_0 are almost perfectly described with the (quantum version of the) two-spin model Eq. (5.22). With increasing time t, the entropy generally increases, while for strong effective fields JS is stays close to zero, i.e., the two-spin model also well captures the dynamics of local observables in this case.

Damping of quantum nutation. To explain the efficient damping of the nutational motion on a very short time scale τ_{N} in the quantum-spin case, we first consider the quantum variant of the two-spin model Eq. (5.22), i.e., both, $\boldsymbol{S}$ and $\boldsymbol{s}$, are considered as quantum spins with spin quantum numbers S and $1/2$, respectively. The time-dependent expectation value $S_z(t)$ after the sudden switch of the field is readily computed and shows oscillations with frequency ω_{N}. Already in the two-spin model those are damped on a time scale τ_{N} which agrees with that seen in the results of the full model in Fig. 5.12 for $S \geq 5$. Writing $S_z(t) = \langle S_z \rangle_t = \sum_{m,n} c_{m,n} \exp(i(E_m - E_n))t$ with energy eigenstates m and n of $H_{2-\mathrm{spin}}$ and coefficients $c_{m,n}$ depending on the preparation of the initial state, it becomes obvious that this damping results from the dephasing of oscillations with the excitation energies $E_m - E_n$ of the system.

Due to the small Hilbert-space dimension of the two-spin model, however, there are strong revivals of the oscillations occurring at finite revival times. In fact, for $S = 5$, the first revival of nutational oscillations of $s_{i_0 z}(t)$ can be seen in the tDMRG result around $t = 20$ (Fig. 5.12, middle panel, lower part). With increasing S and thus with increasing Hilbert space, however, the revival times quickly exceed the time scale accessible to tDMRG in the full model. Furthermore, as the example for $S = 5$ in Fig. 5.12 shows, the revivals themselves are strongly damped in the full theory, opposed to the nearly perfect revivals in the two-spin-model dynamics. As this (secondary) damping of nutation is caused by the residual effective coupling of the two-spin model to the bulk of the system, it becomes less and less efficient with increasing S, while at the same time the revival time strongly increases and the amplitude of the oscillations decreases.

5.2.4 Conclusions

Inertia effects in spin dynamics have been discussed intensively in the recent years, mainly in the context of applications for magnetic devices [Bhattacharjee et al., 2012; Böttcher and Henk, 2012; Butikov, 2006; Evans et al., 2014; Fähnle et al., 2011; Kikuchi and Tatara, 2015; Kimel et al., 2009; Kirilyuk et al., 2010; Olive et al., 2012; Tatara et al., 2008; Wegrowe and Ciornei, 2012]. The most fundamental system which covers the essentials of spin dynamics, however, namely a single spin coupled to a Fermi sea has not yet been addressed in this respect. Applying exact quantum and semiclassical numerical techniques to the Kondo impurity model, we could demonstrate that the

real-time dynamics, initiated by switching the direction of a magnetic field coupled to the spin, not only exhibits spin precession and spin relaxation but also nutational motion known from a gyroscope. The effect not only shows up in the impurity-spin dynamics but also in the dynamics of the conduction-electron local magnetic moments. It is very robust and found in a large regime of coupling constants using quantum-classical hybrid spin dynamics and treating the spin as a classical observable. We find that nutation amplitudes are small as compared to amplitudes in precessional motion. The frequency is, in the strong-coupling limit, linear in J and $S_{\mathrm{cl.}}$.

It has been demonstrated that nutational motion is not restricted to classical-spin systems, but is robust against quantum fluctuations. Despite the fundamental differences between semiclassical and quantum dynamics, quantum-spin nutation is found to be very similar to the classical-spin case in many respects. There is a qualitative, and with increasing spin-quantum numbers also quantitative agreement between quantum and semiclassical dynamics. Kondo screening of the impurity spin represents an important exception which, however, in the present study plays a minor role only as Kondo-singlet formation is inhibited by the external field.

The main effect of the quantum nature of the spin is a very efficient damping of the nutational motion on a very short (femtosecond) time scale which is basically independent of the relaxation time scale for the precessional motion. In the strong-coupling ($JS \to \infty$) limit, the spin dynamics is essentially local and captured by an emergent two-spin model which has served to understand the physical origin of the damping of quantum nutation, namely dephasing of local spin excitations with revivals suppressed by the coupling to the bulk of the system.

An important implication of this study is that direct observation of nutational motion, e.g., of magnetic nanoparticles with a (quantum) macrospin S coupled to the conduction-electron band of a nonmagnetic metallic surface, requires a sub-picosecond time resolution. On the other hand, inertia-driven spin switching in antiferromagnets [Kimel et al., 2009; Kirilyuk et al., 2010] has already been demonstrated successfully.

5.3 Classical spin coupled to a strongly correlated electron system

As up to now, we have concentrated on identifying the cause of relaxation and inertia effects in the real-time dynamics of a classical spin exchange-coupled to a *non-interacting* conduction-electron system, which in the weak-coupling limit can be successfully described on a phenomenological level by the Landau-Lifschitz-Gilbert (LLG) equation [Gilbert, 2004; Landau and Lifshitz, 1935] and extensions of this concept [Bhattacharjee et al., 2012; Tatara et al., 2008] as discussed previously in Secs. 4.3 and 5.1.

In contrast, this section[7] is devoted to the study of a classical spin coupled to a strongly correlated electron system, as electron correlations are expected to have an important effect on the spin dynamics. This has been demonstrated in a few pioneering studies [Garate and MacDonald, 2009; Hals et al., 2015; Hankiewicz et al., 2008] – within different models and using various approximations – but only indirectly by computing the effect of the Coulomb interaction on the Gilbert damping. One hallmark of strong correlations, however, is the emergence and the separation of energy (and time) scales – with the correlation-induced Mott insulator [Gebhard, 1997] as a paradigmatic example.

With the present study we address correlation effects beyond an LLG-type approach and keep the full temporal memory effect. It is demonstrated that correlation-induced time-scale separation has profound and qualitatively new consequences for the spin dynamics. These are important, e.g., for the microscopic understanding of the emerging relaxation time scales in modern nano-spintronics devices involving various transition metals and compounds [Khajetoorians et al., 2011; Loth et al., 2010; Morgenstern, 2010].

Concretely, we consider a generic model with a classical spin $\boldsymbol{S}$ that is antiferromagnetically exchange-coupled ($J > 0$) to a Hubbard system and study the spin dynamics as a function of the Hubbard-U. To tackle this quantum-classical hybrid problem, we develop a new approach which combines the linear-response theory for the spin dynamics (see LR-SD approach in Sec. 4.2) with time-dependent density-matrix renormalization group (tDMRG) [Haegeman et al., 2011, 2016; Schollwöck, 2011] for the correlated electron system. For technical reasons we consider a Hubbard chain, but concentrate on generic effects which are not bound to the one-dimensionality of the model.

In the metallic phase at quarter filling, a complex phenomenology is found where two different channels for energy and spin dissipation, namely dissipation via correlated hopping and via excitations of local magnetic moments, become active on characteristic time scales, depending on U. While magnetic excitations give the by far dominating contribution to the Gilbert damping in the strong-coupling limit, they contribute to the spin

[7] Major parts of this section have been published as M. Sayad, R. Rausch and M. Potthoff: *Relaxation of a classical spin coupled to a strongly correlated electron system* Phys. Rev. Lett. 117, 127201 (2016) - Copyright © 2016 American Physical Society.

dynamics to a much lesser extent and on later and later time scales when U is increased.

It is demonstrated that electron correlations can have extreme consequences: At half-filling and strong U, the spin relaxation is incomplete on intermediate time scales. This represents a novel effect in a quantum-classical hybrid model which is reminiscent of prethermalization [Kollar et al., 2011; Marcuzzi et al., 2013; Moeckel and Kehrein, 2008, 2010] or metastability of excitations due to lack of phase space for decay [Hofmann and Potthoff, 2012; Rausch and Potthoff, 2016; Rosch et al., 2008; Strohmaier et al., 2010], i.e., physics which so far has been observed in purely electronic quantum systems only.

5.3.1 Numerical setup and computational details

The simple LLG equation (4.18) for a classical spin can only provide an overall picture of the spin dynamics and in fact ignores the electronic time-scale separation as discussed in Sec. 4.3. We therefore apply a refined approach which explicitly accounts for the conduction-electron degrees of freedom in a semiclassical Kondo-impurity model with finite Hubbard-U:

$$\begin{aligned} H &= H_e + H_{e-spin} \\ &= -T \sum_{i<j}^{n.n.} \sum_{\sigma} (c^\dagger_{i\sigma} c_{j\sigma} + \text{H.c.}) + U \sum_{i=1}^{L} n_{i\uparrow} n_{i\downarrow} + J \boldsymbol{s}_{i_0} \boldsymbol{S} - \boldsymbol{B} \boldsymbol{S} \,, \end{aligned} \tag{5.23}$$

where the first two terms presents the Hubbard model H_e for N electrons on an open chain of length L as a prototypical model of correlated conduction electrons (see, Sec. 2.1) with nearest-neighbor (n.n.) hopping $T = 1$, which sets the energy and time scale. The third expression includes the local and isotropic coupling between $\boldsymbol{s}_{i_0}$ and the classical spin $\boldsymbol{S}$ ($|\boldsymbol{S}| = 1/2$). Finally, a local magnetic field $\boldsymbol{B}$ is added, which at time $t = 0$, is suddenly switched from $\boldsymbol{B} = B_{\text{ini}}\hat{x}$, forcing the spin to point in x direction, to $\boldsymbol{B} = B_{\text{fin}}\hat{z}$ with $B_{\text{fin}} = 1$ to initiate the spin dynamics. Complete relaxation is achieved if $\boldsymbol{S}(t) \to \frac{1}{2}\hat{z}$ for $t \to \infty$.

As already discussed in Sec. 2.1, at half-filling and in the limit $U \to \infty$ the low-energy physics of the Hubbard model is captured by an antiferromagnetic Heisenberg model,

$$H_s = \sum_i (J_{\text{H}} \boldsymbol{s}_i \boldsymbol{s}_{i+1} + J'_{\text{H}} \boldsymbol{s}_i \boldsymbol{s}_{i+2}) \,, \tag{5.24}$$

where up to order $\mathcal{O}(T^2/U)$ the nearest-neighbor and the next-nearest-neighbor couplings [Buleavskiĭ, 1967] are $J_{\text{H}} = 4T^2/U$ and $J'_{\text{H}} = 0$, and up to order $\mathcal{O}(T^4/U^3)$,

$$J_{\text{H}} = \frac{4T^2}{U} - \frac{16T^4}{U^3} \,, \quad J'_{\text{H}} = \frac{4T^4}{U^3} \,. \tag{5.25}$$

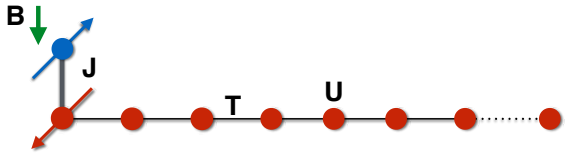

Figure 5.16: Classical spin $\boldsymbol{S}$ with $|\boldsymbol{S}| = 1/2$ coupled via an antiferromagnetic local exchange interaction of strength J to a system of correlated conduction electrons with an on-site interaction U tunneling with nearest-neighbor hopping amplitude $T \equiv 1$ over the sites of an one-dimensional lattice with open boundaries. The spin couples to the site $i_0 = 1$ of the system and is subject to a local magnetic field of strength $\boldsymbol{B}$.

Alternatively, the classical spin S is coupled to a (quantum) Heisenberg chain

$$H = \sum_i (J_{\mathrm{H}} \boldsymbol{s}_i \boldsymbol{s}_{i+1} + J'_{\mathrm{H}} \boldsymbol{s}_i \boldsymbol{s}_{i+2}) + J \boldsymbol{s}_{i_0} \boldsymbol{S} - \boldsymbol{B}\boldsymbol{S} \,, \tag{5.26}$$

for which much larger system sizes and therefore longer time scales are accessible to tDMRG.

The classical-spin approximation is justified for a strong local field B_{fin}, which suppresses the dynamical Kondo effect [Nuss et al., 2015b] that would show up in case of a quantum-spin $S = 1/2$. The quantum-classical hybrid model in Eq. (5.23) also results in the limit of large spin quantum numbers S [Garanin, 2008] of a correlated quantum-spin Kondo impurity model. As previously discussed in Sec. 4.1, the classical spin $\boldsymbol{S}(t)$ satisfies the classical equation of motion $\dot{\boldsymbol{S}}(t) = \boldsymbol{S}(t) \times \boldsymbol{B} - J\boldsymbol{S}(t) \times \langle \boldsymbol{s}_{i_0} \rangle_t$. Furthermore, in Sec. 4.2 it was shown that the electronic degrees of freedom can be integrated out altogether by applying lowest-order perturbation theory in J. To this end, the Kubo formula yields $\langle \boldsymbol{s}_{i_0} \rangle_t = J \int_0^t dt' \, \chi_{\mathrm{loc}}(t - t') \boldsymbol{S}(t')$ where the retarded local spin correlation $\chi_{\mathrm{loc}}(t)$ now plays the role of the linear-response function. Here, we repeat the resulting effective integro-differential equation of motion given in Eq. (4.8):

$$\dot{\boldsymbol{S}}(t) = \boldsymbol{S}(t) \times \boldsymbol{B} - J^2 \boldsymbol{S}(t) \times \int_0^t dt' \, \chi_{\mathrm{loc}}(t - t') \boldsymbol{S}(t') \,, \tag{5.27}$$

with the local (diagonal and isotropic) retarded spin susceptibility

$$\chi_{\mathrm{loc}}(t) = -i\Theta(t) \langle 0 | [s_{i_0 z}(t), s_{i_0 z}(t')] | 0 \rangle \tag{5.28}$$

at the site i_0 where the classical spin is coupled to. In contrast to Sec. 4.2 and Eq. (4.7), $|0\rangle$ is now the ground state of a correlated conduction electron system, i.e. the ground state of the Hubbard Hamiltonian H_e, $s_{iz}(t) = e^{iH_e t} s_{iz} e^{-iH_e t}$, and s_{iz} is the z-component of the local conduction-electron spin $\boldsymbol{s}_i = \sum_{\sigma\sigma'} c^\dagger_{i\sigma} \boldsymbol{\sigma}_{\sigma\sigma'} c_{i\sigma'}/2$. Using the equation (5.27) which is numerically accessible by Runge-Kutta [Verner, 2010] and Newton–Cotes quadrature

rule [Press et al., 2007], we must compute the integral kernel[8] $\chi_{\rm loc}(t)$ (Eq. (5.28)) in advance. To this end, we apply tDMRG and the framework of matrix-product states [Schollwöck, 2011] for systems with $L = 80$–120 sites. Here, the exchange coupling parameter is set $J = 1$ to generate relaxation times accessible to the tDMRG approach.

We choose $i_0 = 1$ for two reasons: (i) As compared to the symmetric choice $i_0 = L/2$, this allows us to double the accessible time scale (before finite-size effects set in). (ii) As previously discussed in Sec. 4.3, the Gilbert damping is given by the expression

$$\alpha^{\rm G} = -\int_0^\infty dt\, t\, \chi_{loc}(t)\,, \tag{5.29}$$

which depends on the Hubbard-U via the local retarded spin susceptibility $\chi_{loc}(t)$. This timeintegral is sensitive to the long-time behavior of $\chi_{\rm loc}(t)$ which, at least for $U = 0$, is related to the strength of the van Hove singularities in the local density of states as explicitly analyzed in Sec. 4.2. At the edge of the open chain, those are weak and characteristic for a three-dimensional system.

Finally, we would like to note that the LR-SD approach in Eq. (5.27) is perfectly reliable even for fairly strong couplings J and up to the time scale necessary for complete spin relaxation, as it has been demonstrated in Sec. 5.1.4 for $U = 0$. This was explained by the observation, that even for moderately strong couplings J, the linear-response contribution $J^2\boldsymbol{S}(t) \times \langle \boldsymbol{s}_{i_0}\rangle_t$ to the equation of motion for $\boldsymbol{S}(t)$ is small (and the quadratic and higher-order corrections are expected to be even smaller).

In the case of correlated conduction electrons, $|\boldsymbol{S}(t) \times \langle \boldsymbol{s}_{i_0}\rangle_t|$ remains small (of the order of 0.1 or smaller), for weak and for strong U, as has been checked numerically for all data that will be presented in this section. This ensures that the spin dynamics is nearly adiabatic and hence the LR-SD approach provides qualitatively correct results.

5.3.2 Correlation effects at quarter filling

Electron correlations are expected to speed up the relaxation of the classical spin since electron scattering facilitates the transport of energy and spin density from i_0 to the bulk of the system. An increasingly efficient dissipation implies an increase of α with U. This can be nicely seen in $\chi_{\rm loc}(t)$, which determines α via Eq. (5.29) and which is shown in Fig. 5.17 (upper panel) for quarter filling $n \equiv N/L = 0.5$ where we have a (correlated) metal in the entire U range. In fact, the absolute value of the integral weight $\int dt\, \chi_{\rm loc}(t)$ grows with increasing U. Note that via the fluctuation-dissipation theorem, the total weight $\int dt\, \chi_{\rm loc}(t)$ is given by the negative local static spin susceptibility. This explains that $\chi_{\rm loc}(t)$ is mainly negative.

[8] The integral kernel $\chi_{\rm loc}(t)$ was provided by Roman Rausch. Concretely, the two-site version of the algorithm suggested in Ref. Haegeman et al. [2011, 2016] was used, which is based on the time-dependent variational principle (TDVP).

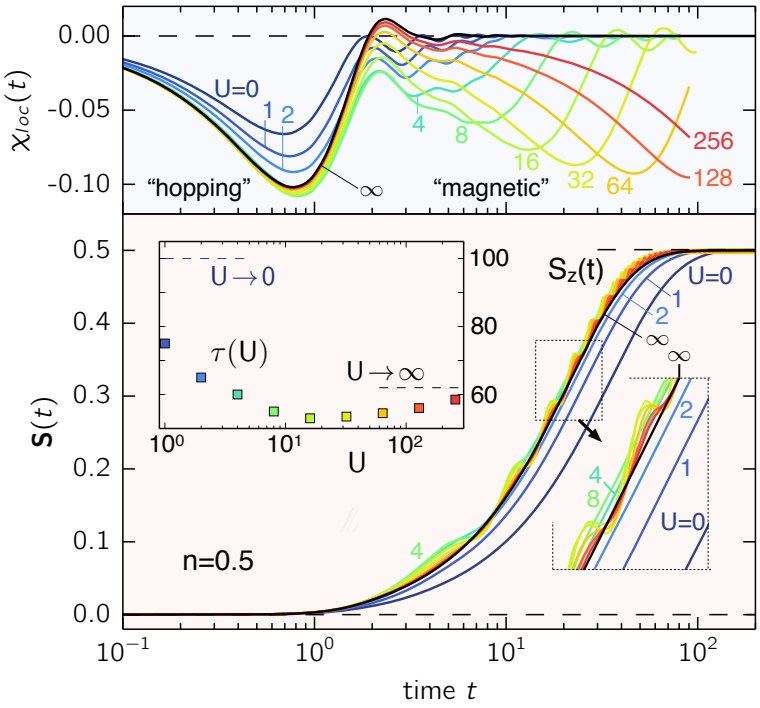

Figure 5.17: *Upper panel:* Local spin correlation $\chi_{\rm loc}(t)$ at $i_0 = 1$ for an open Hubbard chain with $L = 80$ sites as obtained by tDMRG for quarter filling and different U as indicated. ($U \geq 32$: $t-J$ model with three-site terms[9], $L = 100$ sites; $U = \infty$: $L = 120$). Energy and time scales are fixed by the n.n. hopping $T = 1$. *Lower panel:* Resulting real-time dynamics of a classical spin $\boldsymbol{S}(t)$ (with $|\boldsymbol{S}(t)| = \frac{1}{2}$, only $S_{\rm z}$ is shown) coupled at i_0 to the local conduction-electron spin as obtained from Eq. (5.27) for $J = 1$ and different U. The spin dynamics is initiated by switching the local magnetic field in Eq. (5.27) at time $t = 0$ from x- to z-direction ($B_{\rm fin} = 1$). *Inset:* U-dependence of the relaxation time τ, defined as $S_{\rm z}(\tau) = 0.98|\boldsymbol{S}|$.

Separation of time scales. A central observation is that $\chi_{\rm loc}(t)$ develops a pronounced two-peak structure for strong U. For $U = 0$ and in the weak-coupling regime, there is essentially a single (negative) peak around $t \sim 1$ only. This corresponds to fast correlated-hopping processes on a scale set by the inverse hopping $1/T$. As is seen in the figure, the contribution of these processes to the Gilbert damping grows with increasing U.

The second (negative) peak is clearly present for $U \gtrsim 8$. The almost linear shift of its position with U hints towards a time scale set by an effective magnetic interaction $J_{\rm H} \sim 1/U$ between local magnetic moments formed by strong correlations in the conduction-

[9]Strong correlations in the metallic phase is particularly interesting but also difficult to investigate due to the heavy computational costs. However, in the large-U limit $U/T \to \infty$ the Hubbard model can be mapped via a canoncal transformation to an effective $t-J-t_3$ Hamiltonian [Ammon et al., 1995], which is readily accessible to the tDMRG algorithm.

electron system. Even for $U \to \infty$, however, local-moment formation is not perfect at quarter filling: We have $\langle \boldsymbol{s}_i^2 \rangle = \frac{3}{4}n = \frac{3}{8} < s(s+1)$ with $s = 1/2$ for the size of the correlated local moment [Gebhard, 1997]. This explains the residual contributions from correlated hopping processes (first peak).

For strong U the Gilbert damping is dominated by magnetic processes: Because of the extra factor t under the integral in Eq. (5.29), the contribution of the second peak in $\chi_{\mathrm{loc}}(t)$ by far exceeds the hopping contribution (note the logarithmic scale in Fig. 5.17). Clearly, α strongly increases with U, though a precise value cannot be given due to limitations of the tDMRG in accessing the long-time limit.

Correlation effects in the spin dynamics. The resulting spin dynamics (Fig. 5.17, lower panel) is characterized by precessional motion ($S_{\mathrm{x}}(t), S_{\mathrm{y}}(t)$ not shown) with Larmor frequency $\omega_L \propto B$ around the $\hat{z}$ axis, and by relaxation driven by dissipation of energy and spin into the bulk of the electronic system. In the final state there is complete alignment, $\boldsymbol{S}(t) \uparrow\uparrow \boldsymbol{B}$.

Comparing the results for the different U, we observe the following points:

(i) Significant relaxation starts at times $t \sim 1/T$, i.e., on the time scale for dissipation through correlated-hopping processes.

(ii) Correlation effects lead to a considerably shorter relaxation time, e.g., by about a factor two when comparing the results for $U = 0$ and $U = 16$ (see inset).

(iii) To some extent this is due to an additional damping mechanism, namely via excitations of *correlation-induced* magnetic moments – at least for moderate U.

(iv) For strong U, however, the relaxation time *increases* again. This is counterintuitive but easily explained: Since the second, "magnetic" peak in $\chi_{\mathrm{loc}}(t)$ shifts with increasing U to later and later times, relaxation is already completed before dissipation through spin-flip processes can become active. This is most obvious for $U \to \infty$ where magnetic damping is *never* activated, and where a renormalized band picture may apply.

(v) At intermediate U, however, the picture is different. Here, spin-flip processes do contribute to the relaxation but more than an order of magnitude later ($t \gtrsim U/T^2$) than the hopping time scale. *Despite their dominating contribution to* α, their effect is weaker as compared to the correlated-hopping processes. Still, spin-flips leave a clear characteristic in $S_z(t)$: their additional torque produces oscillations (with a period largely independent of U) which superimpose the monotonic relaxation dynamics. The onset of these "magnetic" oscillations grows linearly with U.

Finally, we emphasize that the interpretation of these (and the following) findings does not rely on the one-dimensionality of the model.

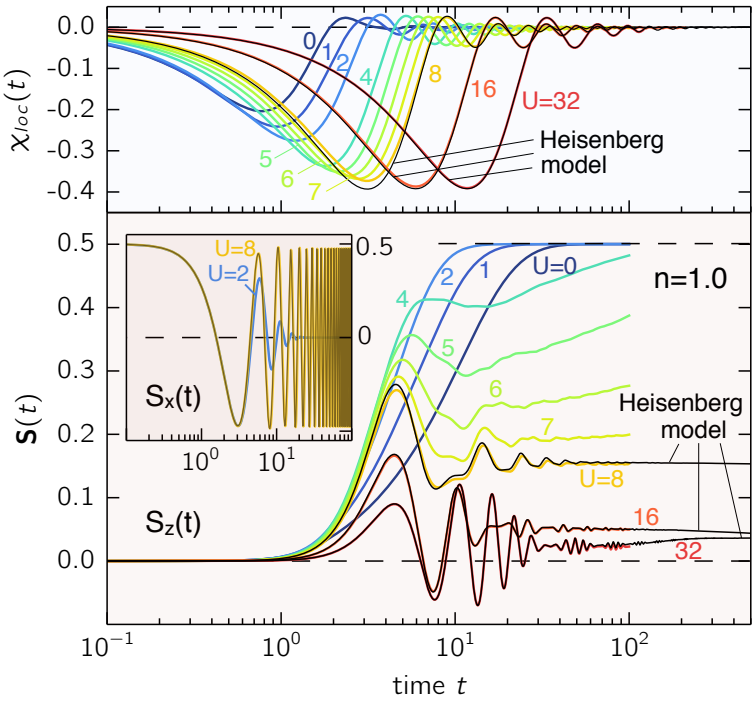

Figure 5.18: The same as Fig. 5.17 but for $n = 1$ ($L = 60$). Thin black lines: Heisenberg model with $J_{\rm H} = \frac{4T^2}{U}$ ($L = 400$) and, for improved accuracy at $U = 8$, with n.n. and n.n.n. couplings $J_{\rm H} = \frac{4T^2}{U} - \frac{16T^4}{U^3}$ and $J'_{\rm H} = \frac{4T^4}{U^3}$ [Buleavskiĭ, 1967] ($L = 300$).

5.3.3 Correlation effects at half -filling

Dissipation through correlated hopping is impeded or even suppressed at half-filling where the system is a Mott insulator for all $U > 0$. Fig. 5.18 (upper panel) shows the tDMRG data for $\chi_{\rm loc}(t)$ at $n = 1$ and different U. Its time dependence is dominated by a single (negative) structure which grows with increasing U up to, say, $U \approx 8$. In the weak-coupling regime, $U \lesssim 4$, the local magnetic moments are not yet well-formed since the charge gap $\Delta \sim e^{-1/U}$ (as obtained from the Bethe ansatz [Ovchinnokov, 1969] for $U \to 0$) is small as compared to T. Hence, residual hopping processes still contribute significantly, as already mentioned in Sec. 2.1. In the strong-coupling limit, on the other hand, spin-flip processes dominate. Here, we observe scaling behavior, $\chi_{\rm loc}(t) = F(4tT^2/U)$ with a universal function $F(x)$. Indeed, due to the suppression of charge fluctuations, the long-time, low-energy dynamics is captured by a Heisenberg chain with antiferromagnetic interaction $J_{\rm H} = 4T^2/U$ between nearest-neighbour $s = 1/2$-spins. As $J_{\rm H}$ is the only energy scale remaining, we have $\chi_{\rm loc}(t) = F(t\, J_{\rm H})$ for arbitrary $J_{\rm H}$ where $F(x)$ is a function independent of $J_{\rm H}$. This implies that the dominant (negative) peak of $\chi_{\rm loc}(t)$ shifts to later and later times as $J_{\rm H}$ decreases as illustrated by Fig. 5.19, upper panel.

As expected, with $F(x)$ obtained numerically by means of tDMRG applied to the Heisenberg chain with $L = 400$ spins at $J_{\rm H} = 1$, the tDMRG data for strong U are fitted perfectly (see Fig. 5.18). Significant deviations from the scaling behavior can be seen in Fig. 5.18 for $U = 8$ and $t \approx 3$, for instance.

Scaling can be exploited to determine the U-dependence of the Gilbert damping for a Mott insulator. From Eq. (5.29) we get

$$\alpha = \frac{J^2}{J_{\rm H}^2} \int_0^\infty dx\, x\, F(x) = \frac{J^2}{J_{\rm H}^2} \alpha_0 = \frac{J^2 U^2}{16 T^4}\, \alpha_0 \,, \tag{5.30}$$

and thus, for fixed J, T, we have $\alpha \propto U^2$. For the universal dimensionless Gilbert damping constant α_0 we find

$$\alpha_0 \approx 4.8 \,. \tag{5.31}$$

For a correlated Mott insulator, Eqs. (5.30) and (5.31) completely describe the U-dependence of the classical-spin dynamics in the weak-J, weak-B limit where the t-dependence of $\boldsymbol{S}(t)$ is so slow, as compared to the typical memory time $\tau_{\rm mem}$ characterizing $\chi_{\rm loc}(t)$, that the Taylor expansion $\boldsymbol{S}(t') \approx \boldsymbol{S}(t) + \dot{\boldsymbol{S}}(t)(t'-t)$ can be cut at the linear order under the t'-integral in Eq. (5.27), such that the LLG equation is obtained (see also Sec. 4.3).

Incomplete spin relaxation. As demonstrated with Fig. 5.18 (lower panel), there is an anomalous U-dependence of the spin dynamics at $n = 1$:

(i) Only in the weak-coupling regime, $U \lesssim 2$, do damping effects increase and lead to a decrease of the relaxation time with increasing U. For $U = 4$, however, the relaxation time *increases* again.

(ii) In addition, as for $n = 0.5$, we note a non-monotonic behavior of $S_z(t)$ with superimposed oscillations (see $U = 6$, for example). With increasing U these oscillations die out at a "critical" interaction $U_{\rm c} \sim 8$.

(iii) For all $U > U_{\rm c}$ the relaxation time seems to diverge. Namely, the z-component of $\boldsymbol{S}(t)$ approaches a nearly constant value which decreases with increasing U while S_x (and S_y) still precess around $\boldsymbol{B}$ (see inset). Hence, on the accessible time scale, $U_{\rm c}$ marks a transition or crossover to an incompletely relaxed but "stationary" state.

(iv) For strong $U > U_c$ the z-component of the spin develops oscillations at short times.

The same type of dynamical transition is also seen for a classical spin coupled to a Heisenberg chain, as can be observed in Fig. 5.19. One clearly notes that for $J \lesssim J_{\rm c} \sim 0.5$ (corresponding to $U_{\rm c} \sim 8$) the time dependence of S_z develops a prethermalization-like plateau on an intermediate time scale $t \sim 100$ (in units of $1/J_{\rm H}$). Moreover, using

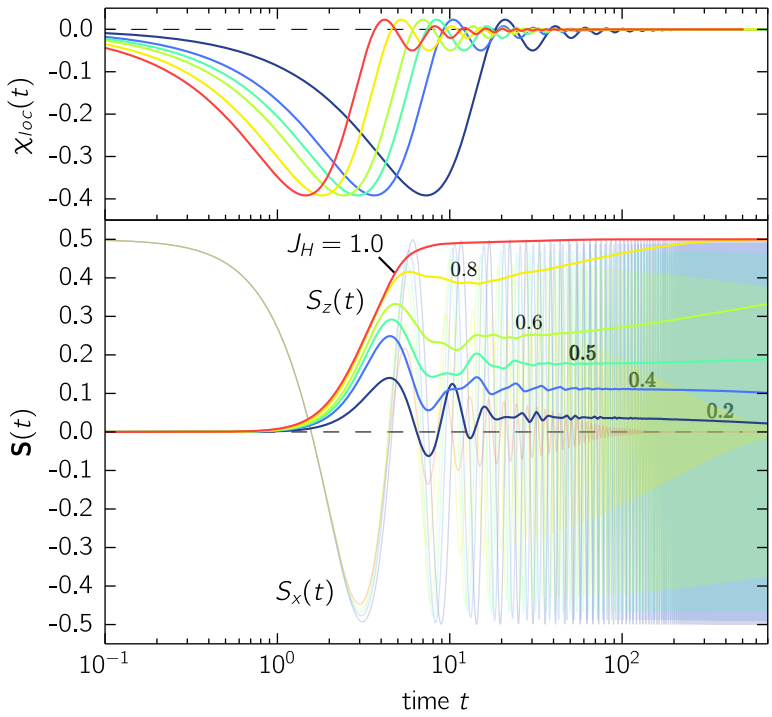

Figure 5.19: *Upper panel:* Local susceptibility $\chi_{\rm loc}(t) = F(tJ_H)$ at $i_0 = 1$ for an open Heisenberg chain with $L = 400$ spins at $J_{\rm H} = 1$ as obtained by tDMRG illustrated for different $J_{\rm H}$ as indicated. *Lower panel:* Resulting real-time dynamics of a classical spin $\boldsymbol{S}(t)$ (with $|\boldsymbol{S}(t)| = \frac{1}{2}$, S_x and S_z are shown) coupled at i_0 to the local spin of the Heisenberg chain as obtained from Eq. (5.27) for $J = 1$ and different J_H (and $J'_H \equiv 0$). The spin dynamics is again initiated by switching the local magnetic field in Eq. (5.27) at time $t = 0$ from x- to z-direction ($B_{\rm fin} = 1$).

the scaling property of $\chi_{\rm loc}(t)$ for the Heisenberg model, it is easily possible to perform calculations up to $t = 1000$. On this longer time scale, it is clearly visible (see Fig. 5.19) that S_z does *not* approach a constant value asymptotically. For $J_{\rm H} = 0.4$ and $J_{\rm H} = 0.2$ the z-component of $\boldsymbol{S}(t)$ is even found to decrease and appears to approach the trivial solution $S_z(t) \equiv 0$. Also, the oscillations of the z-component of the spin at short times are present for weak $J_{\rm H}$.

In addition to the numerical study of the Heisenberg model on the longer time scale, also analytical arguments clearly indicate that a state with $S_z = \text{const.} \neq 1/2$ is unstable and that finally, for $t \to \infty$, the fully relaxed state with $\boldsymbol{S}(t) \uparrow\uparrow \boldsymbol{B}$ is reached. It is straightforwardly seen that a "stationary state" of the form

$$\boldsymbol{S}(t) = S_z\hat{z} + S_\perp \cos(\omega t + \varphi)\hat{x} + S_\perp \sin(\omega t + \varphi)\hat{y} \tag{5.32}$$

with arbitrary parameters $S_\perp, \omega, \varphi$ and with constant (time-independent) S_z does not solve the integro-differential equation (5.27) for $t \to \infty$. There is one exception only, namely

the trivial case where $\chi_{\rm loc}(t) \equiv 0$ which can be realized, up to arbitrarily long times, in the limit $J_{\rm H} \to 0$. For small but finite $J_{\rm H} > 0$, we therefore expect that the classical spin develops a dynamics on an extremely long time scale $t \gg 10^3$, the onset of which is already seen in Fig. 5.19, which finally terminates in the fully relaxed state with $\boldsymbol{S}(t) \to \boldsymbol{S}_0 \uparrow\uparrow \boldsymbol{B}$. It is in fact easy to see from the integro-differential equation that, if there is spin relaxation to a time-independent constant, $\boldsymbol{S}(t) \to \boldsymbol{S}_0$ for $t \to \infty$, the relaxed state has $\boldsymbol{S}_0 = 0.5\hat{z}$. This implies that if there is complete relaxation at all, the spin relaxes to the equilibrium direction.

The Oscillations of the z-component of the spin at short times for weak $J_{\rm H}$, which can also be seen for the case of the Hubbard model for strong U, can be also understood analytically in the following way:

Firstly, by perturbation theory in $x = 4tT^2/U = tJ_{\rm H}$, one verifies the linear short-time behavior of the local susceptibility

$$\chi_{\rm loc}(t) = \Theta(t)\, t\, \frac{2}{3}(J_{\rm H}\langle \boldsymbol{s}_{i_0}\boldsymbol{s}_{i_0+1}\rangle + J'_{\rm H}\langle \boldsymbol{s}_{i_0}\boldsymbol{s}_{i_0+2}\rangle) + \mathcal{O}(x^2)\,, \tag{5.33}$$

valid to leading order for both, the Hubbard and the effective Heisenberg model. Secondly, inserting the expression (5.33) with $J'_{\rm H} = 0$ for the behavior of $\chi_{\rm loc}(t)$ at short times into the LR-SD in equation (5.27), results in

$$\dot{\boldsymbol{S}}(t) = \boldsymbol{S}(t) \times \boldsymbol{B} - \frac{2}{3}J^2 J_{\rm H}\langle \boldsymbol{s}_{i_0}\boldsymbol{s}_{i_0+1}\rangle \boldsymbol{S}(t) \times \int_0^t dt'(t-t')\boldsymbol{S}(t') + \mathcal{O}(t^3J^4)\,. \tag{5.34}$$

Finally, approximating $\boldsymbol{S}(t)$ by the $J = 0$ result $\boldsymbol{S}_0(t) = S(\cos\omega t, \sin\omega t, 0)$ (with $\boldsymbol{B} = B\hat{z}$, $\omega = B$, $S = 1/2$) in the second term on the right-hand side of Eq. (5.34), a straightforward calculation yields:

$$S_z(t) = \frac{2}{3}J^2 J_{\rm H}\langle \boldsymbol{s}_{i_0}\boldsymbol{s}_{i_0+1}\rangle S^2\, \frac{\omega t \sin\omega t + 2\cos\omega t - 2}{\omega^3} + \mathcal{O}(t^4 J^2 J_H^2)\,. \tag{5.35}$$

This is found to perfectly describe the short-time oscillations for weak $J_{\rm H}$ in Fig. 5.19 and for strong U in Fig. 5.18. For longer times the oscillations are damped and eventually die out.

Mechanism for incomplete relaxation. In the following, we describe the mechanism, which leads to the strongly suppressed relaxation of the spin at half filling and large U on the basis of linear-response theory as follows: The x and y components of the linear response

$$\langle \boldsymbol{s}_{i_0}\rangle_t = \int_0^t d\tau\, \chi_{\rm loc}(\tau)\boldsymbol{S}(t-\tau)\,, \tag{5.36}$$

tend to zero if the characteristic memory time $\tau_{\rm mem}$ of the kernel $\chi_{\rm loc}(\tau)$ is much larger than the precession time scale $\tau_{\rm B} = 2\pi/B$ since the integral produces a vanishing average

in this case. This means that the corresponding torque, $-J^2\boldsymbol{S}(t)\times\langle\boldsymbol{s}_{i_0}\rangle_t$, is perpendicular to the field direction and hence there is no relaxation of the spin. The same argument can also be formulated after transformation to frequency space: After some transient effect, we have $\langle\boldsymbol{s}_{i_0}\rangle_\omega = \chi_{\mathrm{loc}}(\omega)\boldsymbol{S}(\omega)$, and thus the x- and y-components of the linear response will vanish if $\chi_{\mathrm{loc}}(\omega = B) = 0$, i.e., if B is stronger than the bandwidth of the magnetic excitations. Note that this can be studied in detail already for $U = 0$, as shown in Sec. 5.1.3 (see Fig. 5.4, right panel), but requires an unrealistically strong field in case of noninteracting conduction electrons.

At half-filling and for strong U, the memory time $\tau_{\mathrm{mem}} \propto J_{\mathrm{H}}^{-1} \propto U$, i.e., τ_{mem} can easily become large as compared to τ_{B}, and thus incomplete spin relaxation can occur at comparatively weak and physically meaningful field strengths. For example, from the Bethe ansatz [Essler et al., 2005] we have

$$W_{\mathrm{spinon}} = 2\int_0^\infty \frac{dx}{x}\,\frac{J_1(x)}{\cosh(Ux/4)} \to \frac{\pi}{2}J_{\mathrm{H}} \quad \text{for } U\to\infty \tag{5.37}$$

for the spinon bandwidth W_{spinon} where $J_1(x)$ is the first Bessel function. Hence, for strong Hubbard interaction, $B_{\mathrm{c}} \approx 2W_{\mathrm{spinon}} = \pi J_{\mathrm{H}}$.

Finally, we also point out that the incomplete spin relaxation can also be understood as a transient "phase" similar to the concept of a prethermalized state. The latter is known for purely electronic systems [Kollar et al., 2011; Marcuzzi et al., 2013; Moeckel and Kehrein, 2008, 2010] which, in close parametric distance to integrability, do not thermalize directly but are trapped for some time in a prethermalized state. Here, for the quantum-classical hybrid, the analogue of an "integrable" point is given by the $U\to\infty$ limit where, for every *finite* t, the integral kernel $\chi_{\mathrm{loc}}(t) \equiv 0$, and Eq. (5.27) reduces to the simple (linear) Landau-Lifschitz equation [Landau and Lifshitz, 1935].

The situation is also reminiscent of *quantum* excitations which are metastable on an exponentially long time scale due to a small phase space for decay. An example is given by doublons in the Hubbard model which, for U much larger than the bandwidth and due to energy conservation, can only decay in a high-order scattering process [Hofmann and Potthoff, 2012; Rausch and Potthoff, 2016; Rosch et al., 2008; Strohmaier et al., 2010]. The relaxation time diverges in the $U\to\infty$ limit where the doublon number is conserved. Here, for a *classical* spin, one would expect that relaxation via dissipation of (arbitrarily) small amounts of energy is still possible. Our results show, however, that this would happen on a longer time scale not accessible to the linear-response approach while the "stationary state" on the intermediate time scale is well captured.

5.3.4 Conclusion

By Combining the tDMRG with non-Markovian classical spin dynamics, we have presented a new method to link the fields of strongly correlated electron systems and spin

dynamics. In addition we could demonstrate that correlation-induced time-scale separation has qualitatively new consequences on the spin dynamics, which is of great importance for the microscopic understanding of the emerging relaxation time scales in modern nano-spintronics devices involving various transition metals and compounds [Khajetoorians et al., 2011; Loth et al., 2010; Morgenstern, 2010]

Concretely, we have studied the spin dynamics of a generic model with a classical spin $\boldsymbol{S}$ that is antiferromagnetically exchange-coupled ($J > 0$) to a Hubbard system as a function of the local Coulomb interaction U.

In the metallic phase at quarter-filling, by comparing the results for different Coulomb interaction U, we have identified the two main electronic dissipation channels, transport of excitations via correlated hopping and via excitations of correlation-induced magnetic moments, become active on largely different time scales. While slow correlation-induced magnetic scales dominate the Gilbert damping α, their contribution to spin dynamics is progressively reduced with increasing U.

At half-filling, we found that electron correlations can have even more extreme impact on the spin dynamics. It has been demonstrated that correlations can lead to a strongly suppressed relaxation which so far has been observed in purely electronic systems only and which is governed here by proximity to the divergent magnetic time scale in the infinite-U limit.

Finally, we pointed out that correlation-induced time-scale separation and incomplete spin relaxation is similar to the notion of prethermalization, which has been studied extensively in purely electronic systems only, [Kollar et al., 2011; Marcuzzi et al., 2013; Moeckel and Kehrein, 2008, 2010] or metastability of excitations due to the lack of phase space for decay [Hofmann and Potthoff, 2012; Rausch and Potthoff, 2016; Rosch et al., 2008; Strohmaier et al., 2010].

6 General conclusions and perspectives

In this thesis, a generalization of the static hybridization mean-field (HybMF) approach [Lacroix and Cyrot, 1979; Yoshimori and Sakurai, 1970] to the nonequilibrium case has been proposed. To this end, the nonequilibrium perturbation theory for Keldysh-Matsubara Green's functions is employed and the full thermal and nonequilibrium self-energy expressions of the correlated many-fermion problem are replaced by the thermal and nonequilibrium Hartree-Fock self-energy contributions to the Kondo-lattice model, respectively. In equilibrium, the previously known static HybMF is recovered. In the nonequilibrium, this leads to a time-dependent hybridization mean-field (tHybMF) theory presented by an equation of motion for the reduced one-particle density matrix which gives access to the time-dependent expectation values of any one-particle observable. The tHybMF approach comprises several advantages; (i) As the Hartree and Fock self-energy contributions can be expressed as functional derivatives of a truncated Luttinger-Ward functional, the tHybMF approach is a conserving approximation in the sense of Baym and Kadanoff [1961b], i.e. macroscopic conservation laws originating from the continuous symmetries of the underlying Hamiltonian are ensured. (ii) The tHybMF approach is a computationally efficient method consisting of a system of non-linear differential equation of first order which can routinely be solved by standard Runge-Kutta methods, see e.g., Verner [2010]. Numerical calculations of large systems consisting of about $L = 10^3$ sites and propagation times up to $t \sim 10^3$ (in units of 1/T) can be performed in a few hours on a standard desktop computer. This is important as small systems suffer from recurrences after only a few propagation steps, which leads to irregular oscillations due to finite size effects. Here, if the impurity is placed at the edge of the chain, finite size effects only occur at $t \sim 10^3$. (iii) The tHybMF method is in general applicable to a wide range of problems concerning classical or quantum spins coupled to a fermionic lattice. The time-dependent Kondo screening as well as the time-dependent competition of Kondo effect versus RKKY indirect magnetic exchange interaction are treatable by this approach. In particular, the transversal and longitudinal dynamics of Kondo impurities are readily accessible, which represents the main focus of this work.

Concerning the spin dynamics, equations of motion for the impurity and conduction-electron spins as well as for the hybridization terms reflecting the time-dependent Kondo effect are derived. This reveals, that the real-time dynamics of a spin in an external mag-

netic field shows a precessional motion. In addition, the spin may relax to a new equilibrium state due to the coupling of the local conduction-electron spin to its environment and the dissipation of spin and energy into the bulk of the electronic subsystem. Furthermore, it has been distinguished between longitudinal and transversal spin dynamics. While the former arises due to the time-dependent Kondo screening, the latter represents a classical phenomenon. Focusing on the classical spin dynamics, we have related our approach to previous ones in the current literature.

Firstly, we have found that the transversal spin dynamics obtained from the time-dependent mean-field approximation of the quantum model is equivalent to the *exact* quantum-classical hybrid spin dynamics (QCH-SD) [Elze, 2012; Hall, 2008] obtained from the classical-spin multi-impurity Kondo model, which is a quantum-classical hybrid model as classical degrees of freedom are coupled directly to quantum-mechanical degrees of freedom. This hybrid model system exhibits non-trivial spin dynamics and is valid for all time scales and coupling strengths. The real-time dynamics of the classical spin is determined via the Liouville-equation by the classical Hamilton function $H^{\mathrm{cl.}} = \langle H \rangle$, which is the only known way to consistently describe the dynamics of quantum–classical hybrids [Elze, 2012; Hall, 2008]. In addition, as in the case of the tHybMF approach, the real-time dynamics of the electronic subsystem is included explicitly in terms of the reduced one-particle density matrix, which obeys the von Neumann equation.

Secondly, in the weak-coupling limit, the conduction-electron degrees of freedom are eliminated by employing standard linear-response theory, which results in the linear-response spin dynamics (LR-SD) presented by an equation of motion for the classical spins only [Bhattacharjee et al., 2012; Onoda and Nagaosa, 2006]. This integro-differential equation possesses a spatially and temporally non-local structure and is numerically accessible by means of a combination of Runge-Kutta method [Verner, 2010] and Newton–Cotes quadrature rule [Press et al., 2007]. As this weak-coupling approach is characterized by the dimensionless small parameter Jt, deviations of the LR-SD from the exact QCH-SD are expected to gradually increase with the propagation time and subsequently the approximation is expected to break down after a propagation time $t \sim 1/J$ at latest. However, if the spin dynamics is nearly adiabatic the perturbation will produce a rather weak torque $\boldsymbol{S}_m(t) \times \boldsymbol{S}_m(t')$ and the LR-SD becomes reliable on rather large time scales $t \gg 1/J$. Both hypotheses have been checked numerically by comparison of the LR-SD with the exact QCH-SD for a classical spin in an external magnetic field and locally exchange coupled to a one-dimensional conduction electron system with open boundaries. The dynamics is initialized by a sudden switch of the field from the x- to the z-direction at $t = 0$. The numerical study revealed that for couplings of the order $J \sim T$ the magnitude of the torque $\boldsymbol{S}_m(t) \times \boldsymbol{S}_m(t')$ is of the order 0.01 as the angle enclosed by $\boldsymbol{S}_m(t)$ and $\boldsymbol{S}_m(t')$ is very close to π for all times t. Hence the process is nearly adiabatic and we find an almost perfect agreement between the results of the ex-

act QCH-SD and the LR-SD during the entire transient dynamics to the new equilibrium state. However, as expected, with increasing J the retardation effects are enhanced, which results in a non-adiabatic process and the LR-SD shows strong deviations as compared to the exact QCH-SD results. Furthermore, it was found that a simple argument based on the dimensionless expansion parameter Jt seems to fail in any case, as this overlooks retardation effects entirely. Summarizing, the LR-SD is a computationally highly efficient approach, as it provides a tractable spin-only effective theory, which is applicable in the nearly adiabatic regime.

Thirdly, the Landau-Lifshitz-Gilbert equation (LLG) [Gilbert, 2004; Landau and Lifshitz, 1935] and in particular the Gilbert-damping and the moment of inertia are re-derived from the QCH-SD in two steps, as the LLG concept is based on two assumptions: (i) The electron-spin coupling is assumed to be weak and hence treatable perturbatively to lowest order. (ii) A separation of time-scales is assumed, i.e. the impurity spin dynamics is taken to be slow compared to the electron dynamics. The first step towards LLG has been taken by the LR-SD, which is simplified further in a second step by applying a Markov approximation. The microscopic derivation of the LLG equation revealed its inherent disadvantages; the Gilbert-damping is ill-defined in the case of an uncorrelated one-dimensional lattice. The moment of inertia is even ill-defined in the case of a (uncorrelated) two-dimensional lattice. This finding has been traced to the strength of the van Hove singularities in the conduction-electron density, on which the Gilbert-damping constant and the moment of inertia are sensitively dependent. As the strength of the van Hove singularities is characterized for all systems by the lattice dimension only [Ashcroft and Mermin, 1976], we can generally conclude that in this case the LLG theory reduces to a purely phenomenological concept without predictive power. However, this conclusion may change for systems where the classical spin is coupled to a correlated electron system. Here, the van Hove singularities are expected to be regularized by the finite imaginary part of the conduction-electron self-energy.

While the emphasis of the first part was on generalizing the static HybMF approach to time-dependent tHybMF theory for describing multi-impurity Kondo systems in non-equilibrium situations and relating our theory concepts for the classical spin dynamics to previous ones in the literature, the second part is devoted to the numerical study of the real-time dynamics of a classical spin subject to an external magnetic field and locally exchange coupled to a one-dimensional system of conduction electrons. The spin dynamics is initialized by a sudden switch of the field direction at $t = 0$. The numerical results are obtained from tDMRG, QCH-SD and LR-SD plus tDMRG approach and can be summarized as follows:

(i) As expected from the equations of motion for the impurity and conduction-electron spins, the exact QCH-SD shows precessional motion with Larmor frequency and damping, which eventually aligns the spin to the final field direction (the new equilibrium state). While the precession term is easily explained by the torque exerted by the magnetic field,

the damping term is more complex, namely it has been found that the relaxation of the spin results from the retarded effects of the local exchange in the coupled electron-spin dynamics, i.e. the classical spin can be interpreted as a local perturbation exciting the conduction-electron system. However, the electronic excitation propagates and feeds back to the classical spin, but at a later time. This non-adiabatic dynamics of the electronic subsystem and its temporally delayed feedback on the spin induces a spin torque parallel to the field direction.

(ii) The QCH-SD approach also provides a precise microscopic picture of the electron dynamics, which revealed that the energy and spin of the initial excitation is locally stored in the vicinity of the classical spin and subsequently dissipated by dispersive wave packets of excitations into the electronic subsystem with the Fermi velocity. This process is a prerequisite for the relaxation of the impurity spin, as the microscopic dynamics is fully conserving.

(iii) Besides precession and damping, the QCH-SD is further suitable to describe inertia effects in the real-time dynamics of classical spins. Moreover, the precise microscopic picture of the electronic subsystem uncovers also nutational motion in the dynamics of the conduction-electron local magnetic moments. It has been found that in both cases nutation amplitudes are small as compared to amplitudes in precessional motion. Furthermore, the frequency scales, in the strong-coupling limit, linearly in J and in $S_{\text{cl.}}$ (length of the classical spin). In addition, in order to identify quantum effects, we have compared the QCH-SD results for the classical-spin Kondo model with the real-time dynamics of the quantum Kondo model studied by means of the tDMRG approach for different spin quantum numbers S. A qualitative, and with increasing spin-quantum numbers also quantitative agreement between quantum and classical spin dynamics has been found. However, also fundamental differences have been observed; Firstly, as expected the quantum spin dynamics exhibits longitudinal fluctuations reflecting the time-dependent Kondo effect. Secondly, we have shown for the first time that nutational motion is not restricted to classical spin systems but is stable against quantum fluctuations. However, in contrast to the classical spin, the nutational motion of a quantum spin is efficiently damped on a femtosecond time scale, which is essentially independent of the relaxation and precession time scales. This can be explained in the strong-coupling ($JS \to \infty$) limit, where the spin dynamics is essentially local and can be described in terms of an emergent two-spin model. Within this simple two-spin model the damping of the quantum nutation is easily understood as a quantum dephasing of the eigenmodes with revivals suppressed by the coupling to the bulk of the system.

Finally, the effect of electron correlations on the spin dynamics has been addressed and it has been shown that correlation-induced time-scale separation, which is one hallmark of strong correlations, has dramatic and qualitatively new consequences for the spin dynamics. In order to link spin dynamics to the field of strongly correlated electron systems, we have introduced a new numerically efficient method, namely a combination of the

LR-SD for the spin dynamics with the tDMRG for the correlated electronic subsystem. Concretely, we have studied the spin dynamics of a classical spin S that is antiferromagnetically exchange coupled to a Hubbard system. Correlation effects are identified by systematic computations for different local Coulomb interactions U.

In the metallic phase at quarter-filling, we have shown that correlation effects induce two main electronic dissipation channels, namely the transport of excitations via correlated hopping and via excitations of correlation-induced magnetic moments, respectively, become active on largely different time-scales as a function of the Hubbard U. With increasing U and up to $U = 16$ correlation effects results in a considerably shorther relaxation time as compared to $U = 0$. To some extent and for moderate U this is due to the additional dissipation channel, namely excitations of correlation-induced magnetic moments. However, in the strong-coupling regime $U > 16$, the relaxation is partially or fully completed, before dissipation through spin-flip processes can become active. This results in an increase of the relaxation time.

At half-filling, the system is a Mott insulator for any finite $U > 0$ and therefore dissipation through correlated hopping is suppressed. However, only in the weak-coupling regime $U \lesssim 4$, the charge gap $\Delta \sim e^{-1/U}$ is small as compared to the hopping T [Ovchinnokov, 1969]. Thus, in addition to dissipation through spin-flip processes, also residual hopping processes still contribute significantly, which leads to a decrease of the relaxation time with increasing interaction strength up to $U \lesssim 2$. In the strong-coupling limit, charge fluctuations are strongly suppressed and only spin-flip processes remain active and indeed the long-time, low-energy dynamics can be also captured by the Heisenberg model. This has strong consequences for the spin dynamics; For $U \geq 4$, the relaxation time increases again. Even more profound changes occur from a "critical" interaction $U_c \sim 8$ onward, where the relaxation time seems to diverge and a transition or crossover to an incompletely relaxed but "stationary" state is observed. The "stationary state" on an intermediate time scale arises whenever the bandwidth of magnetic excitations becomes smaller than the field. We emphasize in particular that this effect has been observed for the first time in a quantum-classical hybrid system and is reminiscent of prethermalization [Kollar et al., 2011; Marcuzzi et al., 2013; Moeckel and Kehrein, 2008, 2010] or metastability of excitations due to the lack of phase space for decay [Hofmann and Potthoff, 2012; Rausch and Potthoff, 2016; Strohmaier et al., 2010], i.e., physics which so far has been demonstrated exclusively in purely electronic quantum systems.

Summarizing, we have introduced two different numerical methods, namely the tHybMF for Kondo systems out of equilibrium, a special case of which comprises the QCH-SD, and a combination of the LR-SD with the tDMRG approach to link classical spin dynamics to the field of strongly correlated electron systems. Both methods have been applied within the scope of this study to systems consisting of a single classical-impurity spin coupled to an elec-

tronic subsystem. However, there are further interesting directions of research which are based on the present work and could be studied with the above numerical methods in the future.

Firstly, the time-dependent Kondo-screening could be studied on a mean-field level and compared to numerically exact methods [Lechtenberg and Anders, 2014; Medvedyeva et al., 2013; Nuss et al., 2015b]. Also longitudinal spin dynamics [Anders and Schiller, 2006] reflecting the time-dependent Kondo effect is accessible to the tHybMF theory, a systematically numerical study of which remains for future works. Secondly, the competition of the Kondo effect with the RKKY interaction for systems with many magnetic impurities on the time-domain has not been addressed. Here, it should be possible to establish a "dynamical" Doniach phase diagram. Thirdly, another line of research comprises classical spin dynamics of systems with more than a single spin where, e.g., the effects of a time-dependent and retarded RKKY interaction can be studied by means of a numerically exact method, as the tHybMF theory reduces in this case to the exact QCH-SD approach. In this context, also the application of the LR-SD plus tDMRG approach to multi-impurity classical-spins coupled to a correlated conduction-electron system to explore the effect of electronic correlations on the time-dependent RKKY interaction appears highly interesting for future research.

Furthermore, the classical-spin Kondo lattice model is highly interesting to address the time-dependent phase transitions [Gebauer, 2015]. However, the combination of the static *mean-field* for the equilibrium phase diagram and the *exact* QCH-SD for the transient dynamics to the new equilibrium state is rather inconsistent. In particular, the long-time limit of the final state dynamics obtained from the *exact* QCH-SD must be compared with statistical predication, in order to determine whether or not the system is equilibrated. Here, we propose a combination of numerically exact methods such as DMRG or Monte-Carlo methods for the thermal state [Yunoki et al., 1998] with the *exact* QCH-SD approach to address the transient dynamics.

Finally, we remark that generally a wide range of quantum and classical concepts, such as eigenstate thermalization, prethermalization, (non)integrability, etc. [Rigol et al., 2008] have not yet been addressed in the context of quantum-classical hybrid systems and remain an important task for future studies.

Bibliography

Alexander, S. and Anderson, P. W. (1964). Interaction between localized states in metals. *Phys. Rev.*, 133:A1594–A1603.

Ammon, B., Troyer, M., and Tsunetsugu, H. (1995). Effect of the three-site hopping term on the *t* - *J* model. *Phys. Rev. B*, 52:629–636.

Anders, F. B. and Schiller, A. (2006). Spin precession and real-time dynamics in the kondo model:time-dependent numerical renormalization-group study. *Phys. Rev. B*, 74:245113.

Anderson, P. (1961). Localized Magnetic States in Metals. *Physical Review*, 124(1):41–53.

Anderson, P. W. (1978). Local moments and localized states. *Rev. Mod. Phys.*, 50:191–201.

Andrei, N. (1980). Diagonalization of the kondo hamiltonian. *Phys. Rev. Lett.*, 45:379–382.

Antropov, V. P., Katsnelson, M. I., van Schilfgaarde, M., and Harmon, B. N. (1995). $AbInitio$ spin dynamics in magnets. *Phys. Rev. Lett.*, 75:729–732.

Aoki, H., Tsuji, N., Eckstein, M., Kollar, M., Oka, T., and Werner, P. (2014). Nonequilibrium dynamical mean-field theory and its applications. *Rev. Mod. Phys.*, 86:779–837.

Ashcroft, N. W. and Mermin (1976). *Solid state physics*. Holt, Rinehart and Winston, 1 edition.

Balzer, M. and Potthoff, M. (2011). Nonequilibrium cluster perturbation theory. *Phys. Rev. B*, 83:195132.

Baym, G. and Kadanoff, L. P. (1961a). Conservation laws and correlation functions. *Phys. Rev.*, 124:287–299.

Baym, G. and Kadanoff, L. P. (1961b). Conservation laws and correlation functions. *Phys. Rev.*, 124:287–299.

Beach, K. S. D. (2005). Ground state properties of a Zeeman-split heavy metal. *eprint arXiv:cond-mat/0509778*.

Bedrich, R., Burdin, S., and Hentschel, M. (2010). Mesoscopic kondo box: A mean-field approach. *Phys. Rev. B*, 81:174406.

Bhattacharjee, S., Nordström, L., and Fransson, J. (2012). Atomistic spin dynamic method with both damping and moment of inertia effects included from first principles. *Phys. Rev. Lett.*, 108:057204.

Bode, M., Heide, M., von Bergmann, K., Ferriani, P., Heinze, S., Bihlmayer, G., Kubetzka, A., Pietzsch, O., Blugel, S., and Wiesendanger, R. (2007). Chiral magnetic order at surfaces driven by inversion asymmetry. *Nature*, 447(7141):190–193.

Böttcher, D. and Henk, J. (2012). Significance of nutation in magnetization dynamics of nanostructures. *Phys. Rev. B*, 86:020404.

Bravyi, S., Hastings, M. B., and Verstraete, F. (2006). Lieb-robinson bounds and the generation of correlations and topological quantum order. *Phys. Rev. Lett.*, 97:050401.

Buleavskiĭ, L. N. (1967). Quasihomopolar Electron Levels in Crystals and Molecules. *Soviet Journal of Experimental and Theoretical Physics*, 24:154.

Butikov, E. (2006). Precession and nutation of a gyroscope. *European Journal of Physics*, 27(5):1071.

Capelle, K. and Gyorffy, B. L. (2003). Exploring dynamical magnetism with time-dependent density-functional theory: From spin fluctuations to gilbert damping. *EPL (Europhysics Letters)*, 61(3):354.

Cappellini, G., Mancini, M., Pagano, G., Lombardi, P., Livi, L., Siciliani de Cumis, M., Cancio, P., Pizzocaro, M., Calonico, D., Levi, F., Sias, C., Catani, J., Inguscio, M., and Fallani, L. (2014). Direct observation of coherent interorbital spin-exchange dynamics. *Phys. Rev. Lett.*, 113:120402.

Carpene, E., Mancini, E., Dallera, C., Brenna, M., Puppin, E., and De Silvestri, S. (2008). Dynamics of electron-magnon interaction and ultrafast demagnetization in thin iron films. *Phys. Rev. B*, 78:174422.

Cinchetti, M., Sánchez Albaneda, M., Hoffmann, D., Roth, T., Wüstenberg, J.-P., Krauß, M., Andreyev, O., Schneider, H. C., Bauer, M., and Aeschlimann, M. (2006). Spin-flip processes and ultrafast magnetization dynamics in co: Unifying the microscopic and macroscopic view of femtosecond magnetism. *Phys. Rev. Lett.*, 97:177201.

Ciornei, M.-C., Rubí, J. M., and Wegrowe, J.-E. (2011). Magnetization dynamics in the inertial regime: Nutation predicted at short time scales. *Phys. Rev. B*, 83:020410.

Clogston, A. M., Matthias, B. T., Peter, M., Williams, H. J., Corenzwit, E., and Sherwood, R. C. (1962). Local magnetic moment associated with an iron atom dissolved in various transition metal alloys. *Phys. Rev.*, 125:541–552.

Coleman, P. (1983). $^1/_N$ expansion for the kondo lattice. *Phys. Rev. B*, 28(9):5255–5262.

Coleman, P. (2016). Introduction to many-body physics. *Cambridge University Press*.

Coqblin, B. and Schrieffer, J. R. (1969). Exchange interaction in alloys with cerium impurities. *Phys. Rev.*, 185:847–853.

Danielewicz, P. (1984). Quantum theory of nonequilibrium processes, i. *Annals of Physics*, 152(2):239 – 304.

de Haas, W. J., de Boer, J., and van dën Berg, G. J. (1934). The electrical resistance of gold, copper and lead at low temperatures. *Physica*, 1:1115–1124.

Delgado, F., Loth, S., Zielinski, M., and Fernández-Rossier, J. (2015). The emergence of classical behaviour in magnetic adatoms. *EPL (Europhysics Letters)*, 109(5):57001.

Donati, F., Rusponi, S., Stepanow, S., Wackerlin, C., Singha, A., Persichetti, L., Baltic, R., Diller, K., Patthey, F., Fernandes, E., Dreiser, J., Ljivan anin, ., Kummer, K., Nistor, C., Gambardella, P., and Brune, H. (2016). Magnetic remanence in single atoms. *Science*, 352(6283):318–321.

Doniach, S. (1977). The kondo lattice and weak antiferromagnetism. *Physica B+C*, 91:231 – 234.

Ebert, H., Mankovsky, S., Ködderitzsch, D., and Kelly, P. J. (2011). *Ab Initio* calculation of the gilbert damping parameter via the linear response formalism. *Phys. Rev. Lett.*, 107:066603.

Elitzur, S. (1975). Impossibility of spontaneously breaking local symmetries. *Phys. Rev. D*, 12:3978–3982.

Elze, H.-T. (2012). Linear dynamics of quantum-classical hybrids. *Phys. Rev. A*, 85:052109.

Essler, F. H. L., Frahm, H., Göhmann, F., Klümper, A., and Korepin, V. (2005). *The One-Dimensional Hubbard Model*. Cambridge University Press, Cambridge.

Evans, R. F. L., Fan, W. J., Chureemart, P., Ostler, T. A., Ellis, M. O. A., and Chantrell, R. W. (2014). Atomistic spin model simulations of magnetic nanomaterials. *Journal of Physics: Condensed Matter*, 26(10):103202.

Fähnle, M., Steiauf, D., and Illg, C. (2011). Generalized gilbert equation including inertial damping: Derivation from an extended breathing fermi surface model. *Phys. Rev. B*, 84:172403.

Fransson, J. (2008). Detection of spin reversal and nutations through current measurements. *Nanotechnology*, 19(28):285714.

Friedel, J. and Blandin, A. (1956). *Can. J. Phys.*, 34:1190.

Fähnle, M. and Illg, C. (2011). Electron theory of fast and ultrafast dissipative magnetization dynamics. *Journal of Physics: Condensed Matter*, 23(49):493201.

Garanin, D., Kladko, K., and Fulde, P. (2000). Quasiclassical hamiltonians for large-spin systems. *The European Physical Journal B - Condensed Matter and Complex Systems*, 14(2):293–300.

Garanin, D. A. (2008). Relaxation of superparamagnetic spins: Classical vs large-spin description. *Phys. Rev. B*, 78:144413.

Garate, I. and MacDonald, A. (2009). Gilbert damping in conducting ferromagnets. ii. model tests of the torque-correlation formula. *Phys. Rev. B*, 79:064404.

Gauyacq, J. and Lorente, N. (2014). Classical limit of a quantal nano-magnet in an anisotropic environment. *Surface Science*, 630:325 – 330.

Gebauer, L.-M. (2015). Semiclassical dynamics and thermodynamics in the kondo lattice model. *M.Sc. thesis, University of Hamburg*.

Gebhard, F. (1997). The mott metal-insulator transition. *(Springer: Berlin)*.

Georges, A., Kotliar, G., Krauth, W., and Rozenberg, M. J. (1996). Dynamical mean-field theory of strongly correlated fermion systems and the limit of infinite dimensions. *Rev. Mod. Phys.*, 68:13–125.

Gerrits, T. H., van den Berg, H. A. M., Hohlfeld, J., BÄR, L., and Rasing, T. H. (2002). Ultrafast precessional magnetization reversal by picosecond magnetic-field pulse shaping. *Nature*, 418:509.

Gilbert, T. L. (2004). A phenomenological theory of damping in ferromagnetic materials. *IEEE Transactions on Magnetics*, 40(6):3443–3449.

Gutzwiller, M. C. (1963). Effect of correlation on the ferromagnetism of transition metals. *Phys. Rev. Lett.*, 10:159–162.

Haegeman, J., Cirac, J. I., Osborne, T. J., Pižorn, I., Verschelde, H., and Verstraete, F. (2011). Time-dependent variational principle for quantum lattices. *Phys. Rev. Lett.*, 107:070601.

Haegeman, J., Lubich, C., Oseledets, I., Vandereycken, B., and Verstraete, F. (2016). Unifying time evolution and optimization with matrix product states. *Phys. Rev. B*, 94:165116.

Hall, M. J. W. (2008). Consistent classical and quantum mixed dynamics. *Phys. Rev. A*, 78:042104.

Hals, K. M. D., Flensberg, K., and Rudner, M. S. (2015). Nonlocal damping of helimagnets in one-dimensional interacting electron systems. *Phys. Rev. B*, 92:094403.

Hankiewicz, E. M., Vignale, G., and Tserkovnyak, Y. (2008). Inhomogeneous gilbert damping from impurities and electron-electron interactions. *Phys. Rev. B*, 78:020404.

Heslot, A. (1985). Quantum mechanics as a classical theory. *Phys. Rev. D*, 31:1341–1348.

Hewson, A. (1993). *The Kondo Problem to Heavy Fermions*. Cambridge University Press, New York, N.Y.

Hofmann, F. and Potthoff, M. (2012). Doublon dynamics in the extended fermi-hubbard model. *Phys. Rev. B*, 85:205127.

Hubbard, J. (1963). Electron correlations in narrow energy bands. *Proceedings of the Royal Society of London A: Mathematical, Physical and Engineering Sciences*, 276(1365):238–257.

Imada, M., Fujimori, A., and Tokura, Y. (1998). Metal-insulator transitions. *Rev. Mod. Phys.*, 70:1039–1263.

Iwai, H. (2016). End of the scaling theory and moore's law. In *2016 16th International Workshop on Junction Technology (IWJT)*, pages 1–4.

Jones, B. A., Varma, C. M., and Wilkins, J. W. (1988). Low-temperature properties of the two-impurity kondo hamiltonian. *Phys. Rev. Lett.*, 61:125–128.

Jullien, R., Fields, J. N., and Doniach, S. (1977). Zero-temperature real-space renormalization-group method for a kondo-lattice model hamiltonian. *Phys. Rev. B*, 16:4889–4900.

Kadanoff, L. P. and Baym, G. (1962). Quantum statistical mechanics. *(Benjamin: New York)*.

Kanamori, J. (1963). Electron correlation and ferromagnetism of transition metals. *Progress of Theoretical Physics*, 30(3):275–289.

Kasuya, T. (1956). A theory of metallic ferro- and antiferromagnetism on zener's model. *Progress of Theoretical Physics*, 16(1):45–57.

Keldysh, L. V. (1965). *Sov. Phys. JETP*, 20:1018.

Khajetoorians, A. A., Wiebe, J., Chilian, B., and Wiesendanger, R. (2011). Realizing all-spin–based logic operations atom by atom. *Science*, 332(6033):1062–1064.

Kikuchi, R. (1956). On the minimum of magnetization reversal time. *Journal of Applied Physics*, 27(11):1352–1357.

Kikuchi, T. and Tatara, G. (2015). Spin dynamics with inertia in metallic ferromagnets. *Phys. Rev. B*, 92:184410.

Kimel, a. V., Ivanov, B. a., Pisarev, R. V., Usachev, P. a., Kirilyuk, A., and Rasing, T. (2009). Inertia-driven spin switching in antiferromagnets. *Nature Physics*, 5(10):727–731.

Kirilyuk, A., Kimel, A. V., and Rasing, T. (2010). Ultrafast optical manipulation of magnetic order. *Reviews of Modern Physics*, 82(3):2731–2784.

Kladko, K., Fulde, P., and Garanin, D. A. (1999). Cumulant expansion for systems with large spins. *EPL (Europhysics Letters)*, 46(4):425.

Kollar, M., Wolf, F. A., and Eckstein, M. (2011). Generalized gibbs ensemble prediction of prethermalization plateaus and their relation to nonthermal steady states in integrable systems. *Phys. Rev. B*, 84:054304.

Kondo, J. (1964). Resistance minimum in dilute magnetic alloys. *Prog. Theor. Phys*.

Koopmans, B., Malinowski, G., Dalla Longa, F., Steiauf, D., Fahnle, M., Roth, T., Cinchetti, M., and Aeschlimann, M. (2010). Explaining the paradoxical diversity of ultrafast laser-induced demagnetization. *Nat Mater*, 9(3):259–265.

Kuneš, J. and Kamberský, V. (2002a). First-principles investigation of the damping of fast magnetization precession in ferromagnetic $3d$ metals. *Phys. Rev. B*, 65:212411.

Kuneš, J. and Kamberský, V. (2002b). First-principles investigation of the damping of fast magnetization precession in ferromagnetic $3d$ metals. *Phys. Rev. B*, 65:212411.

Lacroix, C. and Cyrot, M. (1979). Phase diagram of the kondo lattice. *Phys. Rev. B*, 20(5):1969–1976.

Lakshmanan, M. and Daniel, M. (1983). Comment on the classical models of electrons and nuclei and the generalizations of classical poisson brackets to include spin. *The Journal of Chemical Physics*, 78(12):7505–7506.

Landau, L. D. and Lifshitz, E. M. (1935). A phenomenological theory of damping in ferromagnetic materials. *Phys. Z. Sow. 8 153*, 8:153.

Lechtenberg, B. and Anders, F. B. (2014). Spatial and temporal propagation of kondo correlations. *Phys. Rev. B*, 90:045117.

Lieb, E. H. (1973). The classical limit of quantum spin systems. *Communications in Mathematical Physics*, 31(4):327–340.

Lieb, E. H. and Robinson, D. W. (1972). The finite group velocity of quantum spin systems. *Communications in Mathematical Physics*, 28(3):251–257.

Lieb, E. H. and Wu, F. Y. (1968). Absence of mott transition in an exact solution of the short-range, one-band model in one dimension. *Phys. Rev. Lett.*, 20:1445–1448.

Loth, S., Baumann, S., Lutz, C. P., Eigler, D. M., and Heinrich, A. J. (2012). Bistability in atomic-scale antiferromagnets. *Science*, 335(6065):196–199.

Loth, S., Etzkorn, M., Lutz, C. P., Eigler, D. M., and Heinrich, A. J. (2010). Measurement of fast electron spin relaxation times with atomic resolution. *Science*, 329(5999):1628–1630.

Lundstrom, M. (2003). Moore's law forever? *Science*, 299(5604):210–211.

Marcuzzi, M., Marino, J., Gambassi, A., and Silva, A. (2013). Prethermalization in a nonintegrable quantum spin chain after a quench. *Phys. Rev. Lett.*, 111:197203.

Marx, D. and Hutter, J. (2009). *Ab Initio Molecular Dynamics: Basic Theory and Advanced Methods*. Cambridge University Press, 1 edition.

Matsubara, T. (1955). A new approach to quantum-statistical mechanics. *Progress of Theoretical Physics*, 14(4):351–378.

Maślanka, P. (1988). *Acta Phys. Pol., B*, 19:269.

Medvedyeva, M., Hoffmann, A., and Kehrein, S. (2013). Spatiotemporal buildup of the kondo screening cloud. *Phys. Rev. B*, 88:094306.

Moeckel, M. and Kehrein, S. (2008). Interaction quench in the hubbard model. *Phys. Rev. Lett.*, 100:175702.

Moeckel, M. and Kehrein, S. (2010). Crossover from adiabatic to sudden interaction quenches in the hubbard model: prethermalization and non-equilibrium dynamics. *New Journal of Physics*, 12(5):055016.

Moore, G. E. (1965). Cramming More Components onto Integrated Circuits. *Electronics*, 38(8):114–117.

Morgenstern, M. (2010). Stm ready for the time domain. *Science*, 329(5999):1609–1610.

Mott, N. F. and Peierls, R. (1937). Discussion of the paper by de boer and verwey. *Proceedings of the Physical Society*, 49(4S):72.

Nadj-Perge, S., Drozdov, I. K., Li, J., Chen, H., Jeon, S., Seo, J., MacDonald, A. H., Bernevig, B. A., and Yazdani, A. (2014). Observation of majorana fermions in ferromagnetic atomic chains on a superconductor. *Science*, 346(6209):602–607.

Natterer, F. D., Yang, K., Paul, W., Willke, P., Choi, T., Greber, T., Heinrich, A. J., and Lutz, C. P. (2016). Reading and Writing Single-Atom Magnets. *eprint arXiv:cond-mat/1607.03977*.

Negele, J. W. and Orland, H. (1998). *Quantum Many-particle Systems*. Westview Press.

Nolting, W. and Ramakanth, A. (2009). *Quantum Theory of Magnetism*. Springer, 2010 edition.

Nunes, G. and Freeman, M. R. (1993). Picosecond resolution in scanning tunneling microscopy. *Science*, 262(5136):1029–1032.

Nuss, M., Ganahl, M., Arrigoni, E., von der Linden, W., and Evertz, H. G. (2015a). Nonequilibrium spatiotemporal formation of the kondo screening cloud on a lattice. *Phys. Rev. B*, 91:085127.

Nuss, M., Ganahl, M., Arrigoni, E., von der Linden, W., and Evertz, H. G. (2015b). Nonequilibrium spatiotemporal formation of the kondo screening cloud on a lattice. *Phys. Rev. B*, 91:085127.

Olive, E., Lansac, Y., and Wegrowe, J. E. (2012). Beyond ferromagnetic resonance: The inertial regime of the magnetization. *Applied Physics Letters*, 100(19).

Onoda, M. and Nagaosa, N. (2006). Dynamics of localized spins coupled to the conduction electrons with charge and spin currents. *Phys. Rev. Lett.*, 96:066603.

Ovchinnokov, A. A. (1969). Excitation spectrum in the one-dimensional hubbard model. *Zh. Eksp. Teor. Fiz.*, 57:2137–2143.

Press, W. H., Teukolsky, S. A., Vetterling, W. T., and Flannery, B. P. (2007). *Numerical Recipes: The Art of Scientific Computing*. Cambridge University Press.

Rausch, R. and Potthoff, M. (2016). Multiplons in the two-hole excitation spectra of the one-dimensional hubbard model. *New Journal of Physics*, 18(2):023033.

Read, N., Newns, D. M., and Doniach, S. (1984). Stability of the kondo lattice in the large-n limit. *Phys. Rev. B*, 30:3841–3844.

Rigol, M., Dunjko, V., and Olshanii, M. (2008). Thermalization and its mechanism for generic isolated quantum systems. *Nature*, 452(7189):854–858.

Rosch, A., Rasch, D., Binz, B., and Vojta, M. (2008). Metastable superfluidity of repulsive fermionic atoms in optical lattices. *Phys. Rev. Lett.*, 101:265301.

Ruderman, M. A. and Kittel, C. (1954). Indirect exchange coupling of nuclear magnetic moments by conduction electrons. *Phys. Rev.*, 96:99–102.

Sakuma, A. (2012). First-principles study on the gilbert damping constants of transition metal alloys, fe–ni and fe–pt systems. *Journal of the Physical Society of Japan*, 81(8):084701.

Sarachik, M. P., Corenzwit, E., and Longinotti, L. D. (1964). Resistivity of mo-nb and mo-re alloys containing one percent fe. *Phys. Rev.*, 135:A1041–A1045.

Sayad, M., Gütersloh, D., and Potthoff, M. (2012). Macrospin approximation and quantum effects in models for magnetization reversal. *The European Physical Journal B*, 85(4):125.

Sayad, M. and Potthoff, M. (2015). Spin dynamics and relaxation in the classical-spin kondo-impurity model beyond the landau–lifschitz–gilbert equation. *New Journal of Physics*, 17(11):113058.

Sayad, M., Rausch, R., and Potthoff, M. (2016a). Inertia effects in the real-time dynamics of a quantum spin coupled to a Fermi sea. *EPL (Europhysics Letters)*, 116(1):17001.

Sayad, M., Rausch, R., and Potthoff, M. (2016b). Relaxation of a classical spin coupled to a strongly correlated electron system. *Phys. Rev. Lett.*, 117:127201.

Scazza, F., Hofrichter, C., Hofer, M., De Groot, P. C., Bloch, I., and Folling, S. (2014). Observation of two-orbital spin-exchange interactions with ultracold su(n)-symmetric fermions. *Nat Phys*, 10(10):779–784. Article.

Schollwöck, U. (2011). The density-matrix renormalization group in the age of matrix product states. *Annals of Physics*, 326(1):96 – 192. January 2011 Special Issue.

Schrieffer, J. and Wolff, P. (1966). Relation between the Anderson and Kondo Hamiltonians. *Physical Review*, 149(2):491–492.

Schwabe, A., Gütersloh, D., and Potthoff, M. (2012). Competition between kondo screening and indirect magnetic exchange in a quantum box. *Phys. Rev. Lett.*, 109:257202.

Shastry, B. S. (1986). Infinite conservation laws in the one-dimensional hubbard model. *Phys. Rev. Lett.*, 56:1529–1531.

Skubic, B., Hellsvik, J., Nordström, L., and Eriksson, O. (2008). A method for atomistic spin dynamics simulations: implementation and examples. *Journal of Physics: Condensed Matter*, 20(31):315203.

Spinelli, A., Bryant, B., Delgado, F., Fernández-Rossier, J., and Otte, A. F. (2014). Imaging of spin waves in atomically designed nanomagnets. *Nat Mater*, 13(8):782–785. Letter.

Strohmaier, N., Greif, D., Jördens, R., Tarruell, L., Moritz, H., Esslinger, T., Sensarma, R., Pekker, D., Altman, E., and Demler, E. (2010). Observation of elastic doublon decay in the fermi-hubbard model. *Phys. Rev. Lett.*, 104:080401.

Tasaki, H. (1998). The hubbard model - an introduction and selected rigorous results. *Journal of Physics: Condensed Matter*, 10(20):4353.

Tatara, G., Kohno, H., and Shibata, J. (2008). Microscopic approach to current-driven domain wall dynamics. *Physics Reports*, 468(6):213 – 301.

Thonig, D., Pereiro, M., and Eriksson, O. (2016). Magnetic moment of inertia within the breathing model. *eprint arXiv:cond-mat/1607.01307*.

Tudosa, I., Stamm, C., Kashuba, a. B., King, F., Siegmann, H. C., Stöhr, J., Ju, G., Lu, B., and Weller, D. (2004). The ultimate speed of magnetic switching in granular recording media. *Nature*, 428(6985):831–833.

Umetsu, N., Miura, D., and Sakuma, A. (2012). Microscopic theory for gilbert damping in materials with inhomogeneous spin dynamics. *Journal of Applied Physics*, 111(7).

Van Vleck, J. H. (1953). Models of exchange coupling in ferromagnetic media. *Rev. Mod. Phys.*, 25:220–227.

Verner, J. H. (2010). Numerically optimal runge–kutta pairs with interpolants. *Numerical Algorithms*, 53(2):383–396.

Viola Kusminskiy, S., Beach, K. S. D., Castro Neto, A. H., and Campbell, D. K. (2008). Mean-field study of the heavy-fermion metamagnetic transition. *Phys. Rev. B*, 77:094419.

Wagner, M. (1991). Expansions of nonequilibrium Green's functions. *Physical Review B*, 44(12):6104.

Waldrop, M. (2016). The chips are down for moore's law. *Nature*, 530(7189):144–147.

Wegrowe, J.-E. and Ciornei, M.-C. (2012). Magnetization dynamics, gyromagnetic relation, and inertial effects. *American Journal of Physics*, 80(7):607–611.

Wiegmann, P. (1980a). Exact solution of the s-d exchange model at $t = 0$. *Soviet Phys. JETP Lett.*, 31:392.

Wiegmann, P. (1980b). Towards an exact solution of the anderson model. *Physics Letters A*, 80(2):163 – 167.

Wiesendanger, R. (2009). Spin mapping at the nanoscale and atomic scale. *Rev. Mod. Phys.*, 81:1495–1550.

Wilson, K. G. (1975). The renormalization group: Critical phenomena and the kondo problem. *Rev. Mod. Phys.*, 47:773–840.

Wolf, S. A., Awschalom, D. D., Buhrman, R. A., Daughton, J. M., von Molnár, S., Roukes, M. L., Chtchelkanova, A. Y., and Treger, D. M. (2001). Spintronics: A spin-based electronics vision for the future. *Science*, 294(5546):1488–1495.

Yan, S., Choi, D.-J., J., B. A., Rolf-Pissarczyk, S., and Loth, S. (2015). Control of quantum magnets by atomic exchange bias. *Nat Nano*, 10(1):40–45. Letter.

Yang, K.-H. and Hirschfelder, J. O. (1980). Generalizations of classical poisson brackets to include spin. *Phys. Rev. A*, 22:1814–1816.

Yoshida, S., Aizawa, Y., Wang, Z.-h., Oshima, R., Mera, Y., Matsuyama, E., Oigawa, H., Takeuchi, O., and Shigekawa, H. (2014). Probing ultrafast spin dynamics with optical pump-probe scanning tunnelling microscopy. *Nat Nano*, 9(8):588–593. Letter.

Yoshimori, A. and Sakurai, A. (1970). Functional integral approach to the bound state due to the $s - d$ exchange interaction. *Progress of Theoretical Physics Supplement*, 46:162–181.

Yosida, K. (1957). Magnetic properties of cu-mn alloys. *Phys. Rev.*, 106:893–898.

Yunoki, S., Hu, J., Malvezzi, A. L., Moreo, A., Furukawa, N., and Dagotto, E. (1998). Phase separation in electronic models for manganites. *Phys. Rev. Lett.*, 80:845–848.

Zhang, S. and Li, Z. (2004). Roles of nonequilibrium conduction electrons on the magnetization dynamics of ferromagnets. *Phys. Rev. Lett.*, 93:127204.

List of publication

Parts of this thesis are based on the following publications, which have been published as refereed journal articles:

M. Sayad, R. Rausch and M. Potthoff:
Inertia effects in the real-time dynamics of a quantum spin coupled to a Fermi sea,
Europhys. Lett. 116, 17001 (2016)

M. Sayad, R. Rausch and M. Potthoff:
Relaxation of a classical spin coupled to a strongly correlated electron system,
Phys. Rev. Lett. 117, 127201 (2016).

M. Sayad and M. Potthoff:
Spin dynamics and relaxation in the classical-spin Kondo-impurity model beyond the Landau-Lifschitz-Gilbert equation, New J. Phys. 17, 113058 (2015).

Unrelated publication:

M. Sayad, D. Gütersloh and M. Potthoff:
Macrospin approximation and quantum effects in models for magnetization reversal, Eur. Phys. J. B 85, 125 (2012).

Acknowledgement

I wish to acknowledge and thank the people who helped me to carry out my research project, the results of which are presented in this thesis:

- First and foremost, I wish to express my great gratitude to my advisor Prof. Dr. Michael Potthoff for providing me the opportunity to do my PhD thesis on an exciting scientific field within his group at the university of Hamburg. Your continuous support of my research project with patience, motivation, and knowledge have been an invaluable source for the development of my research project and of this thesis.
- I am grateful to Prof. Dr. Alexander Lichtenstein, who kindly agreed to review my dissertation thesis.
- I sincerely thank my colleague Roman Rausch for providing the tDMRG code and for many valuable discussions.
- I would like to gratefully acknowledge Jan Stockhofe, Felix Hofmann and Roman Rausch for thorough proofreading. I highly appreciated your valuable feedback.
- My special thanks goes to my friends and colleagues Michael Lee and Felix Hofmann for many insightful discussions and all the fun we have had in the last years.
- I also would like to thank Maximilian Aulbach, Daniel Gütersloh, Andrej Schwabe, Lena Gebauer and Christopher Stahl for many insightful discussions.
- It is or was a pleasure to share the office with Maximilian Aulbach, Niklas Rother, Nadine Gdaniec, Daniel Gütersloh, Felix Hofmann and Christian Gramsch.
- For providing a pleasant working atmosphere, I would like to thank all the former and present members of the I. ITP and the Many-Body Systems and Quantum-Statistical Methods group.

Finally, I gratefully acknowledge financial support of this work through the Deutsche Forschungsgemeinschaft within the Sonderforschungsbereich 668 -“Magnetismus vom Einzelatom zur Nanostruktur” (project B3). Numerical calculations were performed on the PHYSnet HPC cluster at the University of Hamburg.

Eidesstattliche Erklärung

Declaration on oath

Hiermit erkläre ich an Eides statt, dass ich die vorliegende Dissertationsschrift selbst verfasst und keine anderen als die angegebenen Quellen und Hilfsmittel benutzt habe.

I hereby declare, on oath, that I have written the present dissertation by my own and have not used other than the acknowledged resources and aids.

Hamburg | January 31, 2017 Mohammad Sayad